Technical University of Denmark

Exploration, modeling and management of groundwater resources in Northern Quintana Roo, Mexico

Master Thesis by Guillaume Charvet
October 2009

Supervised by Associate Professor Peter Bauer-Gottwein

DTU Environment
Department of Environmental Engineering

Abstract

Urban, industrial and touristic development exerts an increasing pressure on the ecosystems and groundwater resources of the Yucatan peninsula, Mexico. The northern area of Quintana Roo is particularly vulnerable since it has the highest development rate in the region. The highly heterogeneous karstic aquifer of the area consists of a shallow freshwater lens floating on top of saline water and represents the only source of drinking water. Groundwater flows partly through the fractured limestone and partly via extensive underground caves. Despite this high complexity, numerical modeling appears to be a useful tool in order to help decision making to ensure the protection of the aquifer. An equivalent porous medium model of the Yucatan peninsula has been built by means of MODFLOW in order to get a quantitative understanding of the hydraulic heads distribution and the flow patterns. A second similar model has been implemented for the northern part of Quintana Roo. The latter aims at determining the influence of the wells supplying drinking water to the city of Cancun. Their protection zones were stochastically delineated by means of Monte Carlo methods. The numerical models have been calibrated using water table elevations measured in the field. The results show the influence of the important differences in the calibrated hydraulic conductivities defined for the different geological formations. The groundwater flow pattern of the peninsula is strongly influenced by the high permeability features inside which water flows rapidly along long distances. This demonstrates the necessity of establishing groundwater management strategies at the scale of the peninsula. The delineated well capture zones present extended areas. Their shapes are affected by the presence of the Holbox fracture zone. Considering the high velocities in the aquifer, restrictive measures should be taken in order to reduce the risks of pollutant release in these areas. The different outcomes of this study have to be confirmed and detailed but propose already valuable inputs for the establishment of groundwater management strategies.

Preface

This master thesis project was carried out from January 2009 to October 2009 at the Technical University of Denmark (DTU), in the Department of Environmental Engineering. It accounts for 35 ECTS and includes a field trip to Yucatan, Mexico, from March 15th 2009 to April 30th 2009.
This project was conducted under the supervision of associate professor Peter Bauer Gottwein and Ph.D. student Bibi Gondwe.

Kgs. Lyngby, Denmark, October 2009

Guillaume Charvet
s070729

Acknowledgements

This project is part of a larger research work which aims at modeling the groundwater resources in the Yucatan Peninsula. It has been initiated and led by associate professor Peter Bauer Gottwein and Ph.D student Bibi Gondwe. I would like to thank both of them for inviting me to be part of this project and for guiding me throughout the entire task. Their answers, advice, feedbacks and support have been of great help for me.

During the field trip in the Yucatan Peninsula, I received a lot of help from many people. I am very grateful to all of them and especially to:

Amigos de Sian Ka´an (ASK) for welcoming me in Cancun, finding me an accommodation, sharing data and helping me for the logistics and transport. A special great thanks goes to Alejandra Fregoso and Gonzalo Merediz Alonso for all their friendship and efforts to make of my trip a long lasting experience.

Mario Rebolledo-Vieyra and Adrien Le Cossec from the Centro del Estudios del Agua (CEA) for measuring ProTEM47 data with me, for lending me the equipment during the field trip and for answering patiently all my questions. A great thank goes also to Anthony Adevah for helping me in all my measurements, facing all the field problems with me and also for the amazing time I had with him during my stay in Mexico.

Luis Marin from the UNAM for lending me the GPS antennas, organizing their transport to Cancun and sending me his Ph.D. thesis, which has been of great help for me.

Patricia Beddows for answering patiently my questions, for providing me useful advice on my project and for giving me the opportunity to discover speleology with her and her friends.

Finally I would like to express my gratitude to Oticon fonden, IDA legater, and the Technical University of Denmark (DTU) for the financial support which made the field trip possible.

Table of Contents

A. INTRODUCTION **1**

1. Motivation and objectives 1
2. Problem statement 2
3. Organization of the report 3

B. PRESENTATION OF THE PENINSULA **4**

1. Geology and Topography 5
   - *1.1. Geological formations* *5*
   - *1.2. Main geological features* *6*
   - *1.3. Topography* *8*
2. Climate and Vegetation 9
   - *2.1. Climate* *9*
   - *2.2. Vegetation* *11*
3. Surface water 12
4. Groundwater 13
   - *4.1. Characteristics of karstic aquifers* *13*
   - *4.2. The Yucatan aquifer* *14*
5. Anthropogenic use 15
6. Water resources management problems 16

C. FIELD WORK **18**

1. Field work strategy 18
   - *1.1. Objectives and strategy of the Fieldwork* *18*
   - *1.2. Location of the measurements* *18*
   - *1.3. Method for the measurements* *20*
2. GPS measurements 20
   - *2.1. Basic concept of GPS* *20*
   - *2.2. Differential GPS positioning* *22*
   - *2.3. Material used during the field trip* *24*
   - *2.4. Data processing* *25*
3. Water table measurement and leveling 26

D. MODELING METHODS **27**

1. Modeling of karst aquifers 27
   - *1.1. The dual flow model* *27*
   - *1.2. Equivalent porous media in the case of karstic aquifers* *29*
2. Modeling of coastal aquifers 29
3. Modeling of groundwater flow in an equivalent porous medium 31
   - *3.1. Flow equation* *31*
   - *3.2. Parameters in the Flow equation* *34*
   - *3.3. Discretization of the aquifer* *36*
   - *3.4. Boundary conditions and initial conditions* *38*
   - *3.5. Transient and steady state flow modeling* *39*
4. Model Calibration 40
   - *4.1. Parameter estimation and inverse problems* *40*
   - *4.2. PEST Presentation* *41*
5. Stochastic catchment delineation 43
   - *5.1. Catchment delineation* *43*
   - *5.1.1. Methods for determining well capture zones* *43*
   - *5.1.2. Presentation of Modpath and the particle tracking method* *44*
   - *5.2. Well protection zones* *47*

5.3. Monte Carlo techniques *48*

E. MODEL SET UP 51

1. HYDROLOGICAL BOUNDARIES AND DISCRETIZATION OF THE MODELS 51
1.1. Model of the Yucatan peninsula (large model) *51*
1.2. Model of the northern area of Quintana Roo (small model) *52*
2. FRESHWATER HEADS 52
2.1. Characteristics of hydraulic heads in the peninsula *52*
2.2. Data obtained from previous studies *53*
2.3. Field Measurements *53*
2.4. Uncertainties in the data *55*
3. THICKNESS OF THE AQUIFER 56
3.1. Interface Freshwater/Seawater *56*
3.2. Data obtained *56*
3.3. Validity of the Ghyben Herzberg relation *57*
4. RECHARGE 57
5. PUMPING WELLS OF CANCUN 58

F. RESULTS OF THE SIMULATION 60

1. MODEL CALIBRATION 60
1.1. Choice of the number of parameters *60*
1.2. Correlation between calculated and observed hydraulic heads *62*
1.3. Calibrated hydraulic conductivities *63*
2. CONFIGURATION OF HYDRAULIC HEADS 64
2.1. Hydraulic heads configuration for the large model *64*
2.2. Hydraulic heads configuration in the north of Quintana Roo *67*
3. FLOW PATTERN IN THE PENINSULA 71
3.1. Flow pattern in the Yucatan peninsula *71*
3.2. Flow pattern in the north of Quintana Roo *73*
4. INFLUENCE OF THE WELLS ON THE POSITION OF THE SALTWATER/FRESHWATER INTERFACE 74
5. STOCHASTIC CATCHMENT STUDY 76
5.1. Implementation of the stochastic well catchment delineation *76*
5.2. Steady state well catchments *78*

G. DISCUSSIONS AND CONCLUSIONS 80

1. DISCUSSION OF THE RESULTS 80
1.1. Groundwater flows at the scale of the Peninsula *80*
1.2. Groundwater flows in the north of Quintana Roo and influence of the pumping wells *82*
2. GROUNDWATER MANAGEMENT POSSIBILITIES WITH REGARDS TO THE RESULTS 83
2.1. Groundwater management plans at the scale of the peninsula *83*
2.2. Well field management plan in the north of Quintana Roo *84*
3. CONCLUSION 85
4. FURTHER WORK 86

REFERENCES 87

A. INTRODUCTION

1. Motivation and objectives

The Yucatan Peninsula is situated in the south-eastern part of Mexico and comprises the Mexican states of Yucatan, Quintana Roo and Campeche, as well as the northern part of Guatemala and Belize. The Peninsula is a limestone platform which leads to the existence of a karstic aquifer. The Groundwater consists of a thin freshwater lens floating on top of saline water and flowing partly via one of the world's largest underground caves system. These caves, combined with sinkholes and wetlands fed by groundwater represent a unique ecosystem with diversified fauna and flora. Due to the high permeability of the limestone, no large surface water bodies can be observed in Yucatan and groundwater represents the main source of freshwater in the Peninsula.

The high velocity of the groundwater in this karstified medium, the irregular flow paths and the presence of numerous sinkholes that can be sources of pollutants make the aquifer very sensitive to pollution (Milanovic, 2004).

The development of major tourism attractions (Cancun, Riviera Maya) in the north-eastern part of the peninsula has led to an extraordinary increase in population. The city of Cancun, which has been created in 1970, has now more than 550,000 inhabitants and comprises more than 27,000 hostel rooms (SEDETUR, 2007). The total population of the state Quintana Roo has experienced an increase of 1220% in population in the last 35 years (INEGI, 2005). The development of northern Quintana Roo is still continuing at a very high rate.
This fast development of the Peninsula leads to an increase of the water demand and so of the exploitation of the Yucatan aquifer. Moreover the number of potential pollution sources is increasing (non treated waste water discharges, leakages in landfills, industry pollution).

Nevertheless the characteristics of the complex Yucatan karstic aquifer are not known sufficiently to ensure its protection and consequently the availability of clean freshwater in the future. Scientific studies have been conducted in different regions of the peninsula but the complexity of the groundwater flow pattern has led for the moment to an incomplete description of the water resources in the peninsula. The groundwater recharge, the groundwater flow pattern, the high permeability features, the thickness of the aquifer have not been determined precisely yet.

Therefore additional hydrogeological studies are needed in order to support the implementation of efficient water management plans. It will allow to determine the groundwater flow connections existing between the different regions and so to be able to establish consistent management strategies at the scale of the Peninsula.
Moreover it is also important at a regional scale to investigate the groundwater flow in order to be able to supply clean freshwater to the population in the present and in the

future. This is especially the case in the northern part of Quintana Roo, area that has been the subject of very few hydrogeological studies and that has experienced a very high development. In order to protect the water pumped in the extraction wells, the delineation of protection zones (areas where polluting activities are restricted or prohibited) is a common efficient strategy.

Despite the fact that the heterogeneities in karstic aquifers are complex to model, numerical modeling of groundwater flow still remains a very useful tool in order to understand the flow patterns of an aquifer and to have a useful decision making tool concerning its protection.

2. Problem statement

Considering the fast and continuous development of northern Quintana Roo and the sensitivity to pollution of the aquifer, Amigos de Sian Ka´an (N.G.O. who aims at conserving biodiversity for present and future generations) and AGUAKAN (company who supplies drinking water in Cancun) have decided to conduct a hydrogeological study in the north of Quintana Roo in collaboration with the Technical University of Denmark (DTU). The objective of the project is to characterize the hydrological system by means of numerical groundwater flow models in order to support the implementation of an efficient water management strategy to ensure the availability of clean drinking water for present and future generations.

To achieve the general objective of the project, different activities are required:

- Determination of the current level of knowledge on the groundwater system in the Yucatan Peninsula and collection of all the data already available.
- Acquisition of additional data in the northern part of Quintana Roo in order to be able to describe as precisely as possible the aquifer characteristics of the hydrological system in the Peninsula
- Setting up two interconnected numerical models of the aquifer at the scale of the Peninsula and of the northern part of Quintana Roo.
- Delineation of protection zones of the wells that supply the water to the city of Cancun, based on the hydrological models previously elaborated.

In order to achieve the objectives of the project and after an evaluation of the data available on the aquifer, it has been decided to organize a field trip to Yucatan to acquire additional data. Therefore a field campaign has been made from the 15th of March to the end of April 2009 aiming at measuring water table elevations and collecting existing data in the northern part of Quintana Roo.

3. Organization of the report

The report is organized as described below.

Chapter B presents the general characteristics of the Yucatan Peninsula with a special focus on the north-eastern part where the fieldwork has been made.

Chapter C presents the work made during the field campaign in Yucatan. The objectives, strategy as well as the different methods and material used are explained.

Chapter D introduces the different methods used to perform the study. This includes the theoretical background concerning the groundwater flow modeling, the model calibration process, particle tracking technique and basics of the Monte Carlo methods. The different software used in the study are also introduced in this part.

Chapter E contains the explanation of the model implementation. The different data and assumptions used are mentioned as well as how they are implemented in the models.

Chapter F presents the results of the flow simulations in the Yucatan peninsula with a special focus on the north-eastern part. The results of the calibration as well as the maps representing hydraulic heads and flow lines are described and interpreted here. Finally the results of the stochastic well catchment delineation are displayed.

Finally chapter H gives discussions, conclusions and propositions for improved groundwater management in the Yucatan Peninsula.

B. PRESENTATION OF THE PENINSULA

The Yucatan Peninsula is situated in the south eastern part of Mexico. It is delineated by the Gulf of Mexico in the west and north and by the Caribbean Sea in the east. The peninsula is located between 18º and 22º North latitude, and 86º and 91º West longitude.
It comprises the Mexican regional states of Quintana Roo, Yucatan and Campeche, the northern part of Belize and Guatemala. Figure 1 shows the states previously cited and the main cities and roads of the Peninsula.

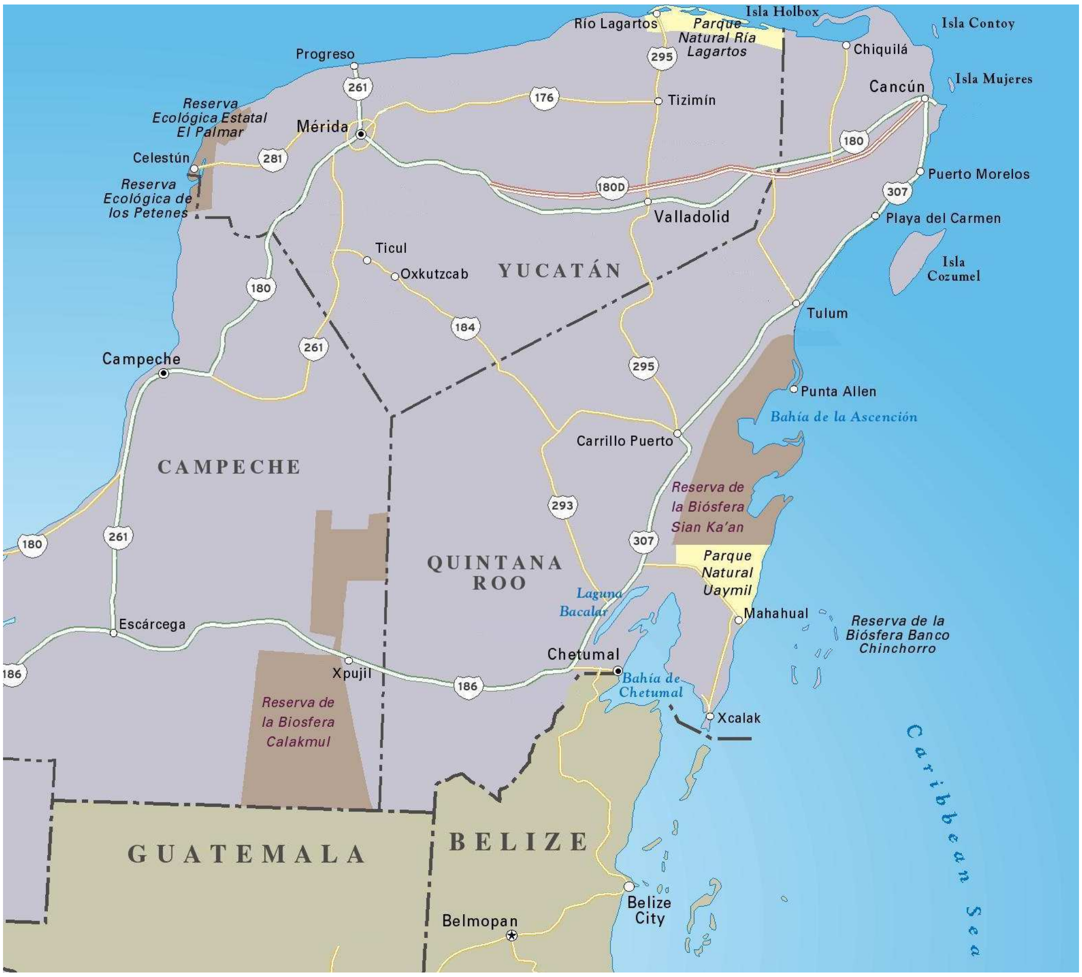

<u>Figure 1:</u> Map of the Yucatan Peninsula (Illustration taken from Moon, 2009)

1. Geology and Topography

1.1.Geological formations

The Yucatan peninsula is a platform composed of marine calcium carbonate deposits ranging in age from the Paleocene up until the Halocene (Butterlin et al., 1963 cited in Villaluso, 2007). Despite the presence of recent deposits (Quaternary deposits) and the reefs still in development in the north and east, it can be considered that the shape of the actual Peninsula was defined after the Miocene (Ward et al., 1985 cited in Schmitter-Soto et al., 2002). Figure 2 represents the different geological formations in the peninsula.

The oldest formations are situated in the southern and central part of the peninsula (Cretaceous, Paleocene and Eocene). The north and east of the peninsula is mainly made of rocks coming from the Mio-Pliocene. Different formations coming from this age have been determined (Formation Bacalar, Carillo Puerto and Estero Franco) (Villaluso, 2007). Next to the coast, recent deposits from the Pleistocene and Halocene can be observed.
The north eastern part of the peninsula consists mainly of Mio-Pliocene with Pleistocene and Ejecta halocene deposits close to the coast.

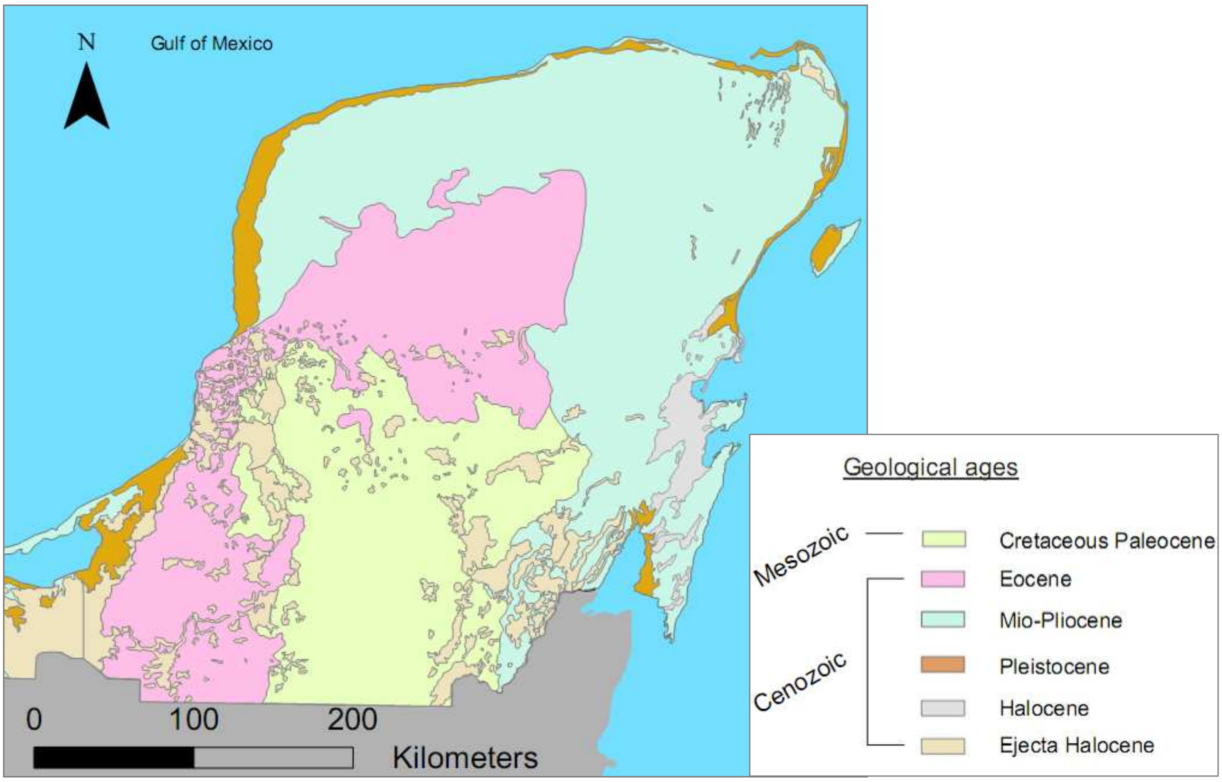

<u>Figure 2:</u> Map of the geological formations (SGM, 2007), the geological ages are classified from the oldest to the youngest.
The dating of the oldest sediments as cretaceous is taken from Schönian et al. (2005), the suggestion the Holocene may be Ejecta is taken from (Perry et al., 2009)

1.2. Main geological features

In the Yucatan peninsula important geological features can be found which affect the hydrology of the peninsula. Four main features can be highlighted: The Holbox fracture zone in the North eastern part, the Sierrita de Ticul fault in the central western part, the Rio Hondo fault in the eastern part (just south from the Holbox zone) and the Ring de Cenotes in the north western part of the peninsula (Perry et al., 2002).

The Holbox fracture zone is a tectonic feature situated in the north eastern part of the Peninsula. It is about 30 km wide and 100 km long. It is composed of large elongated flat bottomed swales (locally called “sabanas”) oriented parallel to the eastern coast (Tulaczik et al., 1993). According to Rosencrantz (1990), the formation of this zone of fractures can be due to Eocene plate movements.
The swales can easily be located on the Landsat images because of the difference in vegetation existing between the swale in itself and the surrounding forest (Tulaczik et al., 1993). Indeed the vegetation observed in the swales is mainly composed of grass and short palms with the presence of wetlands in some of them. These wetlands are believed to be directly related to the groundwater. This particular characteristic of the vegetation in the swales has been observed during the fieldtrip and some pictures showing these observations are available in Appendix 1.
The swales can also be delineated with the topographical map (Figure 3) (especially in the northern part of the Holbox fracture) which shows the difference in elevation between their bottom part and the surrounding ground level.

The Sierrita de Ticul Fault zone is a long escarpment of about 150 km long in the direction northwest-southeast which can be seen in Figure 3. Chemical analyses have demonstrated that this feature carries water from the central part of the peninsula (Lake Chichancanab) and discharges it on the north-western coast (Perry et al., 2002). Nevertheless some other studies considered this feature as a possible low permeability area due to its elevation, the presence of less-permeable strata, and the presence of a normal fault (Gonzalez et al., 2002).

The Rio de Hondo fault zone is situated in the south of the Holbox fracture. There appears to be series of northeast-southwest oriented faults as shown in Figure 3. These faults are believed to be at the origin of the Caribbean coast and of the Island Cozumel (Ward et al., 1985 cited in Schmitter-Soto, 2002). Nevertheless it is only visible on the map in its southern part (around Chetumal and Bacalar).

The Ring of Cenote is a semi circular alignment of sinkholes, overlying the Chicxulub impact structure. The latter is the consequence of a meteorite hit 65 million years ago (Ebbing et al., 2001) and is believed to be the origin of the existence of the Ring de Cenote (Perry et al. 2002). According to Marin (1990), the latter represents a preferential groundwater flow path. Important groundwater springs have been identified at the the intersection between the Ring and the coastline. This Ring de Cenote and more generally the Chicxulub impact structure has, as opposed to the other geological features, been widely studied (among other studies: Marin (1990) Perry et al. (2002, 2008), Pope et al. (1993, 1996), Kinsland et al. (2000), Morgan et al. (1997), Connors et al. (1996)).

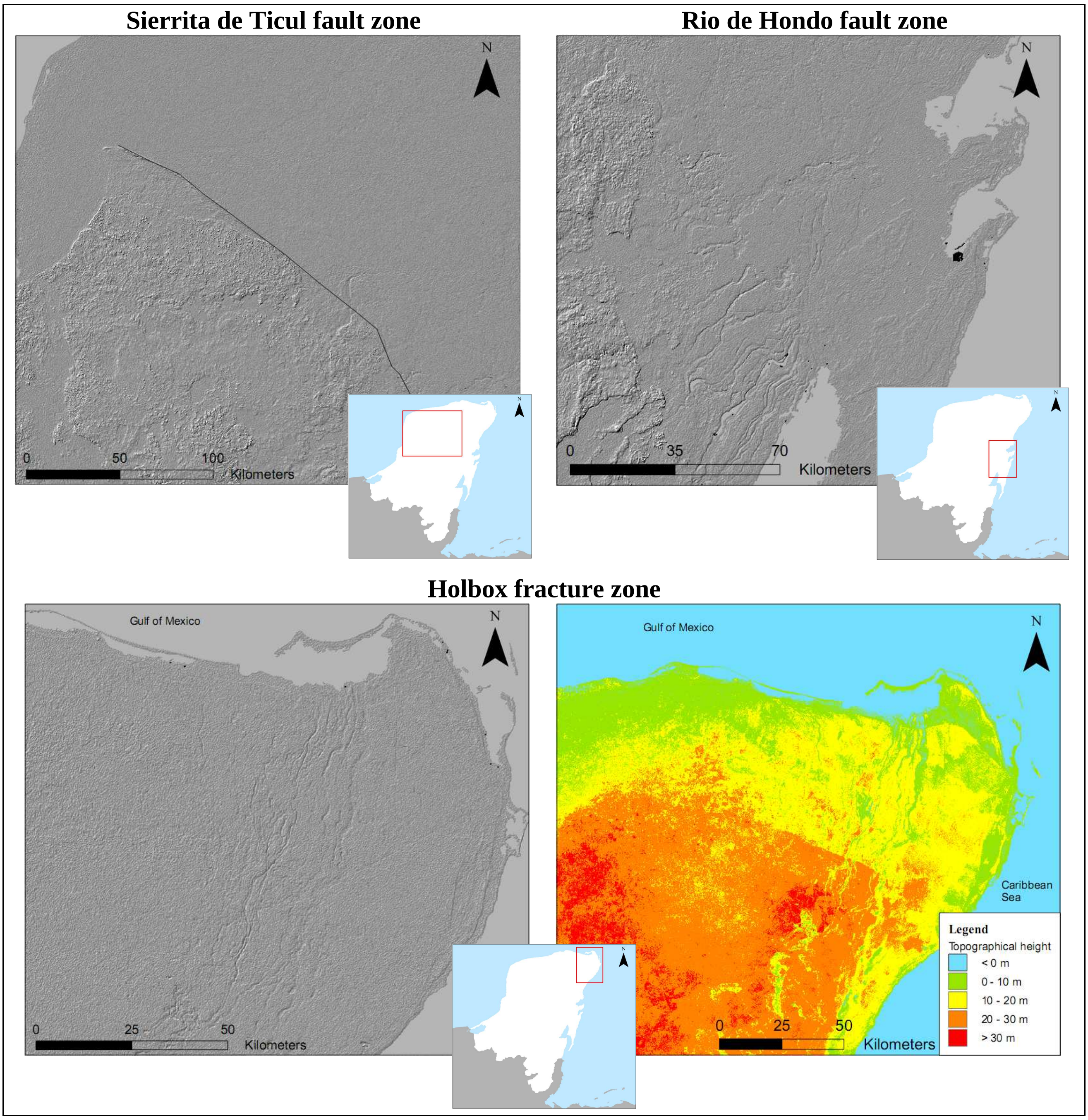

<u>Figure 3:</u> Geological features of the Peninsula displayed from the Shuttle Radar Topography Mission (SRTM) and changed using the "Hillshade" effect in ArcGIS software in the three first pictures (USGS, 2004).

1.3. Topography

The Yucatan peninsula can be considered as a very flat area. The north of the Peninsula presents a ground elevation less than 20 meters above mean sea level (mamsl) in the first 80 km from the coast and less than 40 mamsl 130 km from the coast. The central and southern parts have a significantly higher altitude (up to 300 meters).
Figure 4 highlights the distinct north south separation generated in the topography of the peninsula by the Sierrita de Ticul fault.

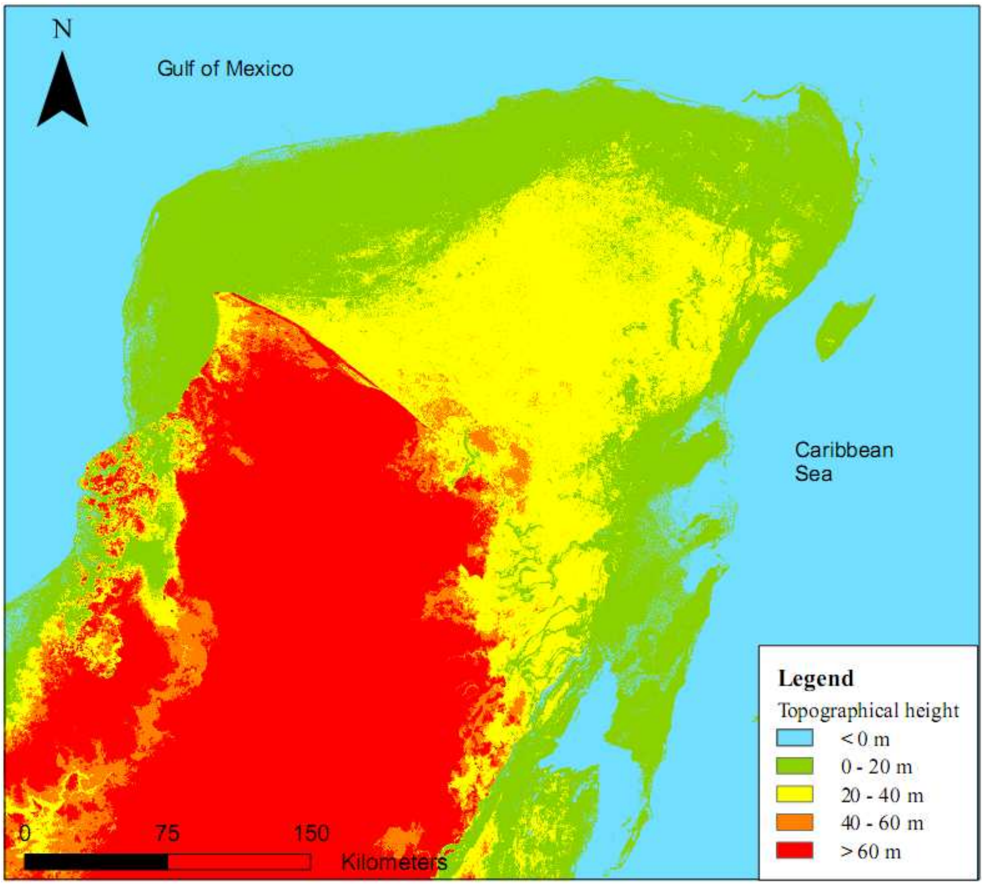

Figure 4: Topographical map of the Yucatan peninsula from SRTM (USGS, 2004)

2. Climate and Vegetation

2.1. Climate

The climate of the Yucatan peninsula can be classified as tropical. Three main seasons can be delineated: warm and dry season (March–May), winter storm season with occasional short showers (November–February), and rainy season (June to October) (Schmitter-Soto, 2002).

The temperatures are not varying much spatially and temporally in the peninsula.
Figure 5 represents the monthly average temperatures in the three cities Campeche, Cancun and Merida (for the period 1990-2005).

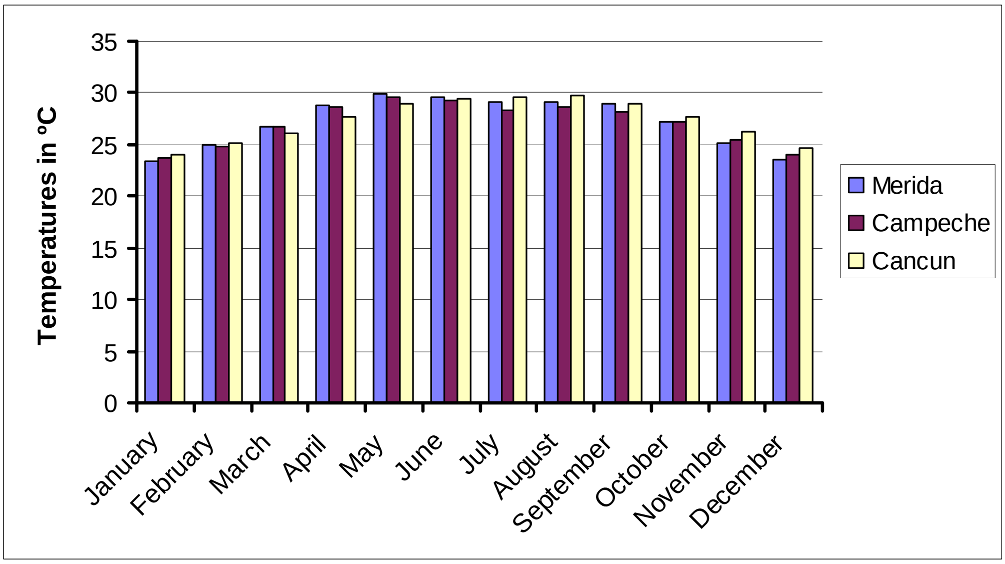

Figure 5: Average monthly temperatures during the period 1991-2005 for the cities of Campeche, Cancun and Merida (CNA, 2008)

Precipitation in the peninsula ranges from 1.5 mm/day (550 mm/year) to 4.5 mm/day (1650 mm/year). The precipitation pattern presents a high seasonal variability (Figure 6) and also important spatial differences in the peninsula (Figure 7). The north-western part is the driest region with a precipitation rate of about 550 mm/year while the southern part is the wettest one.

The Yucatan peninsula is highly affected by tropical hurricanes. Winds that can reach a speed of 250km/h combined with very high precipitation cause considerable damages. The recent hurricane Wilma (2005) is the worst example of these storms. The maximum precipitation recorded was in Isla Mujeres (off the Cancun's coast) with a total rainfall of 1600 mm (CNA, 2008) which represents more than the yearly average precipitation. These storms lead to very important variations in water table levels as the rain percolates very fast in the karstic aquifer.

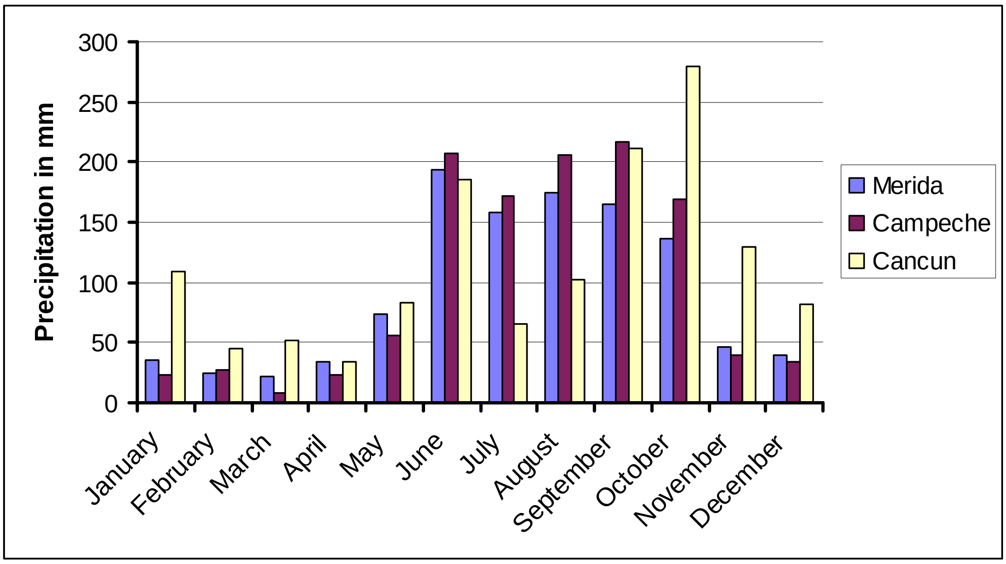

Figure 6: Average monthly precipitation during the period 1991-2005 for the cities of Campeche, Cancun and Merida (CNA, 2008)

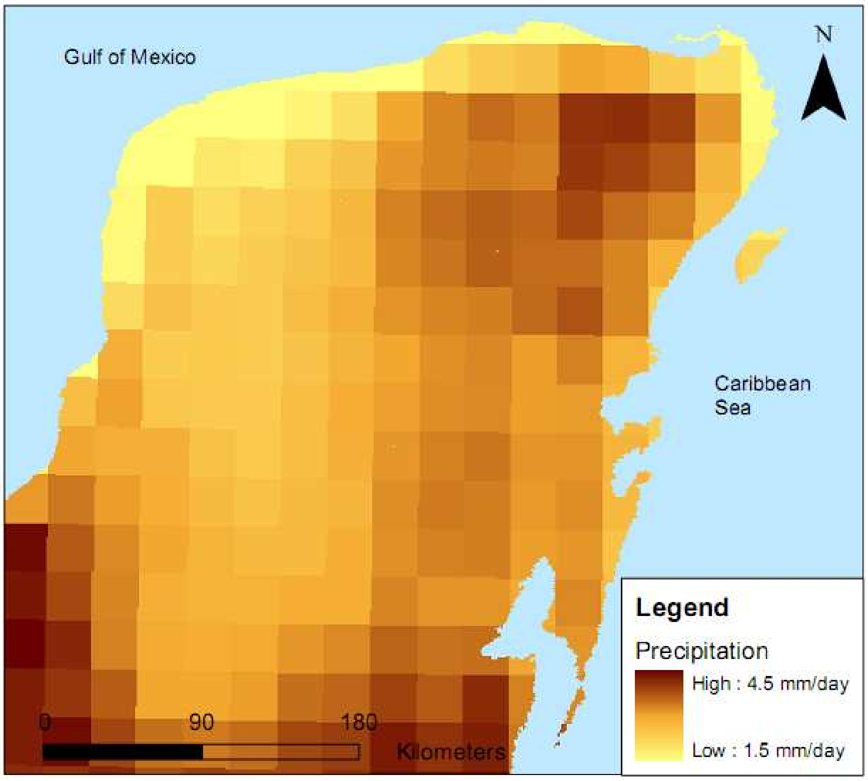

Figure 7: Spatial distribution of average annual precipitation on the Peninsula (mm/year). Yearly average (1998-2008) made from the TRMM 3B43 product, adjusted to ground trusting estimates using a method similar to Wolff et al. 2005.

The evapotranspiration has been evaluated in different studies and ranges from 40% to 95% of the annual precipitation (Schmitter-Soto, 2002, Anonymous 1983 cited in Gonzalez et al., 2002, Beddows, 2004).
Therefore the actual recharge rate is very uncertain, ranging from 5% to 60% of the precipitation. This uncertainty in the recharge determination represents one of the main uncertainties when studying the hydrology of the Yucatan Peninsula. More details about how evapotranspiration and recharge have been determined in this study will be given in chapter D.3.2 (page 35).

2.2. Vegetation

The vegetation changes throughout the peninsula due mainly to the changes in humidity which is gradually decreasing from the southeast to the northwest, following the precipitation gradient (Rzedowski, 2006).

5 main different vegetation types can be identified in the Yucatan Peninsula and will be briefly described here:

- High perennial forest: Situated in the most inland part and in the southern part of the peninsula (wettest areas), high perennial forests are characterized by an important vegetation density. Vegetation height can be higher than 30 m with trunks usually straight.

- Semi deciduous forest: Dominant vegetation in the Yucatan Peninsula, it is characterized by a vegetation height between 15 and 30 m, and presents both species loosing leaves in the dry season and species remaining green throughout the year. A classification of the semi-deciduous forests can be made using the relative percentage of species loosing their leaves in the dry season (Neuman et al., 2006).

- Dry forest: They are observed only in the north-western part of the peninsula and constitute an isolated dry vegetation system surrounded by semi deciduous forests and sea. It is mainly made of thorn scrub and cacti (Valero, no year).

- Low forests and savanna: Situated mainly in the flooded or semi flooded areas they constitute regions with low vegetation density, usually young vegetation. They are particularly observed in the northern part of Quintana Roo.

- Aquatic and sub aquatic vegetation: Situated in the coastal regions or zones with fresh or brackich water, they are composed of popal, tular and mangrove swamps.

Pictures showing some types of vegetation seen during the field work are displayed in Figure 8.
These vegetation patterns have been widely modified by human activities in almost the entire part of the peninsula. The ancestral Mayan slash and burn agriculture is still used and causes important forest fires.

Figure 8: *Pictures of vegetation patterns: Semi deciduous forests (left), savanna (upper right picture), sub aquatic vegetation (lower right picture)*

3. Surface water

Very few surface water bodies can be identified in the Yucatan Peninsula due to the very high permeability of the limestone.
Lakes are present in the center and southern part of the peninsula. 12 lakes with water volumes higher than 50,000 m^3 exist (Doehring et al., 1974; Alcocer et al., 1996). Surface rivers are inexistent in the northern half of the peninsula and very few can be seen in the southern part. The Rio Hondo situated in the south of Chetumal is the largest river in the peninsula.

Contrarily to rivers and lakes, wetlands are present in large areas along the coast. Many of them are completely dry until the beginning of the rainy season but some remain wet throughout the year. They usually constitute very diverse ecosystem and represent in some parts a complex mix of freshwater, brackish water and salt water.

Finally the specificities of the karstic aquifer lead to the existence of numerous open sinkholes (called "Cenote") in the peninsula. Many of them are located in the northern part and have represented for a long time a very important drinking water source for the population. They are now considered as major touristic attractions.
However it should not be forgotten that they are in direct contact with the aquifer and represent a high potential of contamination for the groundwater.

4. Groundwater

The Yucatan aquifer can be considered as a young karstic aquifer (Villaluso et al., 2000). A succinct description of karstic aquifers has to be made first in order to understand specificities of such aquifers.

4.1. Characteristics of karstic aquifers

Karstic aquifers present high heterogeneities that occur over a range of scales. These heterogeneities are due to the properties of the carbonate rocks which can be chemically dissolved in the water (Ford & Williams, 2007).

The karstified medium is basically composed of a rock matrix (primary porosity), a network of fractures or fissures (secondary porosity) and a network of conduits (tertiary porosity). The difference between fractures and conduits is based on the size of the openings (0.1 mm to 10 mm for the fissures, 10mm to 100 mm or more for the conduits) (White, 2002).
It has to be noted that the concept of primary, secondary and tertiary porosity as it has been defined previously is used by hydrogeologists, while sedimentologists use primary porosity when it has been formed during the deposition and, secondary porosity for porosity formed after the deposition (Ford & Williams, 2007).

Due to the high porosity of the karstic aquifers, the precipitation infiltrates rapidly and the water table elevations vary between rainy and dry seasons (Milanovic, 2004).

The groundwater in a karst medium flows in three different zones. The dry zone is characterized with an abundance of dry channels and caves. The rain water percolates in this zone and the water flow is essentially vertical. The flows in the second zone (transition zone) are also mainly vertical. However during rain periods the vertical water flow can be slowed down or stopped leading to the apparition of horizontal flows. Finally the saturated zone is characterized mainly by horizontal flows occurring in the rock matrix and in the fractures and conduits (Milanovic, 2004). These horizontal flows can be considered as Darcian flows in fractures (aperture < 10mm) and turbulent flows in conduits (White, 2002).
The delineation of these zones is not fixed as the karstified medium is in rapid evolution throughout the years (rapid in the geological time scale; in water resources management the aquifers are studied as they exist today).

In the case of coastal karstic aquifers, it is also interesting to highlight the presence of submarine springs. These freshwater flows are visible at the surface as they create remarkable circular areas in the sea water. These submarine springs can even be used for water supply uses in certain cases (Fleury et al., 2007).

4.2. *The Yucatan aquifer*

The Yucatan aquifer is made of a thin freshwater lens floating above saline water. Indeed saltwater intrusion is observed in this aquifer, meaning that there is sea water moving inland. The interface between freshwater and saltwater is called the halocline and can be observed when diving into sufficiently deep sinkholes (Beddows, 2007). This interface is in reality a thin mixing zone. The thickness of it can be considered as small, in comparison with the thickness of the freshwater lens (Beddows, 2004). Further details concerning the interaction between freshwater and saltwater can be found in the chapter D.2 (page 29).

In the northern half of the Peninsula the aquifer top is situated very close to the topographical surface. Water table elevations have been reported to be less than 4m above mean sea level in the northern half (Perry et al., 2002).

Few studies have determined values of hydraulic gradients in the Yucatan Peninsula. These values are very low but are also very different depending on the area where they have been found (7-10 mm/km in the north-western part (Marin, 1990); 20mm/km (Back 1970); and 58mm/km in the eastern part (Beddows, 2003)).

The aquifer can be considered as unconfined except for a narrow band close to the coast (Perry et al., 1989). In addition to the regional aquifer, perched aquifer situated few meters below ground surface can be found in the central elevated part of the Peninsula.

Different studies on the Yucatan aquifer have tried to give estimates of the porosity of the limestone. Values found are ranging between 7% and 41 % in the area of Merida (Gonzalez Herrera, 1984, cited in Steinich et al., 1997), and from 14% to 23% (Harris, 1984, cited in Smart et al. 2006). Nevertheless the spatial variation of porosity (horizontal and vertical) does not allow to get a clear determination of this parameter.

The presence of underground caves has been studied especially in the Caribbean part of the peninsula. In this region Worthington (2000), cited in Beddows (2004), has established that even if the bulk rock matrix represents 96.6% of the water storage, more than 99% of the flows are occurring in conduits. Many caves have been explored and mapped in this area, especially for those close to the coast. More details about these caves can be found in the literature (Neuman et al., 2006; Beddows, 2004; Smart et al., 2006).

Studies have also determined values of hydraulic conductivities in the peninsula. Nevertheless these values depend highly on their locations and methods of determination.

Table 1 displays the different values found for the hydraulic conductivity in the Yucatan aquifer.

Table 1: Horizontal hydraulic conductivities found in the literature

Values of Hydraulic conductivities	Methods used	Area of definition	Reference
K= 0.10 m/s K=1 m/s (high permeability zone)	Numerical modeling	North-western Yucatan	Marin 1990
$K=3.10^{-4} - 5.10^{-2}$ m/s	Experimental determination	North of Merida	Reeve & Perry 1990
1. 10-6 - 5. 10-3 m/s	Laboratory experiments	Merida	Gonzalez-Herrera 1984 (cited in Gonzalez-Herrera 2002)
K=0.55 m/s	Numerical modeling	North-western Yucatan	Gonzalez-Herrera et al. 2002
K= 0.15m/s K= 6m/s (high permeability zone)	Numerical modeling	North-western Yucatan	Gonzalez-Herrera et al. 2002
K=1.115 K=0.0055 m/s (low permeability zone)	Numerical modeling	North-western Yucatan	Gonzalez-Herrera et al. 2002
K=0.19 m/s - 0.65 m/s	Calculated	Playa del Carmen	Moore et al. 1992
K= 0.064 m/s	Used in mathematical model	Merida	Mendez Ramos 1991
$K= 9.10^{-4} – 1.10^{-2}$	Calculated	Merida	Andrade briceno, 1984 (cited in Gonzalez-Herrera et al. 2002)

5. Anthropogenic use

The Yucatan Peninsula has been occupied in the past by the Maya civilization until the ninth century (Curtis, 1998). Numerous archeological sites give evidence of this presence.

Today the population in the three Mexican states of the Yucatan peninsula is 1,130,000 for the state of Quintana Roo, 750,000 for the state of Campeche and 1,820,000 for the state of Yucatan (INEGI, 2005). The three states are among the least populated states in

Mexico. The respective population densities are 22.5 hab/km2, 14.8 hab/km2 and 47.4 hab/km2.
The three major cities of the Yucatan peninsula are the three capitals of the states Quintana Roo, Yucatan and Campeche (Cancun (580,000 inhabitants), Merida (735,000 inhabitants) and Campeche (240,000 inhabitants) respectively) and represent an important part of the population of the three states. The Yucatan peninsula can be considered as urban area even if agriculture represents still in certain parts of the peninsula an important economic sector (INEGI, 2005).

The population density is low but the development of tourism in the Peninsula, which began 30 years ago as a part of a national development plan, has led to extremely high increase of the population and the number of inhabitants continues to increase (especially in the state of Quintana Roo where the tourism is developing the fastest). For example there was between 2000 and 2005 a 10% increase in population in the states of Campeche and Yucatan and a 30% increase in the state of Quintana Roo (INEGI, 2005).

This population growth puts a high pressure on the ecosystems, in terms of pollution and resource consumption or destruction. Only less than 50% of the waste water is treated in the state of Quintana Roo (ASK, 2003) and numerous landfills, that can eventually provoke leaching of pollutants to the soil, are developed near the important cities.

6. Water resources management problems

As it has been seen in this chapter, efficient groundwater management plans have to be set up in order to ensure availability of clean freshwater in the Peninsula and to protect the diverse ecosystems. Different groundwater flow studies have already been made (especially in the north-western part and eastern part). Nevertheless the studies have always focused on one part of the Peninsula and have not tried yet to determine an overall hydraulic head and groundwater flow pattern in the entire peninsula.

At this stage of knowledge, the only flow map of the entire peninsula has been made in a workshop organized by Amigos de Siaan Ka´an in 2003. Figure 9 displays this groundwater flow pattern map.

This map highlights the fact that the different groundwater flows in the different regions of the Peninsula are strongly interconnected. The high permeability features lead to the existence of flows travelling long distances. Therefore when implementing water management plans the overall flow pattern of the peninsula should be considered.

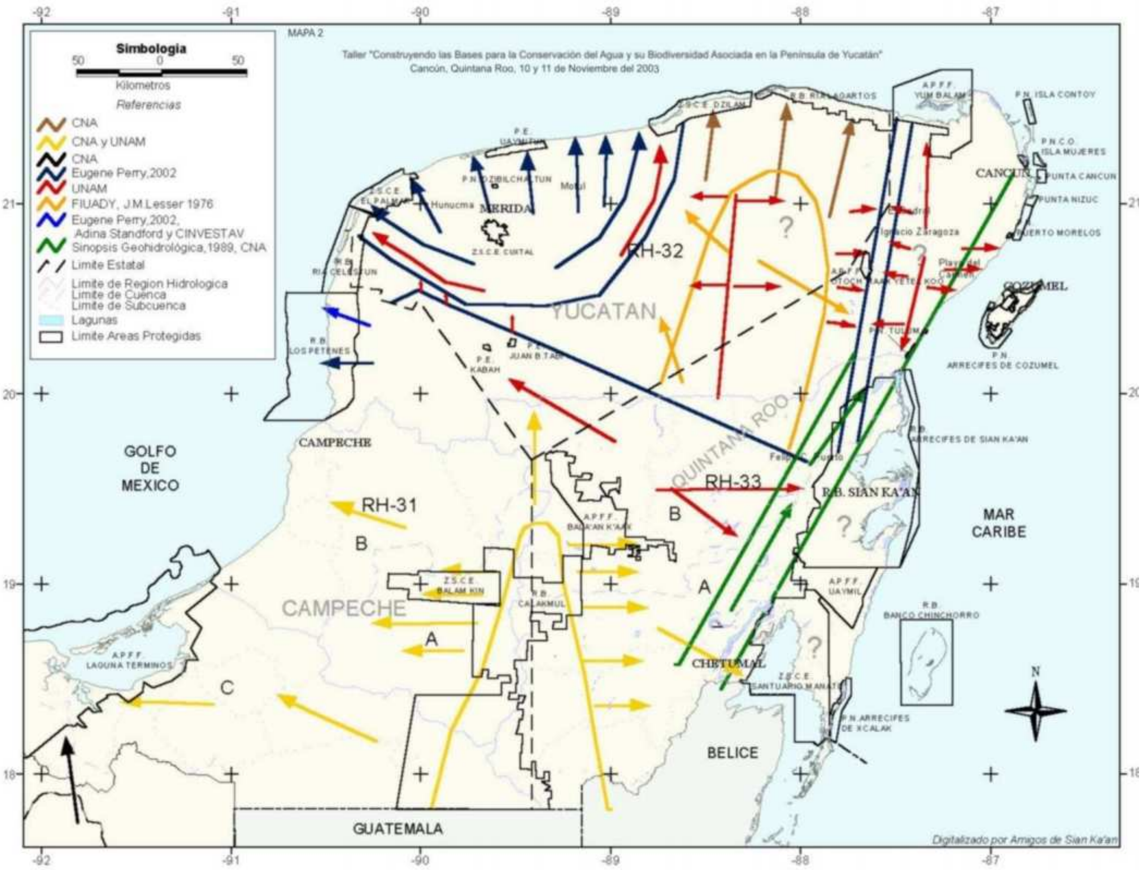

<u>Figure 9:</u> Groundwater flow pattern in the Peninsula (ASK, 2003)

In the north-eastern part, the development of Cancun and the other coastal cities is putting an important pressure on the aquifer. AGUAKAN should ensure availability of clean water in Cancun's pumping areas. This need requires the implementation of an efficient well field management plan.

Two main factors should be considered: the amount of water that can be extracted without threatening the water resources and the prevention of presence of pollutant in the pumped water. In order to ensure good quality of extracted water, the common management solution is to delineate well protection zones, areas where land use and activities are restricted. Basically, if pollution occurs in these areas (for example industrial accidental leakages, leakages from landfills, or agricultural contamination), the travel time of the contaminants between its source and the well will not be long enough for the contaminant to be degraded. In the case of aquifers with sea water intrusion (Yucatan aquifer for example) the possibility of saltwater encroachment has also to be studied.

In addition to the pumping wells, it is important to notice the presence of natural reserves in the north of Quintana Roo (in particular reserves El Eden and Yum Balam). These reserves that are containing large wetlands should also be included in water management plans as the loads of pollutants can have lead to considerable damages for the diversified ecosystems of these areas.

C. FIELD WORK

1. Field work strategy

1.1. Objectives and strategy of the Fieldwork

Studies on the Yucatan aquifer have focused mainly on two areas of interests.
The north-western zone of the peninsula (zone called Chicxulub impact area) has concentrated most of the groundwater studies in the Yucatan Peninsula (among other studies: Marin (1990), Perry (2002, 2008), Pope et al. (1993, 1996), Kinsland et al. (2000), Morgan et al. (1997), Connors et al. (1996)).
The eastern part comprising the Sian Kaan biosphere and numerous underground caves has also been the subject of groundwater studies and caves exploration (Neuman et al., 2006, Beddows 2003, 2004, 2007).

On the contrary the north-eastern zone of the Peninsula has received little attention, especially the inland parts of this area. Nevertheless some hydrological studies have been made (Tulaczik et al. 1993, Southworth 1985 cited in Tulaczik, 1993, Villaluso 2007).

In order to implement effective groundwater management plans, a comprehensive characterization of the hydrology in this region should be made. Therefore it has been decided to include a fieldwork period (15^{th} March 2009 – 30^{th} of April 2009) in order to collect sufficient data to purchase a study of the aquifer in this north-eastern region.

The fieldwork had basically two main objectives: collection of existing data or information available and field measurements in order to acquire water table elevations data for the calibration of the numerical models.

1.2. Location of the measurements

The locations of the measurements have been determined taking into consideration 4 main factors:

- Accessibility of the area: Contrarily to other parts of the peninsula the north-eastern region is sparse populated. Rural activities are not well developed. Therefore the accessibility in large parts of the north-eastern Yucatan is a major constraint when doing field investigations. Moreover roads are not well mapped, and thus no way out roads and bad shapes roads are common. Figure 10 highlights the fact that important parts in the Holbox fracture are not deserved by roads.

- Locations of the data already available: The measurements have been made in an area where no exploitable data were available. Therefore the southern boundary of the Fieldwork area (Figure 10) coincides with the northern boundary of the study area of Neuman et al. (2006), where water table elevation and saltwater elevation data are available.

- <u>Location of the wells and Cenotes:</u> The measurements were made in wells and sinkholes in the area. The wells where the measurements were done were mainly situated in villages or ranches. In the first case the wells were old dug wells constructed to get water in the villages before the introduction of running water. Unfortunately in some parts of the area these non used wells were dry and places with access to groundwater were not easy to find. Many sinkholes are present in the area but in many cases the dense vegetation around these sinkholes does not allow a clear view to the sky and so does not permit GPS measurements.

- <u>Capture zones of Cancun's wells:</u> A preliminary basic model made before the fieldtrip has shown the potential influence of the Holbox fracture on the groundwater flow pattern of the area. Therefore it has been chosen to include entirely this high permeability feature in the fieldwork area in order to get sufficient data coverage in the wellhead catchment zones.

Based on these four main factors a fieldwork area has been delineated before the trip. It has been tried during the field campaign to scatter measurements in order to get the best possible repartition of measurement locations over the entire area.
Figure 10 shows the fieldwork area as it was delineated before the field trip. The measurements made during the fieldwork are also displayed.

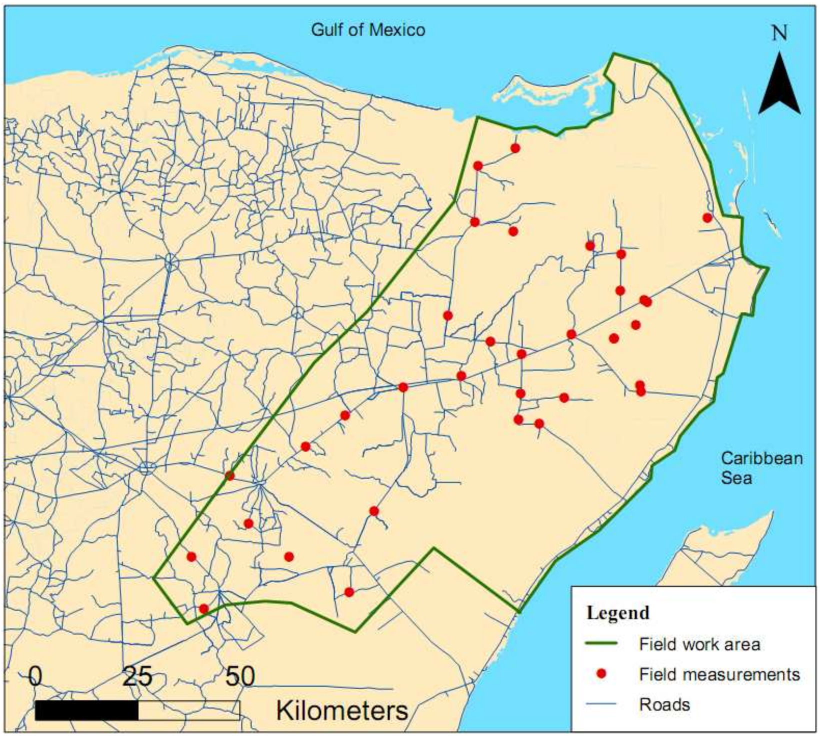

<u>Figure 10:</u> Map of the initial field measurements area delineation

1.3. <u>Method for the measurements</u>

The measurements made during the trip were conducted in order to get indications on the shape of the water table in the study area. 34 wells or cenotes were measured in the north of Quintana Roo. The method for measuring water table elevations used can be described in 3 main stages. First the static carrier phase GPS method has been used to obtain accurate topographical heights. Then leveling was performed to determine the height difference between the position of the GPS antenna and the well, or cenote. Finally the water table elevation was measured by means of an electronic dipper.
Figure 11 presents a sketch explaining the different steps of the measurement method.

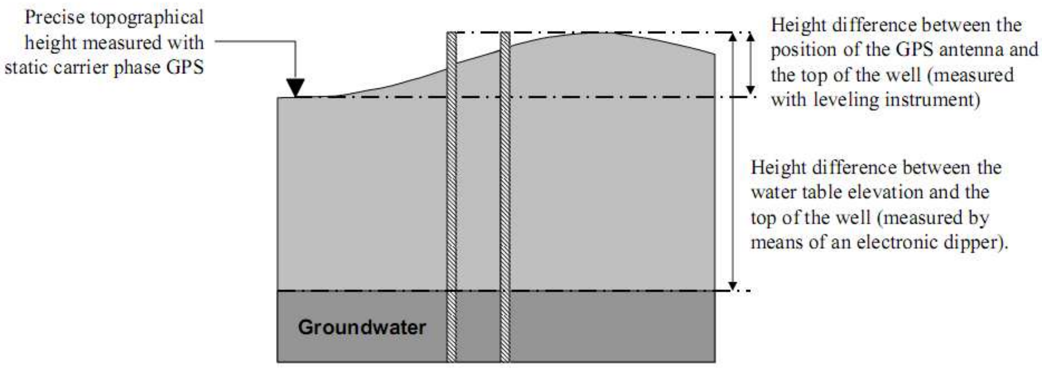

<u>Figure 11:</u> Water table elevation measurement method

2. GPS measurements

2.1. <u>Basic concept of GPS</u>

The Global Positioning System (GPS) is a method to obtain coordinates of locations on the surface of the planet. The system is fully operational since 1995 and comprises between 24 and 32 satellites in orbit around the earth, 4 monitoring stations on Earth and the GPS receivers (Hatzopoulos, 2008). GPS is a method now used in a wide range of fields: scientific uses, map-making, land surveying, surveillance etc…

The coordinates of the GPS receiver are determined by calculating the distance between a receiver placed on the planet surface and a satellite, sending continuously messages, in orbit around the earth. The positions of the satellites around the planet are known precisely with the ephemeresis files downloadable on internet (IGS, 2009). The messages are transmitted from the satellite to the receiver using two carrier waves: L1= 1575.42 MHz and L2= 1227.60 MHz (Hatzopoulos, 2008).

Basically knowing the sending time of the message coming from the satellite (t_1) and the reception time of the message in the receiver, the range between the satellite and the GPS receiver can be computed using the simple equation defining the speed of light in vacuum (Equation C.2.1) (Soon et al., 2008).

$$\rho = c \cdot (t_2 - t_1) \qquad \textbf{Equation C.2.1}$$

<u>*Where:*</u> *t_1 is the sending time of the message (T)*
t_2 is the reception time of the message (T)
c is the speed of the light ($L \cdot T^{-1}$)
ρ is the range from the satellite to the receiver (L)

The coordinates of the receiver can be included in the equation C.2.1 leading to the establishment of equation C.2.2 which shows the necessity of having ranges from three different satellites to solve the equation. Indeed the range p defines a spherical surface, centered in O(x_1, y_1, z_1) (satellite position), comprising the location of the GPS receiver. Three spherical surfaces are needed to determine one single point. (In fact the intersection of three spherical surfaces determines two points, and then the closest point to the earth surface is taken as the coordinate of the receiver).

$$\rho = \sqrt{(x_1 - x)^2 + (y_1 - y)^2 + (z_1 - z)^2} \qquad \textbf{Equation C.2.2}$$

<u>*Where:*</u> *ρ is the range from the satellite to the receiver (L)*
(x,y,z) are the coordinates of the receiver (L)
(x_1,y_1,z_1) are the coordinates of the satellite (L)

This simple calculation is done without taking into considerations the errors. The errors come principally from five different sources: the satellite clock error, the receiver clock error, the ionospheric delay, the tropospheric delay and the errors related to the position of the satellite (ephemeresis) (Farrell et al., 1999). The integration of these errors requires the introduction of the pseudo range (ρ) and the true range (true geometric distance between the satellite and the receiver), defined by the equation C.2.3. It has to be noted that another factor representing the other minor errors is sometimes included in this equation (receiver noise error and multipath error in particular) (Farrell et al., 1999).

$$\rho = r + cdT_k - cdt^p - d\rho^p + d_{ion} - d_{trop} = c \cdot (t_2 - t_1) \qquad \textbf{Equation C.2.3}$$

<u>*Where:*</u> *t_1 is the sending time of the message (T)*
t_2 is the reception time of the message (T)
c is the speed of the light ($T \cdot L^{-1}$)
ρ is the true range from the satellite to the receiver (L)
r is the pseudo range from the satellite to the receiver (L)
dT_k is receiver clock error (T)
dt^p is the satellite clock error (T)
d_{ion} represents the ionospheric delay (L)
d_{trop} represents the tropospheric delay (L)
$d\rho^p$ represents the error on the satellite orbit (L)

The single GPS method does not allow to get sufficient accuracies in the coordinates determination, especially for the vertical coordinates that are less precise than the horizontal coordinates (due to geometrical configurations). In the case of water table elevation, and especially in the case of shallow aquifers, a clear determination of the water table elevation is required.
Therefore methods called differential GPS positioning were used to get satisfactory accuracies.

2.2. Differential GPS positioning

2.2.1. General presentation

Methods have been designed for land surveying in order to minimize the different errors; these methods are called differential GPS methods (DGPS).

Differential positioning requires at least two receivers placed in two different locations. One of the receivers is placed at a location where the coordinates are well known. It is called “base station”. The other is placed at a location with unknown coordinates and is called “rover”. The two receivers are measuring at the same time from the same satellites. This DGPS technique allows better accuracies by minimizing the errors described in chapter C.2.1.
Indeed the base station will basically evaluate the different errors by comparing the calculated coordinates with the real coordinates (known). The base station will transmit these errors to the rover which will use these errors estimates for the calculation of the coordinates of the unknown location.

Two different techniques of DGPS are available: the code phase tracking method and the carrier phase tracking method. The method of the code phase tracking will not be explained here as it has not be used in the fieldwork but details on this method can be found in the work of Guochang Xu (2003).

2.2.2. Static carrier phase GPS

The most accurate DGPS method developed is the static carrier phase GPS method. The carrier phase method measures the difference between the phases of the receiver carrier signal and the satellite carrier signal. The accuracy is therefore high as the wave lengths are short (19 cm for L1 and 24 cm for L2). The receivers are able to compute differences in phase in the order of 2 mm (Gopi, 2005). When doing carrier phase GPS measurements an ambiguity factor (N), representing the number of waves between the satellite and the receiver has to be included.It can not been measured directly by the receiver (every phases of the signal are identical). N remains constant after time, as long as the signal is not lost. Indeed the receiver is able to keep track of the phase changes (El-Rabbany, 2002).

The fundamental equation for carrier phase GPS is described in equation C.2.4 with the same notations than in equation C.2.3 (modified from Guochang Xu, 2007):

$$\lambda \cdot \varphi = \rho - \lambda \cdot N - c\ dT_k + cdt^p + d\rho^p - d_{ion} + d_{trop} \qquad \textbf{Equation C.2.4}$$

<u>*Where:*</u> *φ represents the measured phase*
λ represents the wavelength (L)
N represents the ambiguity factor

As it can be seen in the previous equation, the errors in carrier phase GPS are of the same nature than those described in Chapter C.2.1. Nevertheless one additional error called "cycle slip" can occur. This error occurs when one receiver loses the signal, resulting in a discontinuity in the integer number of cycles. This can lead to a degradation of the positioning results (ASCE, 2000).

Different processing techniques using the presence of the two receivers are used to eliminate some of the errors. Figure 12 presents the concepts of these methods.

First the satellite clock time error is eliminated by doing a single differencing. In practice the two receivers are receiving the signals from the same satellite, so with the same satellite clock error. Therefore a simple difference between the two received signals will give the satellite clock error (Hatzopoulos, 2008).

Then a double differencing which is in fact a difference between two single differences allows to eliminate the receiver clock error. The factor representing the receiver clock error is present in both single differences and so is eliminated by doing the double difference (Hatzopoulos, 2008).

Finally a triple differencing can be made. It is in fact the difference between double differences taken at different moment in time. This leads to the elimination of the ambiguity parameters as they stay constant through the time. This triple differencing is also used to identify possible cycle slips occurring during the measurements as a cycle slip will affect only one triple difference (Hatzopoulos, 2008).

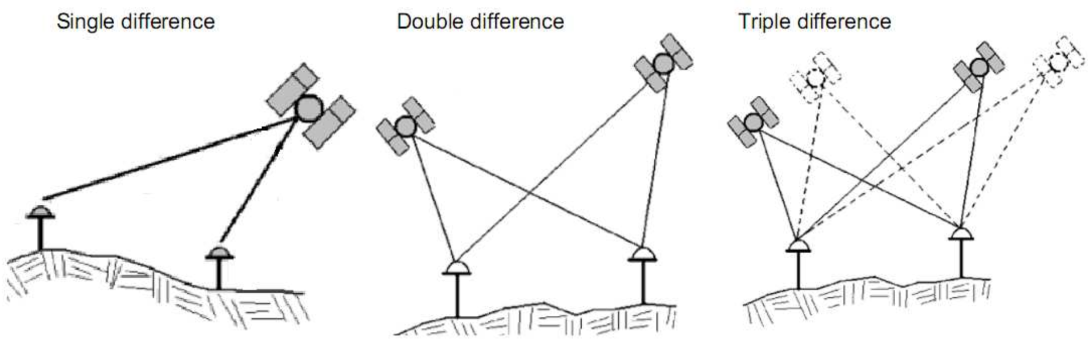

<u>*Figure 12:*</u> *Single, double and triple differencing methods (modified from Hatzopoulos, 2008)*

Different methods are used to perform carrier phase center: static, rapid static, kinematic, stop and go kinematic and pseudo kinematic. The most used and most accurate method is the static one and has been used during the field trip. Long observation time (60-120 minutes) to resolve the phase ambiguity is needed. The other techniques require less time but are providing smaller accuracies (ASCE, 2000).

The accuracy of static carrier phase GPS is dependant and many factors (among others: the type of the antenna, the length of the baseline, the measurement time and the specific measurement method are playing important roles). Nevertheless a general rule to determine the accuracy of these kinds of measurements can be established and is presented in Table 2.

Table 2: Accuracy of carrier phase GPS (Dueholm et al., 2005 cited in Neuman, 2007)

	Base error (mm)	**Distance dependant error (mm/km)**
Single frequency	3	0.8
Dual frequency	2	0.1

The main limitations of the static carrier phase center GPS are the time taken for one measurement (between 60 and 120 minutes minimum) and the need to place the GPS antenna in a location where the view to the sky is clear. This leads to major issues, particularly when measuring in forests or in cities where the view to the sky is obstructed.

2.3. Material used during the field trip

During the field work two antennas (Trimble® Zephir Geodetic) have been available and used as rovers. These antennas were moved at different locations during the day and were measuring at least 90 to 120 minutes in each of the locations. This method permitted to perform 3-4 measurements during a day.
The antennas were connected to two Trimble® 4700 GPS receivers and started with a Trimble® controller. A permanent GPS antenna (Trimble® Zephir Geodetic), placed in the CICY (Centro de Investigación Científica de Yucatan) in Cancun, has been used as the master.

The maximum baseline length among all the measurements was 150 km. With this maximum distance between the base station and the receiver, it can be assumed that the errors are less than 2cm according to the Table 2.
The data stored in the receivers were transferred every day to a laptop using the software Trimble® Data Transfer (Trimble® Navigation Limited, 1999-2007) in order to prevent any data loss.

Figure 13: Picture of one of the GPS measurements

2.4. Data processing

The GPS raw data have been processed using the software Trimble Total Control, Version 2.70 (Trimble® Navigation Limited, 2001). The data measured by the rovers antenna and the permanent GPS station in Cancun have been imported together with the precise ephemeresis (downloaded from IGS, 2009) (GPS week 1526, 1527, 1528 and 1529).

The software Trimble total control is a survey gps processing software which is able to compute the baselines, and so to determine the coordinates of a location from raw GPS data. It basically solves the equations presented in the chapter C.2.2.2.
In the processing process the coordinate system UTM, zone 16 N, was use with the WGS1984 reference system. The WGS1984 is the geodetic system associated to the GPS. The processing mode was set to static as it is the method that has been chosen. The mask angle has been set to 15 º. This parameter refers to an angle under which the satellites are not considered even if they are present. This setting will allow to lower some errors (especially high tropospheric errors).

The Niell mapping function (Niell, 1996) has been chosen for the tropospheric model. This model is used to evaluate and eliminate the tropospheric error which was mentioned previously.

3. Water table measurement and leveling

The leveling was performed using the geometric method between the antenna benchmark (point where the topographical height was measured with the GPS antenna) and the point from where the water depth has been read (usually the top of the well's casing). The leveling was made two times in opposite directions in order to minimize the reading errors. Those errors can be considered smaller than 5mm based on standard deviation calculations.

The water table level was obtained by means of an electronic dipper. This instrument is basically a measuring tape with an electronic lead at its end that produces a sound when it hits the water. Figure 14 shows a picture of the material used. The measurements were made three times at each location to reduce the reading errors. Based on calculations of standard deviations the maximum reading error can be considered smaller than 5 mm.

Figure 14: Picture of leveling (left) and water level measurements (right)

D. MODELING METHODS

1. Modeling of karst aquifers

The presence of triple porosity in karstic aquifers as described in chapter B.4.1 (page 13) leads to the coexistence of two main kinds of models for groundwater flow in karstified medium: the dual flow model and the equivalent porous medium model.

1.1. The dual flow model

The dual flow model, also called conduit-matrix model has been implemented in different studies (Neuman et al., 2006; Cornaton et al., 2002; Cheng 2005; Atkinson, 1977; Worthington, 1993)

The basic concept of this model is to assume that the fractured rock is made of a porous medium in constant hydraulic interaction with conduits. In these models the primary porosity (bulk rocks matrix) and the secondary porosity (fissures) are represented in the matrix continuum. The flows in the tertiary porosity (channels) are represented by flows occurring in conduits.
Figure 15 presents an outline of the flow system in a dual flow model.

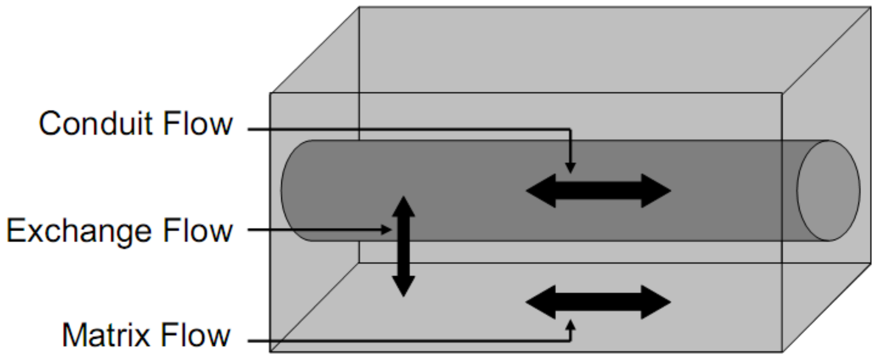

Figure 15: Outline of the dual flow model

The flows occurring in the porous medium are laminar flow and are following the Darcy´s law (Equation D.1.1) (Ford & Williams, 2007). In laminar flows molecules of water are following streamlines.

$$q = -K \cdot \frac{dh}{dl}$$ **Equation D.1.1**

Where: *q is the specific discharge* ($L \cdot T^{-1}$)
K is the hydraulic conductivity ($L \cdot T^{-1}$)
dh/dl is the hydraulic gradient

The flows in the conduits have been modeled in the studies either as laminar flows or turbulent flows. The Reynolds number determines the flow regime occurring in pipes (Ford & Williams, 2007). Its expression is displayed in the equation D.1.2

$$\mathrm{Re} = \frac{\rho \cdot d \cdot v}{\mu}$$ **Equation D.1.2**

Where: *Re is the Reynolds number*
ρ is the density of the fluid ($M \cdot L^{-3}$)
d is the diameter of the conduit (L)
v is the velocity of the fluid ($L \cdot T^{-1}$)
μ is the viscosity of the fluid ($M \cdot L^{-1} \cdot T^{-1}$)

Nevertheless the Reynolds number gives only an indication of the nature of the flows. For open channel or pipe flows the Reynolds number value under which the flow can be considered as laminar is evaluated at 2000 (Hornberger et al., 1998).
By replacing the density and the viscosity by their respective values and d by the minimum diameter for a conduit (d = 10 mm), we obtain $\mathrm{Re}/v = 11.2 \cdot 10^{-5}\ s \cdot m^{-1}$. It means that for flow velocities greater then 0.02 m/s the flow should be considered as turbulent.

According to White (2002), in karst medium the behavior of the flows can be determined as turbulent if the aperture of the channels is superior to 10mm.

The turbulent flows can be described with the Darcy Weisbach equation (equation D.1.3) (Ford & Williams, 2007)

$$q = \sqrt{\frac{8 R_H g}{f} \cdot \frac{dh}{dl}}$$ **Equation D.1.3**

Where: *q is the specific discharge ($L \cdot T^{-1}$)*
g is the gravity acceleration ($L^2 \cdot T^{-1}$)
dh/dl is the hydraulic gradient
R_H is the hydraulic radius (L) defined by the ratio between the conduit cross sectional area and the wetted perimeter
f is the Darcy-Weisbach friction factor ($L \cdot T$)

In reality the two flows are coexisting in conduits depending on the precipitation or locations. But the flows in large channels seem to be most of the time turbulent flows. The coexistence of these two kinds of flows leads to more accurate but more complex models.

1.2. Equivalent porous media in the case of karstic aquifers

The second approach and simplest approach is the one that has been chosen in the study as it is able to provide good outputs in the case of regional scale groundwater models (Ford & Williams, 2007) and is computationally less intensive.

The karstic aquifer is modeled as an equivalent porous medium model. This type of models has been used successfully in different studies (Marin, 1990; Larocque, 1999; Scanlon, 2003). The size of the elementary volumes (cells in the grid of the model) should be large compared to the conduit spacing. In this model the conduits are represented as zones of high permeability.

Figure 16 presents the modeling of conduits in equivalent porous medium models.

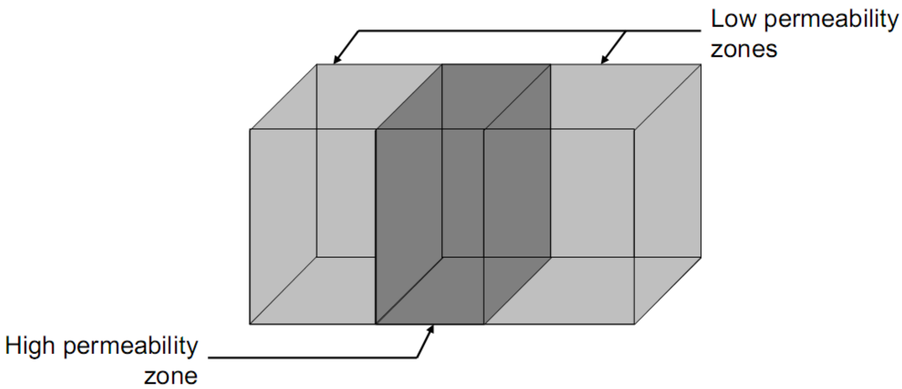

Figure 16: Outline of the equivalent porous medium model

A complete description of the equivalent porous medium models is given in chapter D.3 (page 31)

2. Modeling of coastal aquifers

While modeling coastal aquifers, it is necessary to include in the model the specificities of such aquifers.

In coastal aquifers freshwater is in direct contact with the saltwater. As the density of the freshwater is lower than the density of the saltwater, the freshwater lens is floating on top of the saline water. The simplest view of the problem is obtained by considering the two different kinds of water as immiscible phases (FAO, 1997). This view is illustrated in Figure 17. In this case the interface is a flow line.

In reality freshwater and saltwater are miscible. This leads to the existence of a diffusion zone. In most of the cases this zone can be considered as sharp interface (C.W. Fetter,

2001) because it represents a small fraction of the saturated thickness of the aquifer. In these cases it can be observed flows of freshwater upward to discharge but also cyclic flows of saltwater near the interface (Figure 17).

Saltwater/freshwater interface without diffusion

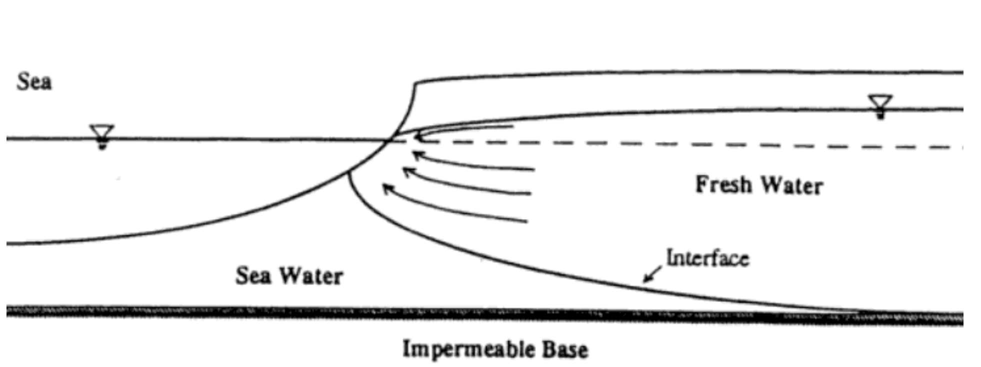

Saltwater/freshwater interface with diffusion

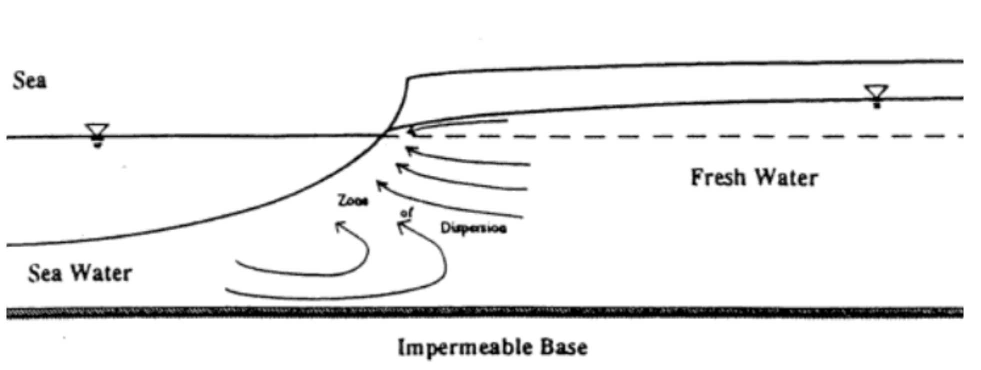

Figure 17: Freshwater/Saltwater interface in the case of sharp interface without diffusion (figure A) and with diffusion (figure B). (FAO, 1997)

In the case of sharp interface, the work of W. Baydon Ghyben (1888-1889) and A. Herzberg (1901) gives a good first approximation of the depth to the interface.
This principle states that the depth to halocline at one specific location in steady state conditions and in the case of unconfined aquifers is linearly related to the hydraulic heads at this point (Equation D.2.1).

$$Z_{(x,y)} = \frac{\rho_w}{\rho_s - \rho_w} \cdot h_{(x,y)}$$ **Equation D.2.1**

Where: $Z_{(x,y)}$ *is the depth to halocline at location (x,y) (L)*
$h_{(x,y)}$ *is the hydraulic head at location (x,y) (L)*
ρ_w *is the density of freshwater* $(M \cdot L^3)$
ρ_s *is the density of saltwater* $(M \cdot L^3)$

The principle described previously gives a good first view of the saltwater intrusion. But most detailed descriptions of the saltwater/freshwater interface can be made. It requires taking into account two equations describing for the first one, the groundwater flow, and for the second one, the movement of salt dominated by advective transport (FAO 2007).
The study of the saltwater/freshwater interface using this method will not be explained here but have been detailed by different authors (Bear, 1989; Segol et al., 1975)

In the study, the Ghyben Herzberg relation has been assumed to be sufficient to determine the depth to saltwater as some previous studies have shown that the interface was sharp (Beddows, 2004; Neuman et al., 2006). Nevertheless a more detailed discussion about the validity of this principle will be made in chapter E.3.3 (page 57).

3. Modeling of groundwater flow in an equivalent porous medium

The software used to make the numerical simulations is the U.S. Geological Survey modular finite-difference ground-water flow model called MODFLOW-96 v3.3 (USGS, 2000). The original development of this software has been made in the early 1980´s. MODFLOW-96 is the second release of the software.
It is a three-dimensional finite-difference groundwater flow in porous medium model that can simulate in steady or non steady state (Mc Donald & Harbaugh et al., 1988).
This chapter describes the theoretical principles used in the software.

3.1.Flow equation

The description of the establishment of the flow equation is based on C.W. Fetter (2001) and Ingebritsen et al. (2006).

The equation characterizing the water flow in a porous medium originates from the *law of mass conservation* applied to an elementary volume as shown in Figure 18.

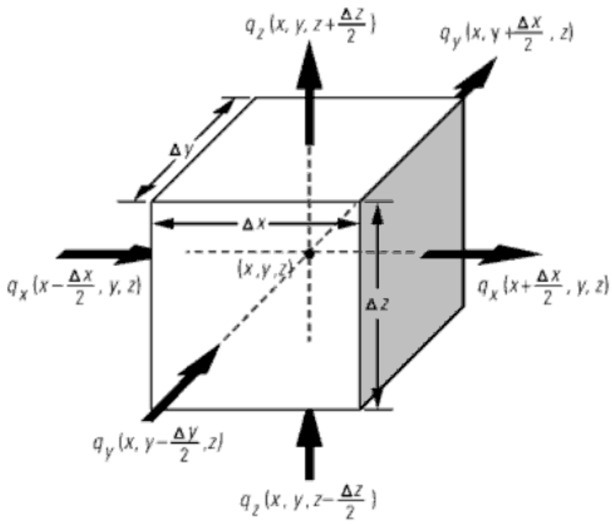

Figure 18: Elementary volume used to elaborate the law of mass conservation. q_x, q_y and q_z represent the volumetric flow rates per unit area.

Based on the law of mass conservation, the equation D.3.1 can be made. It is established by considering that the sum of the outflows minus the sum of the inflows is equal to the variation in mass of fluid in the volume.

$$\begin{aligned}\frac{\partial M}{\partial t}+\rho_f\cdot W=&\left[\rho_f\cdot q_x(x-\frac{\Delta x}{2},y,z)\cdot\Delta y\cdot\Delta z-\rho_f\cdot q_x(x+\frac{\Delta x}{2},y,z)\cdot\Delta y\cdot\Delta z\right]\\&+\left[\rho_f\cdot q_y(x,y-\frac{\Delta y}{2},z)\cdot\Delta x\cdot\Delta z-\rho_f\cdot q_y(x,y+\frac{\Delta y}{2},z)\cdot\Delta x\cdot\Delta z\right]\\&+\left[\rho_f\cdot q_z(x,y,z-\frac{\Delta z}{2})\cdot\Delta x\cdot\Delta y-\rho_f\cdot q_z(x,y,z+\frac{\Delta z}{2})\cdot\Delta x\cdot\Delta y\right]\end{aligned}\qquad\textbf{Equation D.3.1}$$

Where: *M represents the fluid mass in the elementary volume (M)*
ρ_f represents the density of the fluid ($M\cdot L^{-3}$)
qx, qy and qz represents the volumetric flow rates per unit area (L)
W is the volumetric flux per unit volume (T^{-1}) (representing the sources and sinks)

A few assumptions have to be made to simplify this expression.
The control volume is considered to be infinitively small and so the limit of the equation D.3.1 for Δx, Δy and Δz→0 is calculated. The fluid density (ρ_f) is supposed not to vary in space. This gives us the equation D.3.2 (with the same parameters than equation D.3.1):

$$\frac{\partial M}{\partial t}+\rho_f\cdot W=\rho_f\frac{\partial q_x}{\partial x}+\rho_f\frac{\partial q_y}{\partial y}+\rho_f\frac{\partial q_z}{\partial z}\qquad\textbf{Equation D.3.2}$$

The Darcy´s law (equation D.3.3) for an incompressible fluid will now be used to introduce the hydraulic heads in the expression.

$$q_x = -K_x \cdot \frac{\partial h}{\partial x} \;\; ; \;\; q_y = -K_y \cdot \frac{\partial h}{\partial y} \;\; and \;\; q_z = -K_z \cdot \frac{\partial h}{\partial z}$$ **Equation D.3.3**

Where: *K_x, K_y, and K_z are hydraulic conductivities along the directions x, y and z ($L\cdot T^{-1}$)*
h is hydraulic head (L)
qx, qy and qz represents the volumetric flow rates per unit area (L)

The fluid mass (M) can be defined as a function of the hydraulic heads, time and a new parameter called the specific storage (S_s) (Equation D.3.4)

$$\frac{\partial M}{\partial t} = \frac{\partial (n \cdot \rho_f)}{\partial t} = \frac{\partial (n \cdot \rho_f)}{\partial h} \cdot \frac{\partial h}{\partial t} = S_s \cdot \rho_f \cdot \frac{\partial h}{\partial t}$$ **Equation D.3.4**

Where: *M represents the fluid mass in the elementary volume (M)*
h is hydraulic head (L)
n is the porosity of the material
ρ_f represents the density of the fluid ($M\cdot L^{-3}$)
Ss is the specific storage of the porous medium (L^{-1})

All these considerations lead to the establishment of the general flow equation (equation D.3.5):

$$\frac{\partial}{\partial x}(K_x \frac{\partial h}{\partial x}) + \frac{\partial}{\partial y}(K_y \frac{\partial h}{\partial y}) + \frac{\partial}{\partial z}(K_z \frac{\partial h}{\partial z}) - W = S_s \frac{\partial h}{\partial t}$$ **Equation D.3.5**

Where: *K_x, K_y, and K_z are hydraulic conductivities along the directions x, y and z (LT^{-1})*
h is hydraulic head (L)
W is the volumetric flux per unit volume (t^{-1})
S_s is the specific storage of the porous medium (L^{-1})
t is the time (t)

This equation combined with the initial conditions (heads) and boundary conditions (flows and/or heads) determines mathematically the groundwater flow system.
The different parameters of this equation will now be described.

3.2. Parameters in the Flow equation

3.2.1. Hydraulic conductivities (Kx, Ky and Kz)

The hydraulic conductivity (K_x, K_y and K_z) represents the ease of the water to move through porous materials. In many cases the characteristics of the aquifer provide simplifications of these terms and for a regional scale model the porous medium can often be considered as homogeneous and isotropic and so $K_x = K_y = K_z$.

Different methods are available to determine experimentally the values of hydraulic conductivities in the laboratory or directly in the field. Most of them are evaluating hydraulic conductivities by measuring flow rates and using the Darcy´s law (equation D.3.3) (Oosterbaan et al., 1994).
In practice hydraulic conductivities in numerical models are often found by performing a calibration of the model using hydraulic heads measurements. This procedure will be detailed in chapter D.4 (page 40).
The typical values of hydraulic conductivities in porous medium depend highly on the material constituting the porous medium and range from 10^{-9}m/s (clay materials) to 1m/s (gravel) (Fetter, 2001).

3.2.2. Specific storage (S_s)

The specific storage (S_s) has been defined before by the relation:

$$S_s = \frac{1}{\rho_f} \frac{\partial(n \cdot \rho_f)}{\partial h}$$ **Equation D.3.6**

<u>Where:</u> *ρ_f represents the density of the fluid ($M \cdot L^{-3}$)*
h is hydraulic head (L)
n is the porosity of the material
Ss is the specific storage of the porous medium (L^{-1})

The specific storage can also be called elastic storage coefficient and represents the volume of water stored or expelled from storage per volume of saturated formation per unit of head change. It is a constant of the aquifer materials. The storage of an aquifer has a very different meaning when applied to confined or unconfined aquifers.

An unconfined aquifer is made of continuous layers of permeable materials. The upper boundary is the water table and so the saturated thickness of the aquifer is variable. A decrease in hydraulic head will induce a decline in storage. This decrease is due to the fall of the water level (water drains from pore spaces) and represented by the specific yield (S_y). The specific storage is neglected in this case as it is several orders of magnitude lower than the specific yield (Fetter, 2001)

A confined aquifer is overlain by a confining layer. The groundwater is under pressure and a potentiometic surface, which is the surface representing the level to which water would rise if a well is drilled into the aquifer, can be defined. A decrease of potentiometric head will induce a decline in storage but the saturated thickness of the aquifer will remain the same. As water can be considered as uncompressible fluid, the drop-off of storage is due only to the specific storage. It corresponds in fact to a decrease in the effective porosity which represents the volume of material pores filled with water (Fetter, 2001) (the water is considered as an incompressible fluid.

Therefore the specific storage is used only in the case of confined aquifers. The storage characteristics of an aquifer can be determined by tests on aquifer samples or direct tests on aquifers (McWorther et al., 1977).
It has to be noted that in steady state simulations the value of S_s is not required as the term ($S_s \cdot \partial h / \partial t$) is equal to zero.

3.2.3. Sinks and sources (W)

The term W is the volumetric flux per unit volume (T^{-1}) and represents the sinks and sources of an aquifer (McDonald & Harbaugh, 1988). Different types of sinks and sources can be defined.

The wells represent sources in the case of recharge wells or sinks in the case of pumping wells. In both cases the pumping rate (usually in $L^3 \cdot T^{-1}$) defines the volume extracted or incorporated in the aquifer per unit of time. The characteristics of the wells are most of the time well known as they have been set during the construction of them.

Surface water bodies (rivers, lakes, wetlands…) are interacting often with groundwater. There is a water mass transfer from surface water and groundwater, mass transfer that can be either positive (source) or negative (sink) (Fetter, 2001).
In the case of the Yucatan Peninsula these interactions will not be studied. Indeed the surface bodies are rare (inexistent in the northeast), and for a wide study area with few surface bodies, the interactions between surface water and groundwater are supposed not to be of great influence.

Finally the groundwater recharge (GWR) represents the last main type of sinks (negative recharge) and sources (positive recharge). In order to determine it, a soil water balance has to be made (equation D.3.7) (Stewart et al., 2003).

$$P = AET + R + GWR + \Delta S \qquad \textbf{Equation D.3.7}$$

R is the runoff; it represents the water that flows from the hillslope to the stream channel. In the case of flat areas without any substantial runoff this term can be neglected.
ΔS is the storage term; it represents the difference of water volume stored in the plant root zone during a time ΔT (time during which the water balance is calculated). If Δt is long enough, the change in storage can be neglected.

P represents the precipitation in the studied area; it is relatively easy to measure with pluviometers situated on the earth surface or satellites (Tropical Rainfall Measuring

Mission) and is in most part of the world well determined. A map of the precipitation in the Yucatan Peninsula is displayed in Figure 7 (page 10).

AET represents the actual evapotranspiration; it is very complex to measure or determine this value theoretically. It represents often a great source of uncertainties in the determination of the recharge.
Evapotranspiration is basically a combination of two processes: the evaporation of water from surface water, bare soils and vegetation surfaces and the transpiration of plants.
Direct measurements of evapotranspiration are not possible and therefore different indirect methods to determine the evapotranspiration have been developed. The description of the different methods available will not be given here but can be found in the literature (Allen et al., 1998; Hargreaves, 2003)

In this study the AET was determined in the Peninsula using remote sensing data and a correlation between vegetation and AET by S. Lerer (2008). The method used for the determination of AET is called triangle method which is basically based on the fact that the surface radiant temperature is dependant on surface water soil content. The description will not be given here but can be found in the works of Lerrer (2008) or Carlson (2007).
The data used were NDVI index obtained from MODIS (NASA, 2008) which is a remote sensing sensor. The difference in day night temperature was also taken from MODIS LST.

The recharge maps obtained are displayed in Figure 27 (page 58)

In Modflow the sinks and sources are implemented using stress packages (wells, recharge, evapotranspiration, river, drain…)

3.3. Discretization of the aquifer

Except in the case of very simple problems, it is not possible to obtain an analytical solution of the groundwater flow equation. Thereby different methods have been implemented to solve this equation. One possibility, used in Modflow, is to replace the continuous system by a finite set of points distributed in space and time. With this discretization the derivatives are transformed into differences and the equation can be solved. Figure 19 shows an example of discretization of one model area. The limit of the model area is shown with the dashed line; cells situated inside this limit and marked with black points are active , the others are inactive.

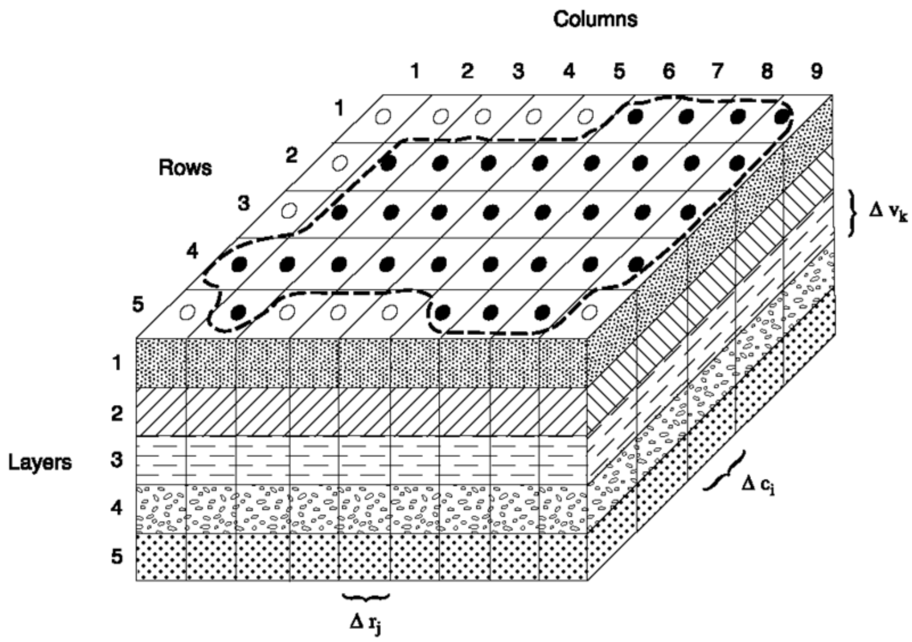

Figure 19: Discretization of the model area (McDonald & Harbaugh, 1988)

The horizontal discretization is obtained by defining the number of columns and rows as well as the width of each row and column. Hydraulic parameters are set individually to each cell or set by defining zones comprising a certain number of cells.

The vertical discretization is achieved by defining the number of layers of the model and a set of hydraulic properties of the layers including the thickness of the layers. Three different kinds of layers can be defined in Modflow: unconfined, confined and mixed confined/unconfined.

Unconfined layers can be defined only for the first layer as the upper boundary is set to the water table. The top of this layer is defined with the water table elevation, so the saturated thickness varies with the hydraulic heads.
Confined layers are characterized by constant transmissivities (saturated thickness of the aquifer × hydraulic conductivity) during the simulation. The specific storage of the cells is defined using the confined storage coefficient and is used to calculate the rate change in the storage throughout the simulation.
Finally layers convertible between unconfined and confined can be defined either with transmissivities varying with saturated thickness through the simulation or constant transmissivities. The confined storage coefficient is used to calculate the rate change in the storage throughout the simulation

3.4. Boundary conditions and initial conditions

To solve the flow equation (Equation D.3.5), the boundary and initial conditions of the model have to be defined.
There are basically three types of hydrological boundaries: fixed head boundary, fixed flow boundary and head dependant flux boundaries (Yeh G., 2000).

The first type, known mathematically under the name *Dirichlet condition*, defines a boundary where the hydraulic heads are known and may vary with the time in a prescribed way. The hydraulic head (h) is characterized at the boundary by the equation:

$$h = H(t) \;\; on \;\; B_d$$ **Equation D.3.8**

Where: *B_d is the boundary segment*
H(t) is the prescribed head (L)

This type of boundaries occurs mainly when the aquifer is in direct freely interaction with surface water bodies (Sea, lakes, rivers) and so the hydraulic head is set at the elevation of the surface water body (Spitz and Moreno, 1996).
In Modflow the cells situated at the location of the fixed head boundary should be defined as constant head cells. It means that the Hydraulic heads in these cells has to be defined in advance and will not change between the different stages of the simulation.

The second type of boundary, also known as *Neumann condition*, is characterized by the fact that the flow through the boundary is known. The equation representing this type of boundary is:

$$-K\frac{\partial h}{\partial x} = q \;\; on \;\; B_d$$ **Equation D.3.9**

Where: *h hydraulic head at the boundary (L)*
q is the specific discharge ($L \cdot T^{-1}$)
K hydraulic conductivity ($L \cdot T^{-1}$)

A fixed flow boundary can be modeled by different tools in Moflow.
To model no flow conditions through the boundary with Modflow, the boundaries of the model array are placed at the location of the no flow boundaries of the aquifer. Indeed in an inactive cell (cell out of the model array) inflows and outflows are prohibited (Mc Donald & Harbaugh 1988).
In the case of a boundary with areas of constant flow (different from zero), the use of external source terms is required.

Finally the third type of boundary called head dependant flux boundaries or mixed boundaries define a boundary where the flow through it is linearly dependant from the hydraulic head at the boundary. The heads and flows are following the equation (Spitz and Moreno, 1996):

$$K.\frac{\partial h}{\partial x} - c(h_b - h) = 0 \ on \ \ B_d$$ **Equation D.3.10**

Where: *h hydraulic head at the boundary (L)*
H surface water elevation (L)
K hydraulic conductivity ($L \cdot T^{-1}$)

The definition of this boundary can be used in the cases of leakages or exchanges between a stream and an adjacent aquifer.
This type of hydrological boundary is modeled by using one of the two stress packages available in Modflow: General head boundary package or River package. In these two cases the cell defined by using one of these tools should be adjacent to an inactive cell.

Initial conditions are required in transient flow models as well as in steady state models. In transient flow simulation, initial conditions (t=0) have to be defined to solve the flow equation while in the case of steady state model it is only the starting point of the different iterations occurring during the simulation.

3.5. *Transient and steady state flow modeling*

The flow simulations in Modflow can be made either in steady state or in non steady state (transient flow simulation).

In steady state flow simulation the flow equation (equation D.3.5) is simplified as there are no changes in time. So the basic groundwater flow equation becomes with the notations previously defined:

$$\frac{\partial}{\partial x}(K_x \frac{\partial h}{\partial x}) + \frac{\partial}{\partial y}(K_y \frac{\partial h}{\partial y}) + \frac{\partial}{\partial z}(K_z \frac{\partial h}{\partial z}) = W$$ **Equation D.3.11**

In reality groundwater flow is nearly always transient. Seasonal variations in recharge, impacts of extreme rain events can not be simulated with steady state flow simulations. Steady state flow simulations should be interpreted as long term average conditions.
Transient flow simulations require more complicated model and much more input data than steady state simulations. Indeed it requires the specific storage of the aquifer as the term $\partial h / \partial t$ is not equal to 0. It requires also extensive data time series (especially for the recharge and hydraulic heads measurements) (Haitjema, 1995).

4. Model Calibration

4.1.Parameter estimation and inverse problems

The calibration of the model is a necessary and critical stage in groundwater modeling. Basically it refers to the estimation of some of the parameters used in the numerical model.

The calibration process is an inverse process. It means that its objective is to estimate parameters by using real field data. Equation D.4.1 represents an inverse process: the objective of the problem is, contrarily to a forward process, given d to find m (Aster et al., 2005)

$$m = G^{-1}(d)$$ **Equation D.4.1**

Where *G is the function that links m and d*
d represent the field data
m represents the parameter to be estimated

More precisely in the case of groundwater modeling the inverse process is often non linear, meaning that the function that links field data (d) and parameters (G) is not linear.
Two main types of calibration processes can be chosen for a study: a manual calibration or an automatic calibration. The manual calibration has been used in many studies but is time consuming and very subjective whereas the automatic calibration invoking the use of an algorithm allows to get results faster and in most of the cases better (Bahremand et al., 2007). The calibration algorithm generally aims at minimizing an "objective function" which is able to measure the fit between field data and simulated values. The usual objective function (φ) is called the weighted least squares function and is defined by the equation D.4.2:

$$\varphi = (d - c)^t \cdot Q \cdot (d - c)$$ **Equation D.4.2**

Where: *d represents the observed values (field data)*
c represents the simulated
Q is the matrix of squared observations weights

It has to be noted than in a calibration, different weights can be assigned to the different observed values. This permits to minimize the influence of non trusted measurements. The squared of these weights are incorporated in a diagonal matrix Q. The typical value for Q is given by the equation D.4.3 where σ_i represents the standard deviation of the measurement i.

$$Q_{ii} = \frac{1}{\sigma_i^{\,2}}$$ **Equation D.4.3**

A calibration does not necessarily give a unique set of estimated parameters. Given the heterogeneity of most aquifers it is even unlikely to get a unique solution. Indeed the number of parameters to be estimated is often too high compared to the number of field values. Nevertheless in that case a unique solution can still be found by simplification. The first solution to get uniqueness in the solution is to regroup the parameters in different zones, inside which the values of the parameters are identical. The second solution is to implement restrictive conditions to the parameters (for example a range of variations). This second technique is called regularization (Moore et al., 2006).

4.2.PEST Presentation

In this study the parameter estimation package PEST v4.1 (PEST, 2002) has been used.
PEST is a non-linear parameter estimation algorithm which performs inverse modeling. The main advantage of PEST is that no changes are necessary in the model. PEST adapts to this model. It uses the Levenberg-Marquardt algorithm, which is briefly described in the next paragraph. The basic description of the algorithm used in PEST is given here based on the PEST user manual (Doherty, 1994) and the work of Madsen et al. (2004), more details can be found in these works.

The Levenberg-Marquardt algorithm is an iterative method used to solve non linear problems. The goal of the algorithm is to minimize the objective function φ which represents the sum of squared deviations between simulated values (calculated with the model) and observed values (measured on the field). Basically it will adjust the parameters iteratively until the best fit between observed values and simulated values is found.

An initial set of parameters (b_0) should be defined. From this set of parameters a set of simulated values is found (c_0) and the objective function can be calculated. Then a new set of parameters (b) is determined by summing the initial set (b_0) with the parameter upgrade vector ($u=b-b_0$). A set of simulated values is generated (c) and the objective function can be recalculated. This procedure continues until the minimum of the objective function is found. It is necessary to translate this procedure into equations.

The model is represented by the non linear function M. If b_0 represents a set of parameters, c_0 a set of simulated values (ie $c_0=M(b_0)$); in the case of small variation of b_0, the approximation described in equation D.4.4 can be made:

$$\begin{aligned} M(b) &= M(b_0+\delta) \\ &= M(b_0)+J.\delta \\ &= c_0+J.(b-b_0) \end{aligned}$$ **Equation D.4.4**

<u>*Where:*</u> *b_0 is the set of parameters*
M is the function representing the model
δ is a small variation of b_0 ($b=b_0+\delta$)
c_0 is the set of simulated values
J is the Jacobian matrix of M

In the equation D.4.4, the Jacobian matrix (J) is a matrix such as J_{ij} is the derivative of the i´th simulated value with respect to the j´th parameter.

Using the equation of the objective function (φ) (equation D.4.2) can now be rearranged (equation D.4.5). b and c represent respectively the set of parameters and simulated values in the second iteration and, b_0 and c_0 represent respectively the initial set of parameters and initial simulated values.

$$\begin{aligned}\varphi &= (d-c)^t \cdot Q \cdot (d-c) \\ &= (d-c_0-J\cdot(b-b_0))^t \cdot Q \cdot (d-c_0-J\cdot(b-b_0))\end{aligned}$$ **Equation D.4.5**

<u>Where:</u> *b_0 is the initial set of parameters*
c_0 is the initial set of simulated results
b is the set of parameters for the second iteration
c is the set of simulated results for the second iteration
J is the Jacobian matrix of M
M is the function representing the model
Q is the matrix of squared observations weights
d is a set of observed values

From the equation D.4.5, the parameter upgrade vector (u) can be determined. It represents the variation of b between two iterations (equation D.4.6)

$$u = (J^t \cdot Q \cdot J)^{-1} \cdot J^t \cdot Q \cdot (d-c_0)$$ **Equation D.4.6**

<u>Where:</u> *c_0 is the set of simulated results*
J is the Jacobian matrix of M
M is the function representing the model
Q is the matrix of squared observations weights
d is a set of observed values

The major contribution of Levenberg and Marquardt to the algorithm is to introduce a damping parameter called Marquardt parameter (α) in the equation D.4.6. This damping parameter influences highly the first steps of the iteration. It changes the size of the steps and also the direction of the steps and allows to achieve convergence much faster. The modified expression of the parameter upgrade vector is given in equation D.4.7:

$$u = (J^t \cdot Q \cdot J + \alpha \cdot I)^{-1} \cdot J^t \cdot Q \cdot (d-c_0)$$ **Equation D.4.7**

<u>Where:</u> *c_0 is the set of simulated results*
J is the Jacobian matrix of M
M is the function representing the model
Q is the matrix of squared observations weights
d is a set of observed values
α is the Marquardt parameter
I is the identity matrix

The choice of the value of this Marquardt parameter implemented in PEST is user specified. The initial value of the parameter is set by the user to λ_0. This value is then lowered by a user specified factor to give a new value for λ. This procedure is made as long as the objective function is lowered.
On the contrary if φ raised when the initial value λ_0 is lowered, instead of lowered, λ_0 will be raised by the same user specified factor as long as φ is lowered.

The implementation of the algorithm in PEST is not described here but is detailed in the user manual (Doherty, 1994).

5. Stochastic catchment delineation

5.1. Catchment delineation

5.1.1. Methods for determining well capture zones

In theory the capture zone of a well can be determined directly on the field by means of tracers. But this technique is applicable only to certain types of aquifers where the residence time is not too long (Vassolo et al., 1998). Moreover restrictive regulations on the nature of tracers injected in the area of a drinking well make this method complicated to implement (Holmbeck-Pelham, 2000).
Therefore groundwater modeling is a very useful tool to delineate these captures zones. Many different computational methods have been established both analytical and numerical method.

Bear and Jacobs (1965) introduced an analytical solution in the case of time related capture zone. His theory was applied to homogeneous isotropic aquifers, with uniform background flow and a single steady state extraction well.
Further different analytical solutions for the delineation of capture zones with different flow conditions were proposed (Lerner, 1992; Kinzelbach et al., 1992)

Nevertheless in the case of distributed recharge and hydraulic conductivities it is not possible to determine analytically capture zones. In these cases numerical modeling is required (Vassolo et al., 1998). Determination of capture zone using numerical models has been successfully implemented in different studies (Kinzelbach et al., 1992; Franssen et al. 2003; Springer et al. 1992).

The most popular method used to determine capture zone numerically is the particle tracking method.

5.1.2. Presentation of Modpath and the particle tracking method

Modpath v3.2 (MODPATH, 2000) is a particle tracking post processing package that computes 3D flow paths using the results of flow simulations obtained by means of Modflow.
This particle tracking software uses the output files of Modflow combined with the definition of the particle locations to compute either pathlines, times series, or endpoint files. This package can track particles backward and forward, in steady state conditions or transient conditions.

A short description of the particle tracking method in steady state is given here based on Modpath user manual (Pollock, 1994).

The partial differential equation of the groundwater flow has been described in equation D.3.2. and D.3.5. In these equations it is possible to introduce the velocity of the flow using the existing relation between volumetric flow rate per unit area and velocity (Equation D.5.6). It gives the starting point of the particle tracking method (Equation D.5.7). As the method is described in steady state condition, the time dependant term in the groundwater flow equation is set to 0.

$$V_x = \frac{q_x}{n_e} \ ; \ \ V_y = \frac{q_y}{n_e} \ ; \ \ V_z = \frac{q_z}{n_e}$$ **Equation D.5.6**

<u>*Where:*</u> *V_x, V_y, V_z are the average linear groundwater velocities along the directions x, y and z ($L{\cdot}T^{-1}$)*
q_x, q_y, q_z are the volumetric fluxes per unit area along the directions x, y and z ($L{\cdot}T^{-1}$)
n_e is the effective porosity of the medium

It has to be noted that the velocities are directly related to the effective porosity of the material. The effective porosity represents the volume of material pores in which water can flow (pores have to be big enough and interconnected to let water flow) (Fetter, 2001). The average values of effective porosity in karst massif aquifers range generally from 0.1% to 1% (Bonacci et al., 2006). They are significantly lower than the porosity. Equivalent porous medium are not able to compute effectively effective porosity in karst aquifers as it is not equivalent to the specific yield of the material.

$$W = \frac{\partial(n_e \cdot V_x)}{\partial x} + \frac{\partial(n_e \cdot V_y)}{\partial y} + \frac{\partial(n_e \cdot V_z)}{\partial z}$$ **Equation D.5.7**

<u>*Where:*</u> *V_x, V_y, V_z are the average linear groundwater velocities along the directions x, y and z ($L.T^{-1}$)*
W is the volumetric flux per unit volume (T^{-1})
n is the porosity of the medium

We will now consider a cubic control volume with x_1, x_2, y_1, y_2, z_1 and z_2 the faces of the volume. This volume is displayed in Figure 20.

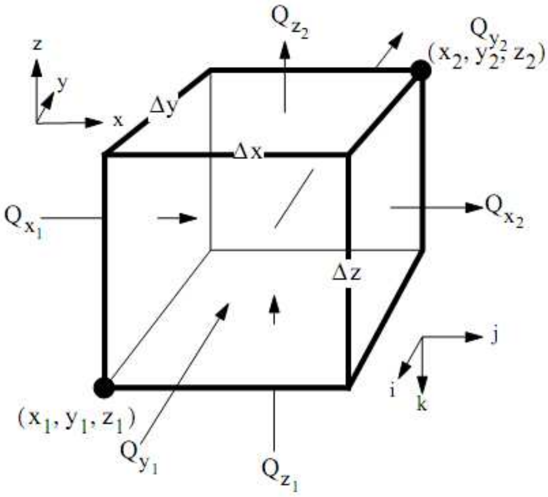

Figure 20: Control volume for the implementation of the particle tracking method (Pollock, 1994)

The expressions of the velocities (at the point with coordinates (x,y,z)) V_x, V_y, and V_z can be determined using a linear interpolation (Equation D.5.8). This technique produces a continuous velocity field in each of the cells.

$$\begin{cases} V_x = A_x(x - x_1) + V_{x_1} \\ V_y = A_y(y - y_1) + V_{y_1} \\ V_z = A_z(z - z_1) + V_{z_1} \end{cases}$$ **Equation D.5.8**

Where: *V_x, V_y, V_z are the average linear groundwater velocities at point (x,,y,z) ($L \cdot T^{-1}$)*
V_{x1}, V_{y1}, V_{z1} are the average linear groundwater velocities at point (x1, y1, z1) ($L \cdot T^{-1}$)
A_x, A_y and A_z are constants

The movement of a particle p within a cell is described now. Some rearrangements of equation D.5.8 can be made to get the equation D.5.9 with the notations defined previously:

$$\begin{cases} \left(\frac{dV_x}{dt}\right)_p = \left(\frac{dV_x}{dx}\right) \cdot \left(\frac{dx}{dt}\right)_p = A_x \cdot V_{x_p} \\ \left(\frac{dV_y}{dt}\right)_p = \left(\frac{dV_y}{dx}\right) \cdot \left(\frac{dy}{dt}\right)_p = A_y \cdot V_{y_p} \\ \left(\frac{dV_z}{dt}\right)_p = \left(\frac{dV_z}{dx}\right) \cdot \left(\frac{dz}{dt}\right)_p = A_z \cdot V_{z_p} \end{cases}$$ **Equation D.5.9**

A new rearrangement of equation D.5.10 can be made to obtain equation D.5.10:

$$\begin{cases} \dfrac{1}{V_{x_p}} \cdot dV_{x_p} = A_x \cdot dt \\ \dfrac{1}{V_{y_p}} \cdot dV_{y_p} = A_y \cdot dt \\ \dfrac{1}{V_{z_p}} \cdot dV_{z_p} = A_z \cdot dt \end{cases}$$

Equation D.5.10

Integration between (t_1 and t_2) of the equation D.5.9 gives the equation D.5.10:

$$\begin{cases} \ln\left(\dfrac{V_{x_p}(t_2)}{V_{x_p}(t_1)}\right) = A_x \Delta t \\ \ln\left(\dfrac{V_{y_p}(t_2)}{V_{y_p}(t_1)}\right) = A_y \Delta t \\ \ln\left(\dfrac{V_{z_p}(t_2)}{V_{z_p}(t_1)}\right) = A_z \Delta t \end{cases}$$

Equation D.5.11

<u>*Where:*</u> *Vx_p Vx_p Vx_p are the average linear groundwater velocities at point (x_1, y_1, z_1) ($L \cdot T^{-1}$)*
A_x, A_y and A_z are constants

By taking the exponential of each side of the equation D.5.11, and incorporating the equation D.5.8 it gives the equation D.5.12:

$$\begin{cases} x_p(t_2) = x_1 + (\dfrac{1}{A_x}\left\{V_{x_p}(t_1)\exp(A_x \Delta t) - V_{x_1}\right\} \\ y_p(t_2) = y_1 + (\dfrac{1}{A_y}\left\{V_{y_p}(t_1)\exp(A_y \Delta t) - V_{y_1}\right\} \\ z_p(t_2) = z_1 + (\dfrac{1}{A_z}\left\{V_{z_p}(t_1)\exp(A_z \Delta t) - V_{z_1}\right\} \end{cases}$$

Equation D.5.12

<u>*Where:*</u> *Vx_p Vx_p Vx_p are the average linear groundwater velocities at point (x_1, y_1, z_1) ($L \cdot T^{-1}$)*
A_x, A_y and A_z are constants

The characteristics of the velocity vector are known in $t=t_1$ and so can be computed at any time within the cell. The last step of the method is now to define the coordinates of the location where the particle leaves the cell. These coordinates are determined by calculation of the time of leaving of the particle. After the determination of this time, the coordinates can be calculated with the equation D.5.12. This calculation has to be made for each consecutive cell until the end of the particle path.

5.2. Well protection zones

Many different definitions of wellhead protection zones have been made depending on the country and on the characteristics of the aquifer.

Usually three different zones are defined: the zone of strict protection (or inner zone), the middle zone (or inner protection zone) and the outer zone or (contributing area).

- The inner zone is defined to protect the water supply wells from short cut pollution. It is in most of the cases a distance based zone; it means that the zone is usually a circular area with a fixed radius (Kresic, 2007; Schmoll et al., 2006). The radius is fixed as 10 to 50 meters (Milanovic, 2002).
- The middle zone is generally based on time of travel analysis. The definition of this time limit is highly dependant on the aquifer properties. In some aquifers with high hydraulic conductivities, the middle zone can be very large, and so to respect this protection zone can be very challenging (Kresic, 2007; Schmoll et al., 2006). The delay time is usually set to 50 days (Milanovic, 2002)
- The outer zone corresponds to the steady state well catchment for most of the countries (Kresic, 2007; Schmoll, 2006).

This definition is in accordance with the Table 3 giving examples of the wellhead protection zones in some countries. Other values are given in the work of Parise et al. (2007).

Table 3: Definition of wellhead protection zone (Schmoll et al., 2006)

Country	**Inner zone**	**Middle zone**	**Outer zone**
Australia	50 m	10 years	Whole catchment
Austria	< 10 m	60 days	Whole catchment
Denmark	10 m	60 days or 300 m	10-20 years
Germany	10-30 m	50 days	Whole catchment
Ghana	10-20 m	50 days	Whole catchment
Indonesia	10-15 m	50 days	Whole catchment
Ireland	100 days or 300m		Whole catchment
Oman	365 days	10 years	Whole catchment or 1000m
Switzerland	10 m	Individually defined	Double size of middle zone
United Kingdom	50 days and 50 m	400 days	Whole catchment

In the case of karstic aquifers the definition of protection zones has to be different. Indeed due to the very high velocity of groundwater, the delay time between sinking and discharge of water is less than 50 days (criteria for zone II). The water can be transported along a distance of more than 100 km during this period, leading to a very restrictive urbanization in many locations (Milanovic, 2002).

The three different zones presented previously are still defined but important differences appear in the definition of the middle zone. The middle zone is separated in two distinct time related zones. The first one (zone 2a) is the distance corresponding to a 24h transit time of pollutant. The zone 2b is the distance corresponding to a 50 days transit time of pollutant (Leibundgut et al., 1998).

Milanovic (2002) defined even more complicated protection zones for karstified medium. He defined the zone 2 with a distance corresponding to a 24h transit time of pollutant. But he also includes a fourth zone, between the middle zone and the outer zone. This zone comprises the swallow holes which have direct connection with springs or intake structures.

5.3. Monte Carlo techniques

The Monte carlo techniques have been used in many studies to delineate stochastic wellhead catchment zones (among other studies: Guha (2008); Vassolo et al. (1998); Franzetti et al. (1995); Stauffer et al. (2004); Riva et al. (1999)).

The Monte Carlo techniques are methods used to model particular phenomena with important uncertainties in inputs. It is hard to define precisely the characteristics of these methods as they are numerous and present high differences.
Nevertheless most of the methods present three main steps: characterization of the inputs, simulations using the set of inputs generated and computation of the results. The second and third stages are highly dependant on the study conducted whereas the first stage is more common to all the studies (Fishman, 1995).

The set of inputs is generally sampled randomly using a probability density function. It means that the samples generated are independent and identically distributed from the target distribution which is defined by the probability density function.

The most widely used algorithm to generate the set of inputs is the Metropolis Hastings algorithm which is a Markov chain Monte Carlo (Neal, 1993).
The principle of this method is to determine samples from a probability distribution using a procedure of acceptance or rejection of proposed values. Basically two functions should be defined in order to use this algorithm.

- A random number from the uniform distribution
- A probability density function

A complete description of the algorithm is available in the work of Neal (1993).

The probability density function used in this study is called the log-normal distribution or Galton distribution. It represents the probability distribution of a variable whose logarithm is normally distributed. This distribution is useful to generate samples of values that are all positive. Considering a set of N data whose logarithm are spared around a mean value (μ) with a define standard deviation (σ), the log-normal distribution function of this data set is given by the equation D.5.13. It has to be noted that the standard deviation can be directly related to confidence intervals.

$$f(x) = \frac{1}{\sigma \cdot x \cdot \sqrt{2\pi}} \exp\left(-\frac{(\ln x - \mu)^2}{2\sigma^2} \right)$$ **Equation D.5.13**

<u>Where:</u> σ is the standard deviation of the logarithm of the data
μ is the mean of the logarithm of the data

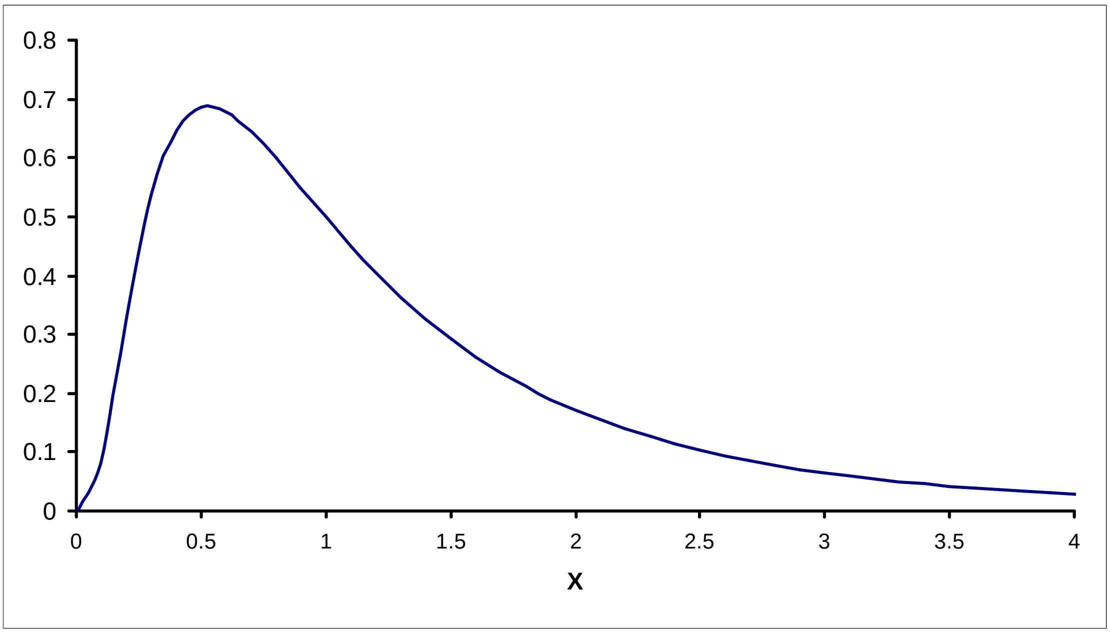

<u>Figure 21:</u> Log-normal probability density function of the variable X (μ =0; σ=0.8)

In the case of input data sets composed of different correlated parameters, the problem becomes more complicated even if the principle of the algorithm remains the same. The probability function should be a multivariate probability density function. The covariance matrix needs to be determined in order to establish the multivariate log-normal distribution. The equation and characteristics of this function will not be described here but can be found in the work of Hansen (2008).

In order to get the correlated random number from the uniform distribution, the Cholesky decomposition is used. By applying the Cholesky decomposition, the covariance matrix is decomposed in order to obtain a lower-triangular L. The latter can be multiplied with a vector of uncorrelated data to obtain a random vector comprising the properties of the covariance matrix.

In our study the characteristics of the input parameters (standard deviations and covariance matrix) used to generate the probability density function and the random numbers have been extracted from the results of the calibration made in PEST. The sampling of the data, successive launching of the groundwater flow and backward particle tracking simulations and the data treatment were made using MATLAB® v7.7 (Matlab, 2008) which is basically a numerical computing environment.
More information about how these Monte Carlo simulations have been conducted will be given in Chapter G.

E. MODEL SET UP

Two models have been developed in parallel by means of MODFLOW: a model for the entire Yucatan peninsula (called "large model" in the rest of the report in order to avoid confusions) and a model for the north of Quintana Roo (called "small model").

1. Hydrological boundaries and discretization of the models

1.1. Model of the Yucatan peninsula (large model)

The model of the entire Yucatan peninsula covers an overall area of 143,616 km^2. The cell size has been set to 2km×2km, which corresponds to a sufficient discretization in order to get a characterization of the hydrological properties of the aquifer. The model consists of one unconfined layer. The grid is composed of 35,904 cells.
The model area is delineated to the west and north by the Gulf of Mexico, and to the east by the Caribbean Sea. At the coast hydraulic heads have been fixed to 0 mamsl and thus the boundary is a fixed head boundary.
The south boundary of the model area has been determined with the use of digital elevation maps by Fratini (2007). The remote sensing and GIS software ILWIS 3.3 Academic (ILWIS, 2007) is able to determine flow directions comparing topographical heights within neighboring pixel. So the accumulation points are determined by performing a cumulative count of the number of pixels that naturally drain into the same outlet (ILWIS, 2007). The groundwater is supposed to flow from the edge (defined at the boundary), and consequently this boundary is a no flow boundary. Figure 22 represents the area of the Yucatan peninsula model.

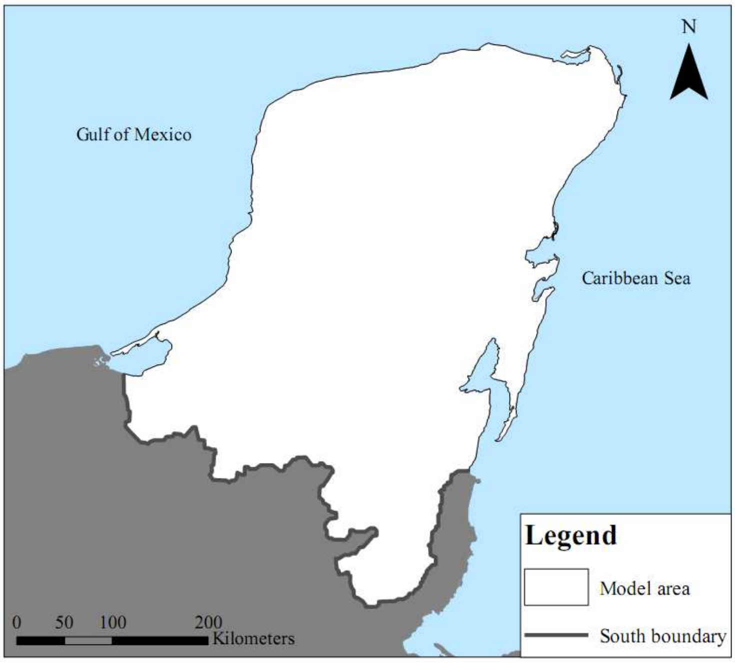

Figure 22: Area of the Yucatan peninsula model

1.2. Model of the northern area of Quintana Roo (small model)

The model of the north of Quintana Roo presents a total area of 25,784 km^2. The cell size is 0.5×0.5 km. The model is made of one unconfined layer and thus represents a total number of 103,138 cells.
The model is delineated to the north by the Gulf of Mexico and to the east by the Caribbean Sea. The south and east boundaries are defined as fixed head boundaries and the heads are fixed to the values found through the simulations made in the large model. The east and north boundaries are also defined as fixed head boundaries with hydraulic heads at the coast set to 0 mamsl. Figure 23 represents the area of the small model.

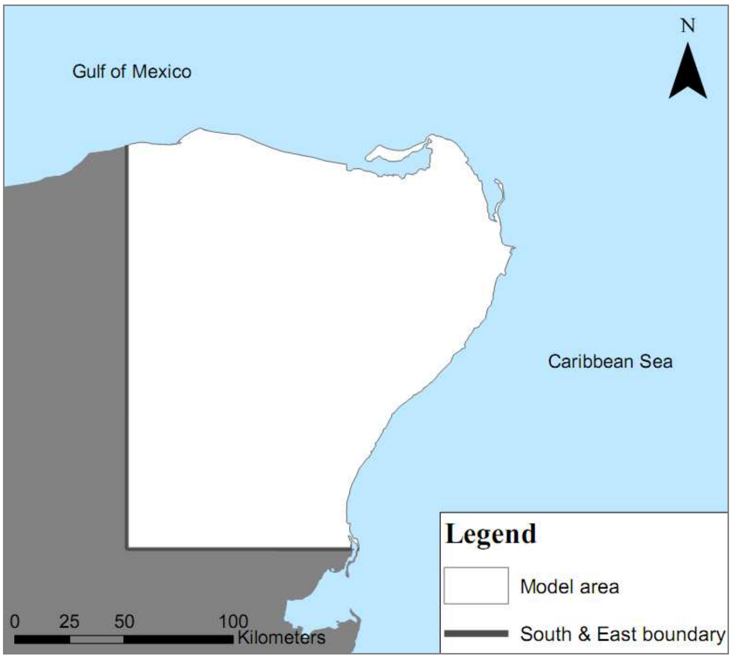

Figure 23: Area of the small model

2. Freshwater heads

For the calibration of the large model, data of water table elevation have been used. This chapter describes the general hydraulic head pattern in the peninsula based on the data obtained.

2.1. Characteristics of hydraulic heads in the peninsula

Previous studies have reported low water table elevations, less than 3-4m above mean sea level, even in the inland part of the peninsula (Perry et al., 2002; Marin, 1990; Neuman et al., 2006). This is mainly due to a very high hydraulic conductivity (Marin, 1990; Gonzalez et al., 2002) and small hydraulic gradient (between 7 and 50 mm/km) (Marin, 1990; Back et al., 1970; Beddows, 2004).

Little data is available concerning the seasonal water table elevation variations. Some studies tend to prove that these fluctuations are far from being negligible. Steinich et al. (2003) reported variations up to 60% in some wells in the north-western part of the peninsula. But other studies were not able to confirm this phenomenon (Beddows, 2004). Thus it is difficult to determine if these variations are really due to seasonal differences or to single rain events.

The temporal variations due to tropical storms or hurricanes can also be very important. The Yucatan peninsula is often affected by such extreme events. During the fieldwork, many villagers have been spoken about the hurricane Wilma (2005). Few villages were flooded during more than 2 months and the water table elevations rose dramatically.

2.2. Data obtained from previous studies

Water table elevation data (relative to mean sea level) are hard to find in the literature and should be very accurate as the freshwater lens is shallow in the Yucatan peninsula.

The head elevations data used here have been taken from three previous studies.

L. Marin has conducted a hydrological study of the north-western part of Quintana Roo (1990) and for this purpose has made measurements of water table elevation in this part of the peninsula. Measurements were made at different periods during the years 1987 and 1988. For our steady state study, only 28 measurements puchased in April 1988 will be considered as it is necessary to use data from the same period of the year in order to reduce the influence of seasonal variations.

C. Fratini (2007) has also conducted some measurements of water table elevation in July 2007. Most of the measurements are located in the central part of the peninsula where the topography is very different, and the ground elevation at least 100 meters above mean sea level. Most of the water table elevations are very high and probably elevations of perched aquifers. Consequently only a few measurements from Fratini were used in the model.

B. Gondwe has conducted a hydrological study of the Siaan Kaan Biosphere and performed water level measurements in this part of the peninsula at different period of the year. In the model only the measurements from February, March and April 2007 were taken into consideration.

Figure 25 (page 55) shows the location of all these measurements.

2.3. Field Measurements

In the period from April 5th to April 30th, I measured water table elevations in sinkholes, and wells in the north of Quintana Roo. 34 measurements were conducted during this period. All water table elevation measurements have been made in the area of the small model, and especially in the Holbox fracture zone. Indeed no data were available in this part of the peninsula and the influence of this high permeability feature on the regional ground water flow pattern is supposed to be important. The table displaying all water table elevation measurements is available in Appendix 2.

Figure 24 represents the water table elevations (mamsl) relative to the distance from the coast.

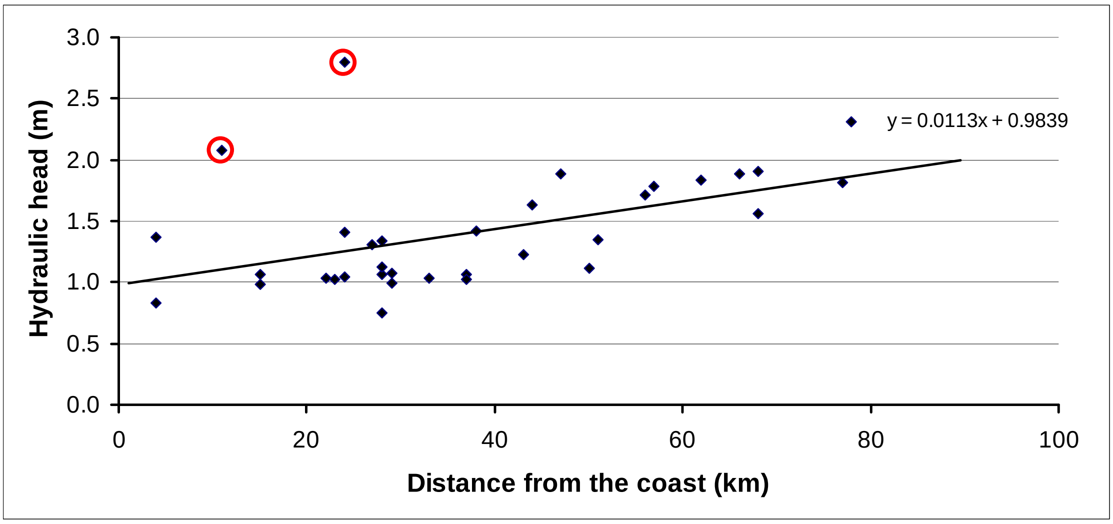

Figure 24: Hydraulic head vs Distance from the coast

It is not surprising to see that the water table elevations are not really following a clear trend. Indeed the characteristics of a karstic aquifer are varying a lot in space and the measurements are sparse over a large area. Nevertheless it has been tried to find the function that fits the best with the experimental values. A global linear trend has been determined. Two measured values have been excluded from the regression because of their high differences compared to the others (bordered in red in Figure 24). These values are measurements taken close to the coast and in the center of the Holbox fracture zone. The equation of the linear function is displayed in Figure 24.

Two important observations can be made from this equation.
First it can be seen that the linear function does not cross the origin (x = 0, y = 0). The water table elevation at the coast does not seem to be 0 mamsl. Different factors can explain this observation and they will be more detailed in Chapter F.2.1.3 (Page 65).
Secondly the slope of the function (0.0113m/km) gives information about the order of magnitude of the hydraulic gradient in the northern part of the peninsula. This value is in the same order of magnitude that the values of hydraulic gradient found in the literature for different part of the Yucatan aquifer (7-10mm/km found by Marin (1990), 20mm/km found by Back et al. (1970), and 58mm/km found by Beddows (2004)).

Figure 25 represents the location of each water table elevation used in the calibration of the model. It can be seen that no data are available in the central and southern part of the peninsula.

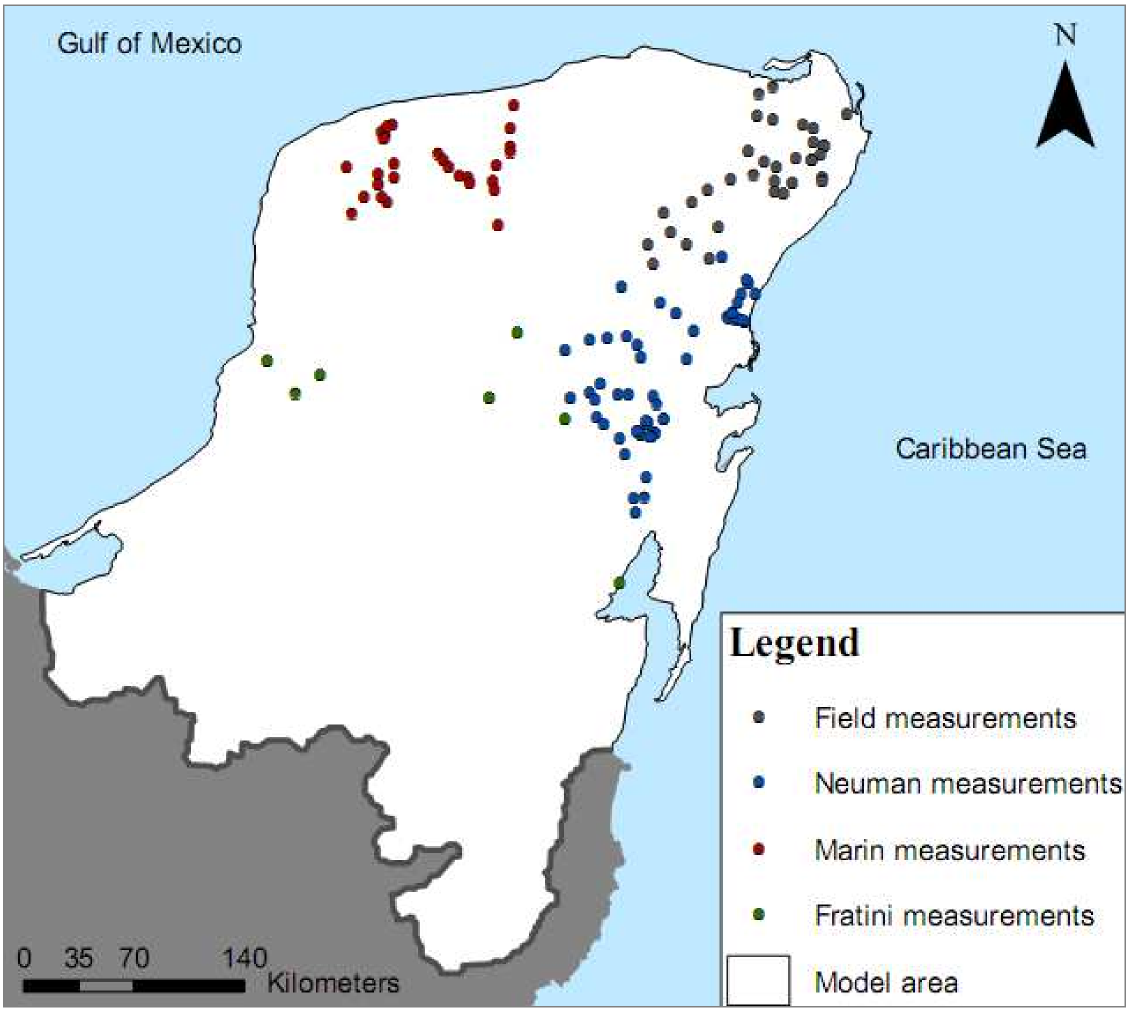

Figure 25: Geographical locations of the water table elevation data

2.4. Uncertainties in the data

It is important to evaluate the uncertainties of the data available. It is assumed, as all the freshwater heads have been measured with the same method and material, that the accuracies are the same for water table elevations coming from the different sources.
The measurement uncertainty comprises three main factores that have been evaluated in chapter C:

- Uncertainty in the topographical height determination: σ_1 = 2cm
- Uncertainty in the leveling σ_2 = 0.5cm
- Uncertainty in the level of the water table σ_3 = 0.5cm

Another source of uncertainty has to be added; the uncertainty related to the time of measurement. As it has been explained in chapter E.2.2, the data have not been collected the same year (and even not collected at the same exact period of the year). The water table level is varying throughout one year and also between years. This uncertainty can be estimated to $\sigma_4 = 10$cm.

The total standard deviation of the measurements will be:

$$\sigma_{tot} = \sqrt{\sigma_1{}^2 + \sigma_2{}^2 + \sigma_3{}^2 + \sigma_4{}^2} = \sqrt{2^2 + 0.5^2 + 0.5^2 + 10^2} = 10.22$$ **Equation E.2.1**

3. Thickness of the aquifer

3.1.Interface Freshwater/Seawater

The validity of the Ghyben Herzberg principle in the case of the Yucatan aquifer has been already studied and different results have been found.
Marin (2001) found that the thickness of the freshwater lens was not significantly overestimated in the north-western part of Yucatan. Electrical resistivity surveys from Steinich et al. (2006) had confirmed this result.
On the contrary, Moore (1992) found that the depth to halocline calculated from hydraulic heads using the Ghyben Herberg principle is overestimated. According to his study the slope of the function describing the relation between hydraulic head and depth to halocline should be around 24 instead of 40.

3.2. *Data obtained*

During the fieldwork in Yucatan, measurements of depth to halocline have been made with the time domain electromagnetic equipment ProTEM47D. Unfortunately the results were not convincing, probably due to a malfunctioning of the equipment.

Nevertheless few profiles of electrical conductivities were made in 2008 by the company Aguakan in the north-eastern part of the peninsula. From these profiles the depth to saline water can be determined as the electrical conductivity of the saltwater is by far higher than the freshwater one's. These profiles are available in Appendix 4.
Moreover B. Gondwe, in 2007, conducted electromagnetic measurements in different locations in the eastern part of the peninsula.

It should be noticed that these data of depth to halocline have a high uncertainty and are all located in the eastern part of the peninsula. The use of these data to prove the validity of the Ghyben Herzberg principle is not possible. But it can still give an idea on the possibility of using this principle in our study.

3.3. *Validity of the Ghyben Herzberg relation*

Figure 26 represents the experimental relation between the water table elevation and the depth to halocline.

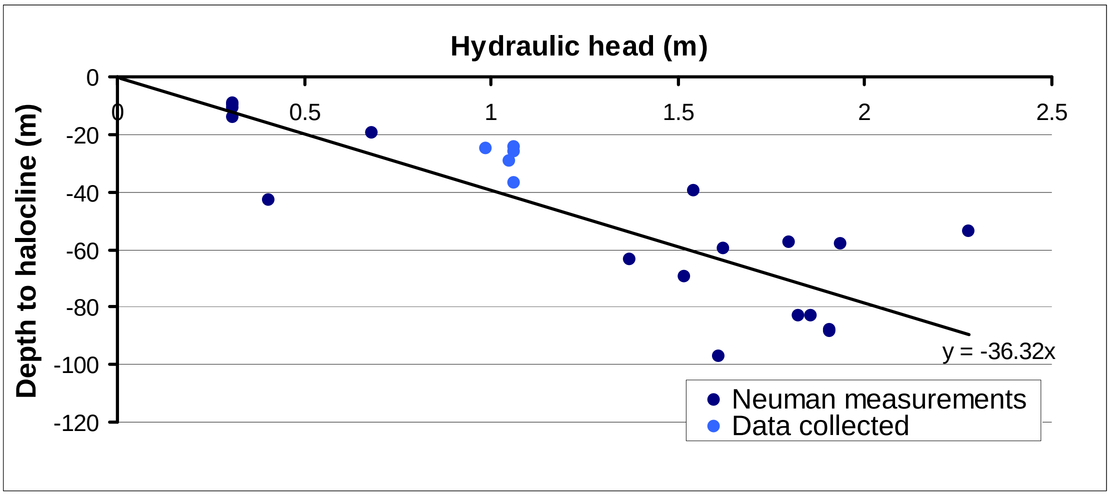

Figure 26: Hydraulic head vs depth to halocline

The best linear regression has a slope of -36 as it is displayed on the plot. This is relatively close to the analytical formula and thus tends to confirm the validity of the relation. Nevertheless, considering the uncertainties of the data, the uncertainty of the linear regression and the small number of measurement points, further studies should be made to confirm the validity of the principle.
In the two models the thickness of the aquifer has been implemented using the Ghyben Herzberg relation. In practical terms it means that an iterative method has been used. The water table was calculated, and then the bottom of the aquifer was set using the Ghyben Herzberg relation. Those two stages were achieved several times until convergence was found.

4. Recharge

The yearly average recharge in the peninsula has been determined by Lerrer (2007).

The method used to elaborate the recharge maps has already been described in the chapter D.3.2 (page 34).

The recharge maps for the two model areas are displayed in Figure 27. It can be seen that the recharge does unfortunately not cover the entire area of the large model. For the area where the recharge is not defined a value of 7 mm/day was used.
In some parts of the peninsula, especially near the coast, the recharge is negative. The possibility of negative recharge has been confirmed by Tulaczik et al., (1993) in the northeastern part of the peninsula. The recharge in the model is applied to the top layer.

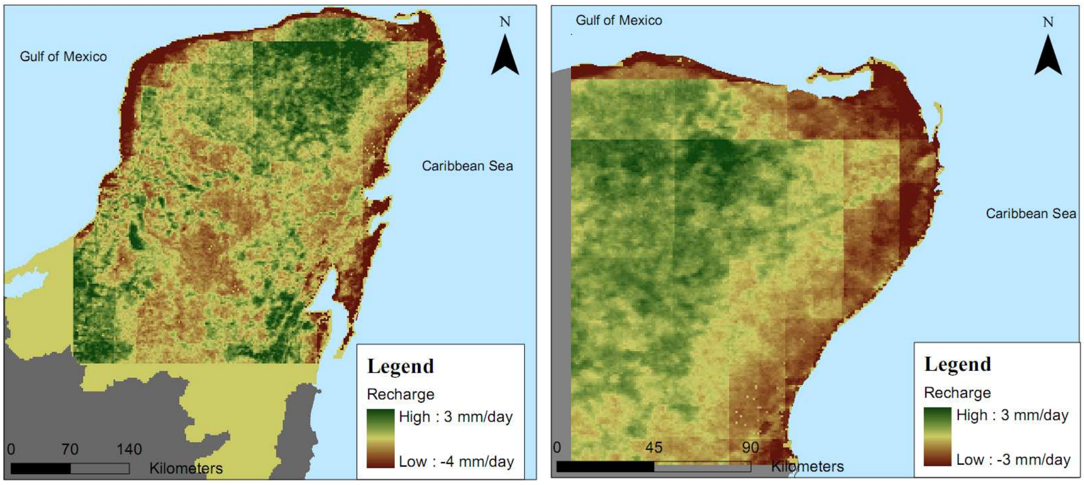

Figure 27: Recharge maps

5. Pumping wells of Cancun

The wells supplying drinking water to the city of Cancun are located in 6 different pumping zones. The locations of the six pumping areas are shown in Figure 28. The total pumping rate of the wells is 1900 L/s for a total of 142 wells (Aguakan, 2009).

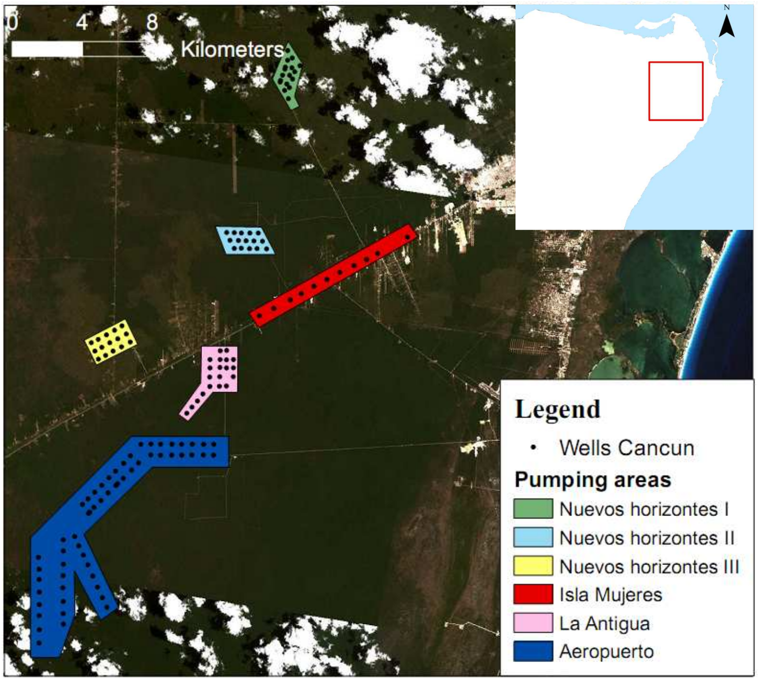

Figure 28: Pumping areas and wells locations

It is supposed that all the wells have the same pumping rate; it means that the 142 wells are pumping 13.38 L/s each.
As the discretization of the model does not allow to define the wells individually, pumping areas have been implemented in the model. The global pumping rate of each zone has been calculated (knowing the number of wells in each zone) and divided by the number of cells contained in the zone in order to obtain the pumping rate of each cell.

The wells have been implemented only in the small model. Indeed it is supposed that they do not influence significantly the hydraulic heads and the flows at the scale of the peninsula. The validity of this hypothesis will be confirmed in chapter F.2.2.3, (page 68). Moreover the locations of the pumping wells in the entire peninsula are not known.

As the pumping depth is not known, the wells are supposed to pump over the entire thickness of the aquifer.

Table 4 summarizes the implemented values.

Table 4: Characteristics of the different pumping zones

Zone name	**Number of wells**	**Number of cells**	**Global pumping rate**	**Pumping rate /cell**
Nuevos horizontes I	18	10	0.240 m^3/s	0.0240 m^3/s
Nuevos horizontes II	15	21	0.200 m^3/s	0.0096 m^3/s
Nuevos horizontes III	15	12	0.200 m^3/s	0.0167 m^3/s
Isla Mujeres	11	41	0.147 m^3/s	0.0036 m^3/s
La Antigua	20	24	0.268 m^3/s	0.0112 m^3/s
Aeropuerto	63	168	0.842 m^3/s	0.0050 m^3/s

F. RESULTS OF THE SIMULATION

1. Model Calibration

The hydraulic conductivities in the peninsula model have been calibrated using water table elevations measured and obtained from various sources. The calibration was made only in the large model.

1.1. *Choice of the number of parameters*

The different zones of identical hydraulic conductivities were defined in accordance with the different geological formations (Figure 2, page 5).
It is necessary in a calibration to find the right number of zones that need to be specified.
On one hand choosing a too important number of parameters gives in some zones very broad 95% confidence interval. The number of field data available is then not sufficient. Moreover too many parameters will lead to a dramatic increase of the computational time.
On the other hand, when calibrating a large area like the Yucatan peninsula, it is necessary to take into consideration the geological and hydrological differences between the different parts of the model in order for the latter to be realistic.

The model was successively calibrated with 2, 3, 4 and 5 parameters in order to determine the best compromise. The same importance has been assigned to all measurements as they have been measured with the same uncertainties.
The maps of the geological areas taken into consideration in these calibrations are displayed in Figure 29.

The results of the four calibration attempts (95% confidence interval and normalized root mean square deviation) are displayed in Table 5.

Table 5: Results of the four different calibrations

	Calibration with 2 parameters	**Calibration with 3 parameters**	**Calibration with 4 parameters**	**Calibration with 5 parameters**
P1 (95% interval)	1.94 – 2.42 m/s	3.24 - 4.28 m/s	0.72 - 2.48 m/s	0.52 – 1.35 m/s
P2 (95% interval)	0.019 – 0.11 m/s	0.029 – 0.17 m/s	7.38 - 295.8 m/s	5.14 – 168.8 m/s
P3 (95% interval)		0.12 - 0.28 m/s	0.014 - 0.059 m/s	0.017 – 0.084 m/s
P4 (95% interval)			0.70 - 1.40 m/s	0.53 – 1.57 m/s
P5 (95% interval)				3.62 - 55.8 m/s
Normalized root mean square deviation	6.84	6.28	3.83	3.77

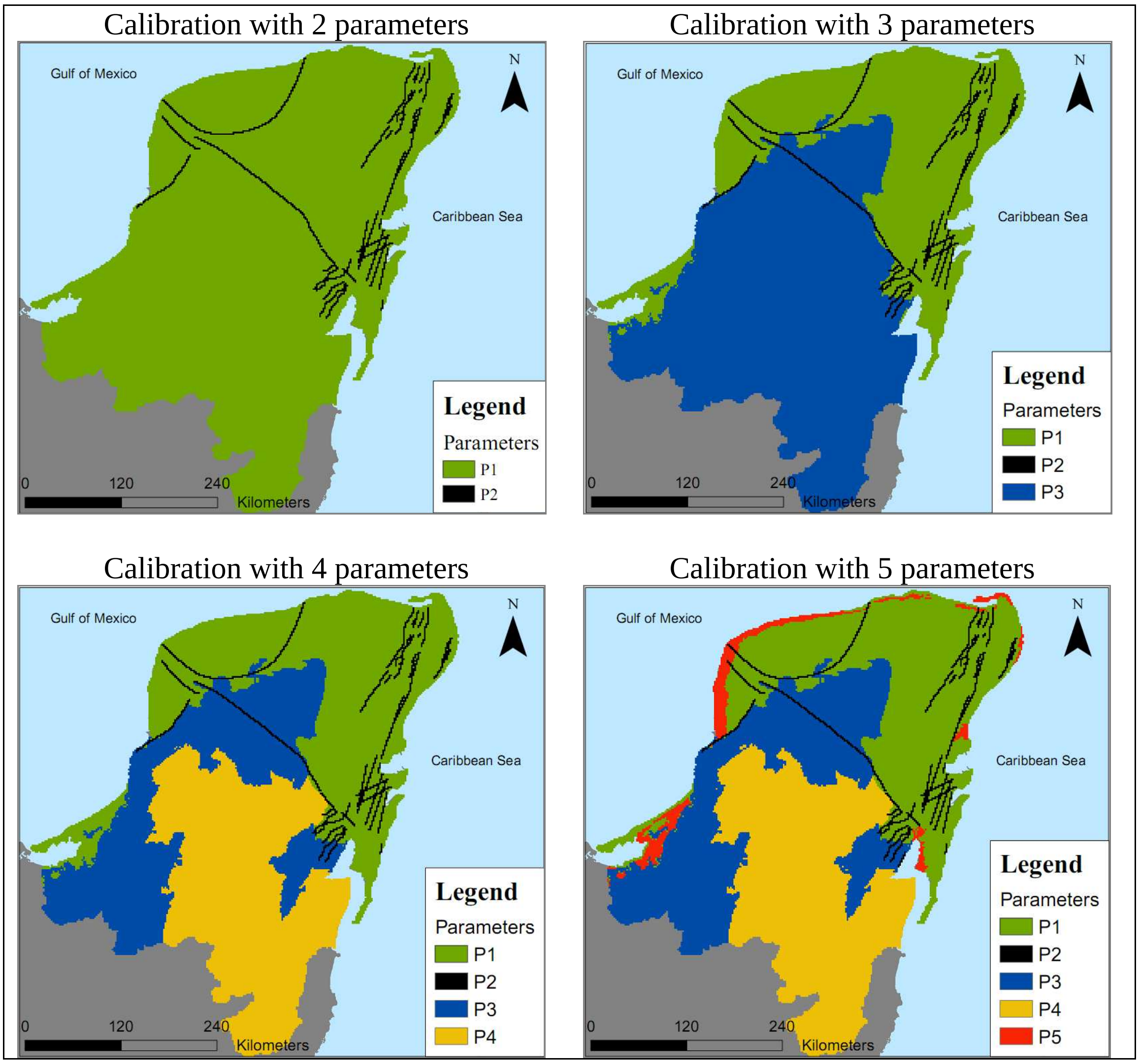

Figure 29: Geological zones in the different calibrations

Based on these results, it has been chosen to implement in the model 4 parameters. The two first calibrations (with 2 and 3 parameters) showed normalized root mean square deviation (NRMSD) much higher than the two other calibrations. Moreover the hydraulic conductivities found do not reflect the reality of the aquifer (the high permeability areas (P2) have hydraulic conductivities lower than the other areas).

The calibrations with 4 and 5 parameters give results relatively close in terms of NRMSD and hydraulic conductivities. Despite a small decrease in NRMSD between the two attempts, it has been chosen to define only 4 parameters in order to keep the model as simple as possible.

It should be noted that for the calculation of NMSD, the standard deviation of the measurements has been set to σ_{tot} = 10.22 cm as it was calculated in chapter E.2.4.

1.2. Correlation between calculated and observed hydraulic heads

Figure 30 shows the relation between the measured hydraulic heads and the calculated hydraulic heads over the peninsula.

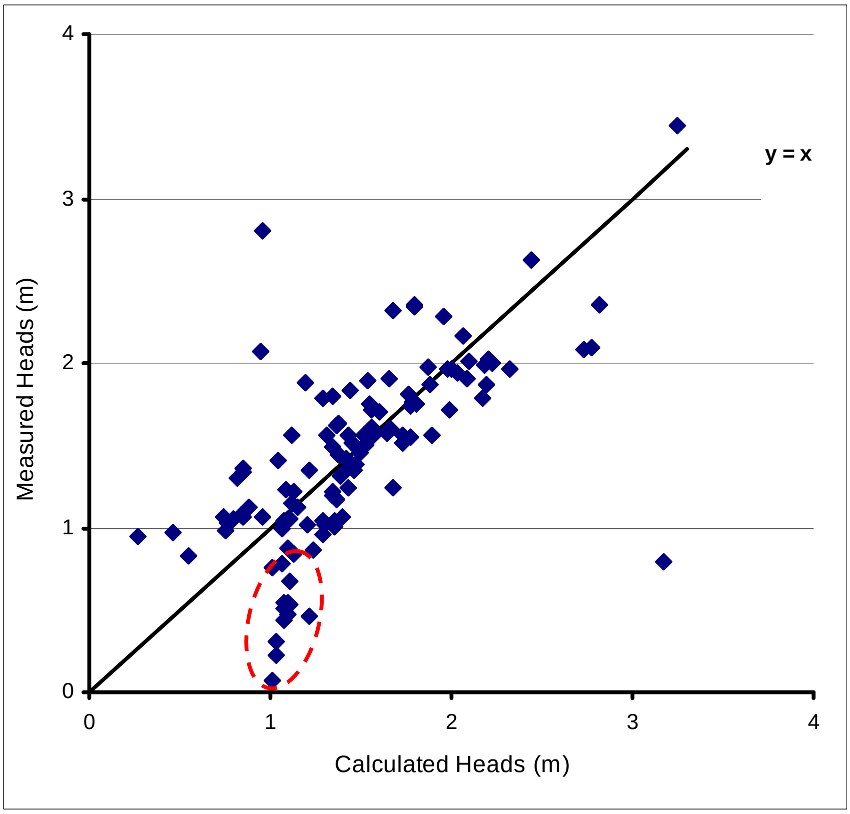

Figure 30: Measured heads vs calibrated heads,
The red shape refers to the red shape in Figure 31

The points scatter around the function y = x. Nevertheless the value of the normalized root mean square deviation highlights the fact that the correlation is far from being perfect. This reflects the difficulties of calibrating a large simple model for a complex karstic aquifer.

Figure 31 shows a map of the residuals (difference between measured heads and calculated heads). It can be seen that they are not really following an obvious trend in their geographical distribution. However some interesting observations can be formulated.

The residuals in the north-eastern part of the peninsula (bordered in blue in Figure 31), situated in the holbox fracture zone, seem to be in average significantly higher than in the other parts. It means that the model is underestimating the hydraulic heads in this region and thus overestimating the hydraulic conductivity.

On the contrary the area bordered in red in Figure 31 seems to be an area where the measured heads are lower than the calculated heads. These measurement points can also be identified in the plot Figure 30 (bordered in red). In this area, situated close to the coast, the water table elevations are low (between 0 and 0.6 mamsl). It is in fact the only part of the peninsula where the measurements seem to show that the hydraulic heads are reaching an elevation of zero at the coast without any drop in the last few kilometers. This issue will be further discussed in the chapter F.2.1.3 (Page 65).

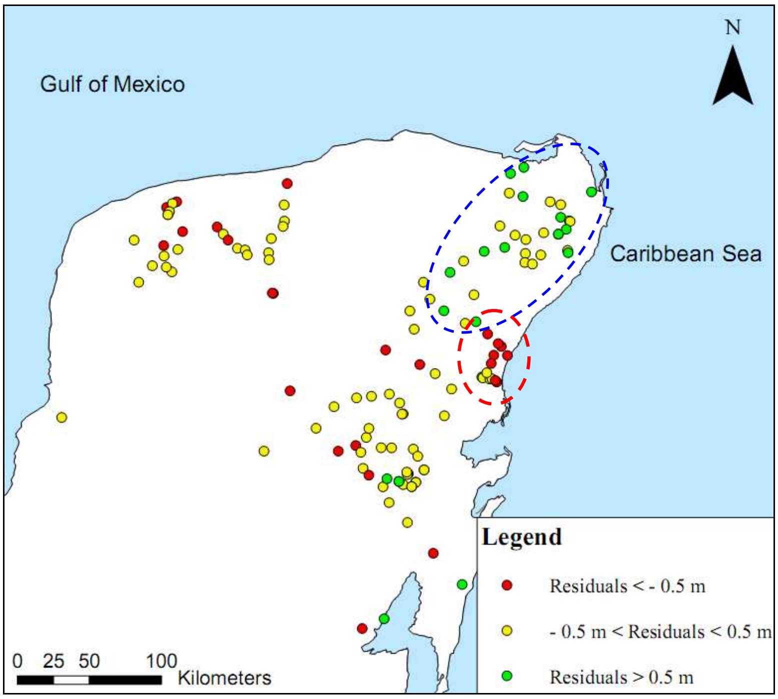

Figure 31: *Map of residuals (measured heads – calculated heads)*
The blue shape highlights a zone where the residuals are high
The red shape highlights a zone where the residuals are low

1.3. Calibrated hydraulic conductivities

As it has been described in page 60, 4 different zones of hydraulic conductivities have been defined in the model area. The different values obtained for the 4 different areas are shown in the Table 6. The names of these zones refer directly to those given in Figure 29.

Table 6: *Calibrated hydraulic conductivities*

	Hydraulic conductivity	95 % confidence interval	
		Lower limit	Upper limit
Zone P1	**1.34 m/s**	0.72 m/s	2.48 m/s
Zone P2	**46.73 m/s**	7.38 m/s	295.79 m/s
Zone P3	**0.029 m/s**	0.014 m/s	0.059 m/s
Zone P4	**1.00 m/s**	0.70 m/s	1.40 m/s

Few studies have already determined values for the hydraulic conductivity in the Yucatan aquifer and values are displayed in Table 1 (page 15).

Numerical models have most of the time given quite high hydraulic conductivities while measurements led to lower values. Most of the values, as it can be seen in Table 1 were found in the north-western part of the aquifer. The calibration of the model has given hydraulic conductivities that are situated in the same order of magnitude than those found by means of numerical models in the literature.

2. Configuration of Hydraulic Heads

2.1. Hydraulic heads configuration for the large model

2.1.1. General shape of the simulated hydraulic heads

Figure 32 shows the hydraulic heads distribution in the large model.

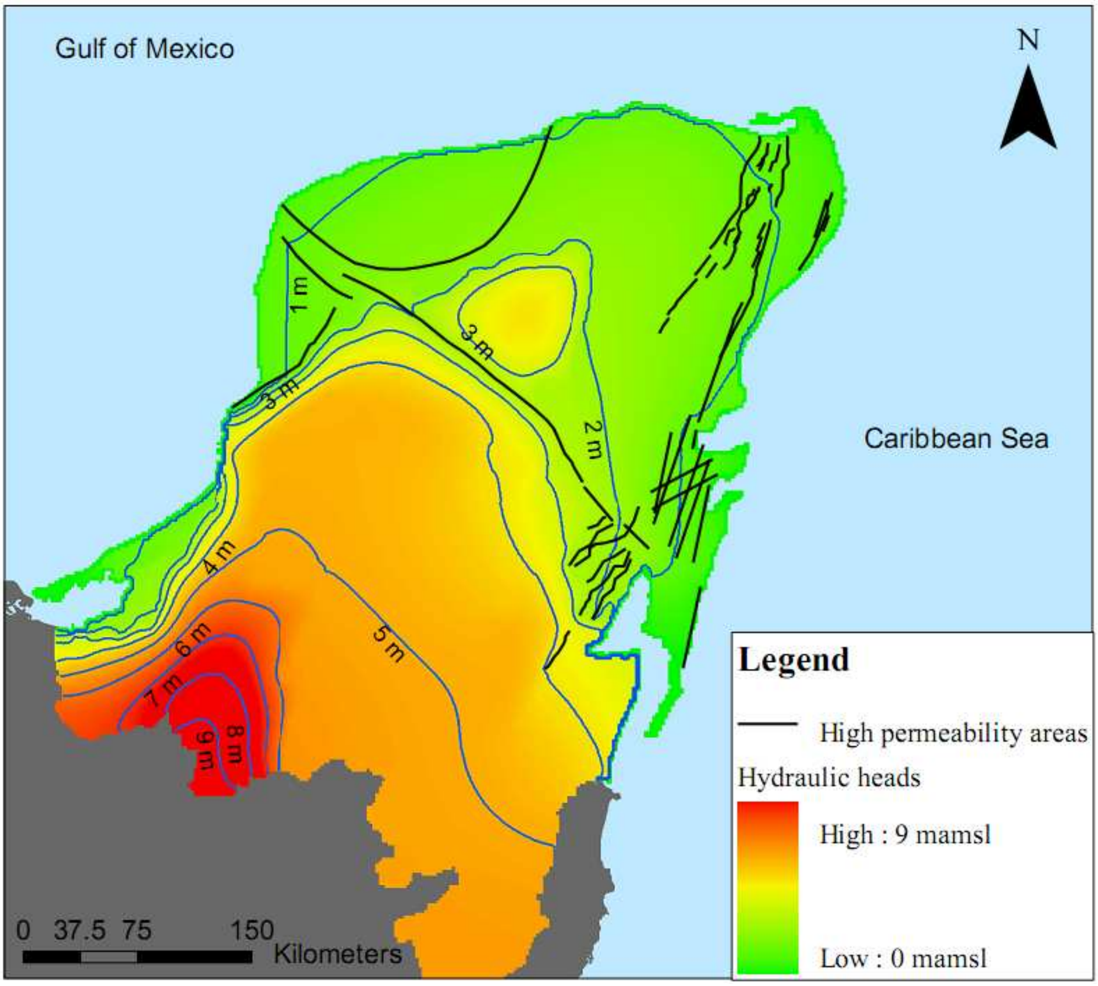

Figure 32: Hydraulic heads in the Yucatan peninsula

The hydraulic heads in the peninsula range from 0 to 6 mamsl, except from a small area situated in the south west of the peninsula. The values are globally decreasing from the south to the north, except for a small area situated in the north of the Sierrita de Ticul fault where a local hydraulic heads maximum can be found.

2.1.2. Correlation between horizontal hydraulic conductivity and hydraulic heads

It is interesting to see that the shape of Figure 32 is highly correlated with the map describing the different hydraulic conductivity zones (Figure 29, page 61). The zone P1 (K=1.34m/s) located in the northern part of the peninsula is characterized by very shallow water table elevations while the zone with the lowest hydraulic conductivity (zone P3, K=0.029m/s) is situated where the highest values of hydraulic heads are found. This observation is not surprising because of the high difference in the values of hydraulic conductivities for the different zones. Nevertheless it shows the importance of their definition in the establishment of a model on a large area like the Yucatan peninsula.

2.1.3. Water table elevations next to the coast

As it has been defined in the hydrological boundaries of the model, the hydraulic head at the coast has been fixed to 0 mamsl. The simulated hydraulic heads near the coast (distance from the coast under 5km) are far from being 0 mamsl. This leads to an important drop of the water table elevations just a few kilometers from the coastline. This phenomenon can be observed for example on the north coast in Figure 33.

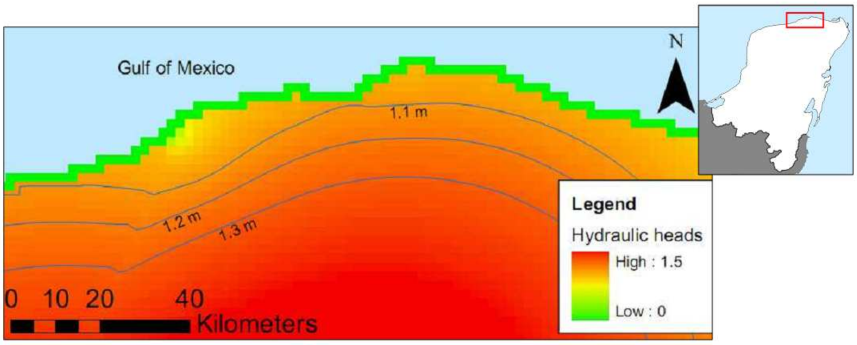

Figure 33: Hydraulic heads on the north coast

This drop of the water table elevations has already been observed by looking at the measured hydraulic heads (Figure 24, page 54). It has also been seen with the measured hydraulic heads that, in one area, this phenomenon is not happening (area bordered in red in Figure 31, page 63). This specificity is not represented in the model as no additional hydraulic conductivity zone has been defined for this part of the peninsula.

Another explanation to this drop is directly related to the manner that the freshwater thickness has been modeled. The bottom of the freshwater layer has been set using the Ghyben Herzberg principle, and thus, as the hydraulic heads are set to 0 mamsl at the

coast, the aquifer thickness is also set to 0 mamsl. In reality this situation is not true as it can be seen by looking at Figure 34.
Nevertheless it is believed that this fall of hydraulic heads at the coast does not lead to changes in the groundwater flow pattern, as the flows are governed by differences in hydraulic heads.

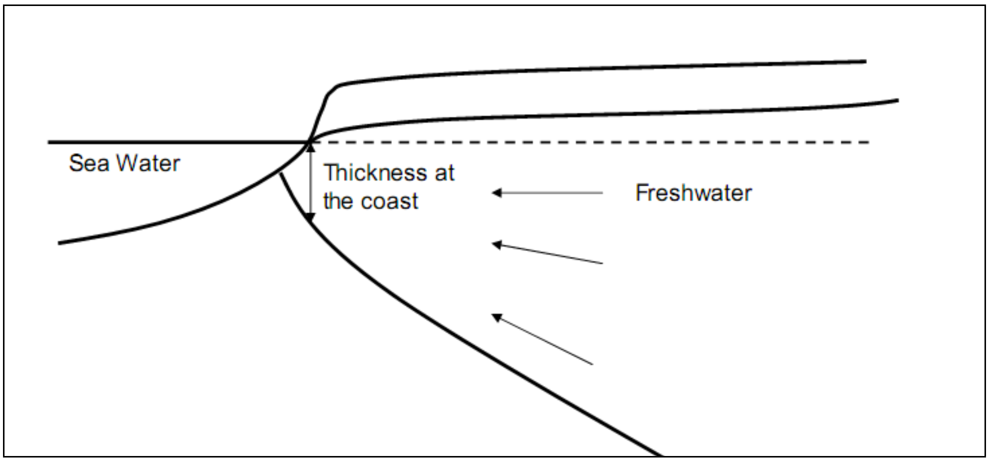

Figure 34: Thickness of the aquifer at the coast

2.1.4. Influence of high permeability areas

The influence of the high permeability areas is not obvious on the shape of Figure 32 (page 64), except concerning the Sierrita de Ticul fault. The major influence of this feature results in a significant decline of water elevations in its area. A careful interpretation of this outcome should be made, as there are major uncertainties in the definition of this high permeability area. The mapping of it is not well known and neither is the characterization of it.
It has been modeled as one continuous high permeability feature in the model as suggested by Perry et al. (2002). Nevertheless some other modeling studies have included this fault as a low permeability area (it acts in this case as a flow barrier) (Gonzalez Herrera at al., 2002).

In order to evaluate the influence of such consideration, a scenario has been made describing the Sierrita de Ticul fault as a horizontal flow barrier with a constant transmissivity of 0.0005 m^2/s. The map of the hydraulic heads distribution is displayed in Figure 35. It can be seen that the local hydraulic heads maximum observed in Figure 32 in the north of the fault has disappeared. However a hydraulic head maximum can be seen on the location of the Sierrita de Ticul fault zone.

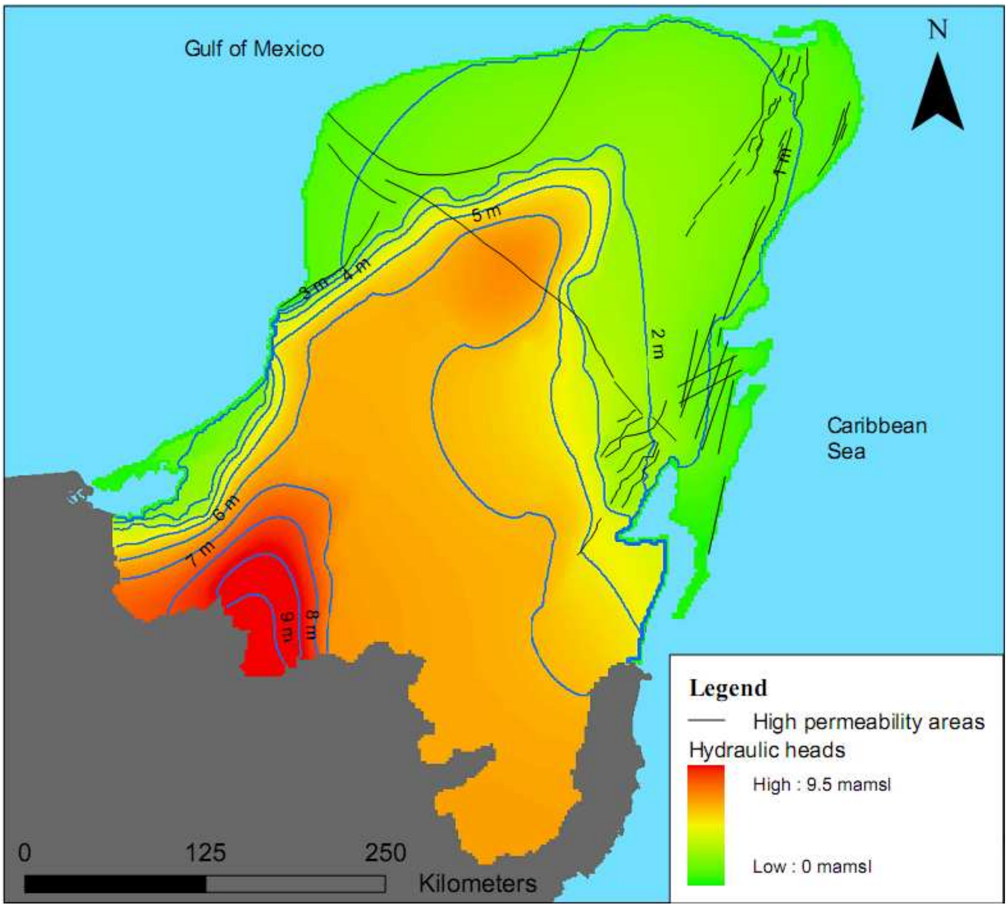

Figure 35: *Hydraulic heads in the Peninsula considering the Sierrita de Ticul as a flow barrier*

2.2.Hydraulic heads configuration in the north of Quintana Roo

2.2.1. General shape of the simulated hydraulic heads

Figure 36 shows the hydraulic heads configuration obtained in the small model.

The hydraulic heads in the model area range from 0 to 2.5 mamsl. The maximum water table elevation is situated in the west of the model area in a zone where the hydraulic conductivity is lower than in the other parts (K=0.029m/s in the western part, K=1.34m/s in the rest of the area). As it was already seen in Figure 32, the high permeability features (the Holbox fracture zone) do not have an obvious influence on the shape of the hydraulic heads.

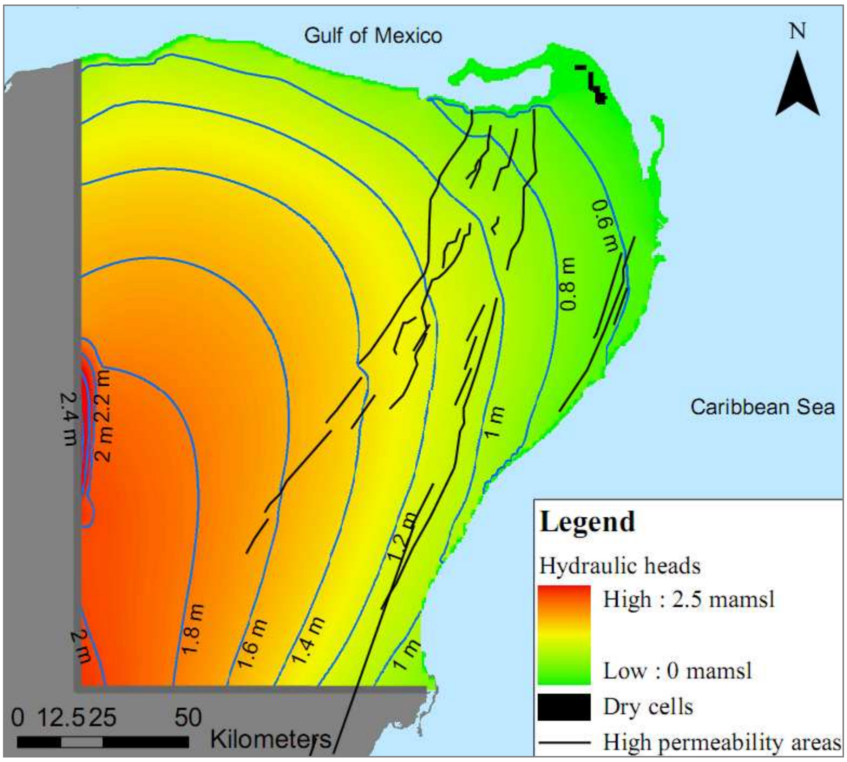

Figure 36: Water table elevations in the northern peninsula

2.2.2. *Presence of Dry cells in the simulated area*

It has to be noticed that there are dry cells in the north-eastern part of the model area. This presence is directly related to the negative recharge in this part of the area. It means that the yearly average evapotranspiration rate is higher than the yearly average precipitation rate and that the inflows in these cells are not sufficient to cover this difference. This fact seems to be unrealistic and is probably due to the uncertainties linked with the recharge map and the definition of the model.

2.2.3. *Influence of the pumping wells*

The wells supplying water to the city of Cancun are included in the small model. The characteristics of these wells have been described in chapter E.5 (page 58).
They do not seem to have any obvious influence on the hydraulic heads as it can be seen in Figure 37. This tends to confirm the fact that including the wells in the large model is not necessary.

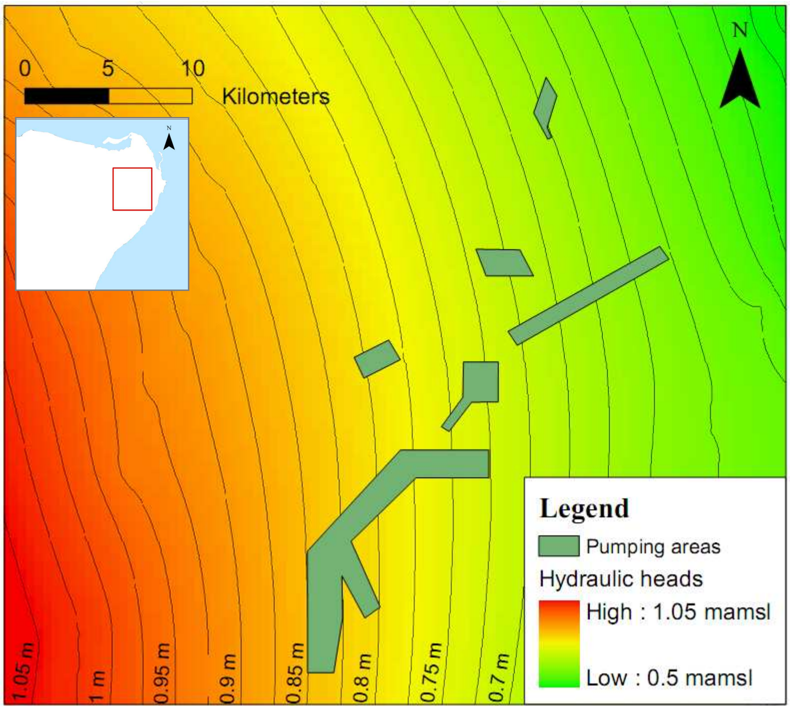

Figure 37: Influence of pumping wells on the hydraulic heads

Nevertheless it is important to see if an increase of the pumping rates, in the future will lead to changes in the hydraulic heads pattern. That is the reason why four different scenarios have been implemented with different pumping rates (2.5, 5, 7.5 and 10 times the actual pumping rate). The distribution of the hydraulic heads in these scenarios is shown Figure 38.

By looking at the four scenarios it can be seen that no major differences in the hydraulic head pattern can be seen in the two first scenarios (2.5 times and 5 times the actual pumping rate). On the contrary in the two others, the influence of the pumping wells is obvious. The heads isolines are modified significantly and the shape of the aquifer is changed.

This scenario analysis shows that the actual pumping rate should be increased dramatically to cause any changes in the hydraulic head pattern (at least more than 5 times).

Scenario 1: 2.5 times of actual pumping rate

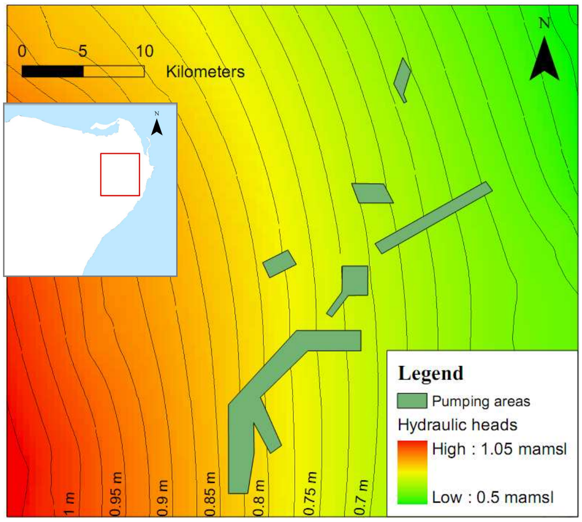

Scenario 2: 5 times of actual pumping rate

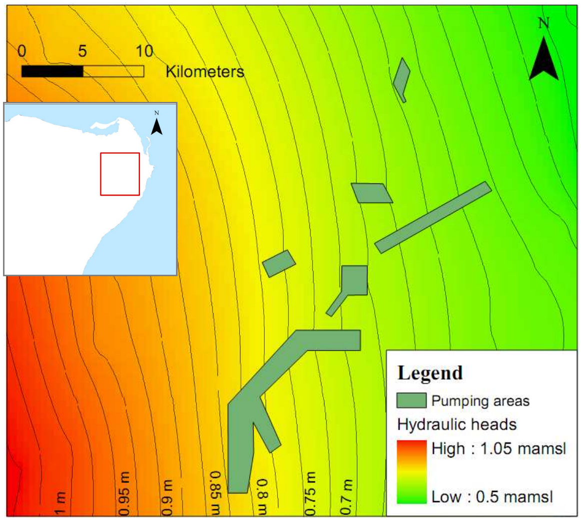

Scenario 3: 7.5times of actual pumping rate

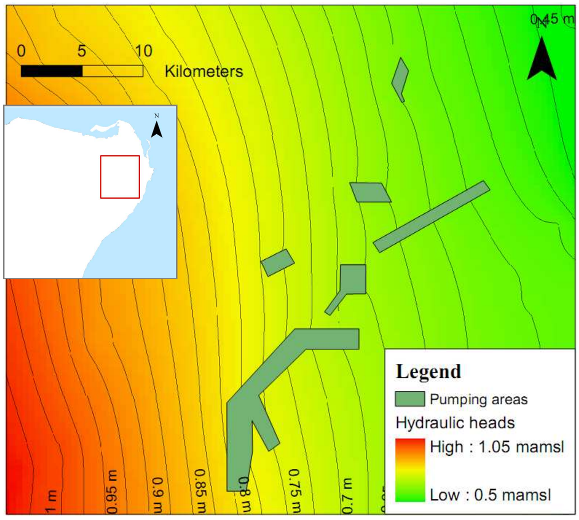

Scenario 4: 10 times of actual pumping rate

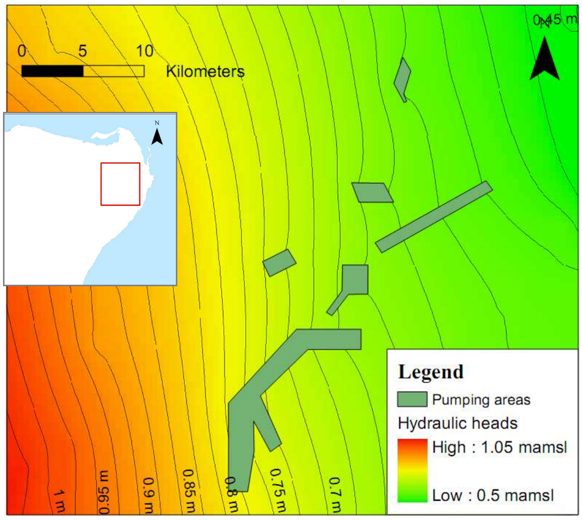

Figure 38: Scenarios with changes in pumping rates

3. Flow pattern in the peninsula

The technique of backward particle tracking permits to obtain flow lines in an aquifer. In this chapter all flow lines figures have been obtained by assigning particles at the coast and by performing a backward particle tracking simulation.

3.1.Flow pattern in the Yucatan peninsula

Figure 39 shows the overall flow pattern in the Yucatan peninsula.

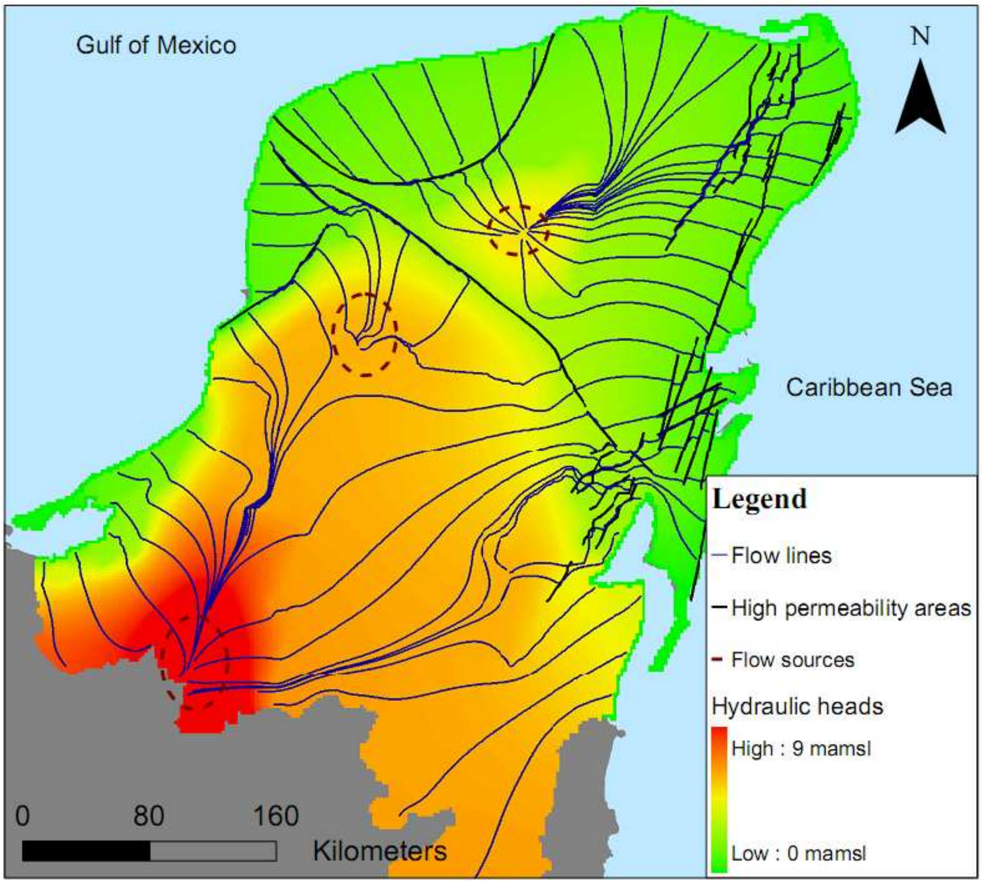

Figure 39: Flow pattern in the Yucatan peninsula

These flow lines point out the existence of three flow sources, corresponding to three local hydraulic heads maximum. The flows in the northern part of the peninsula originate from a flow source situated in the central-north of the peninsula (source 1). As it has been already described in the chapter F.2.1.4 (page 66), this hydraulic heads local maximum is mainly due to the combination of the Sierrita de Ticul fault and of the difference in hydraulic conductivity between zone P1 and P3.
The second flow source (source 2), which was not seen in Figure 32, originates from the difference of hydraulic conductivities between the zone P3 and P4 (respectively 0.029m/s and 1m/s). As this maximum is less marked than the two other flow sources, fewer flow

lines are coming from it. Finally the third source (source 3) is located on the south-western part of the peninsula and is the flow source of the majority of the flows in the south.

This flow pattern figure highlights the importance of the high permeability features in the shape of the flow lines. The most important high permeability areas (Holbox fracture, Sierrita de Ticul, Ring de Cenotes) are representing preferential flow paths.

A flow pattern in the Peninsula has also been made considering the Sierrita de Ticul fault zone as a low permeability area (Figure 41). It is interesting to see that the picture does not change significantly. The three different flow sources are still present (even if the source 2 is now located on the fault). The flow source situated in the north of the Peninsula concentrates more flows in this scenario. On the contrary the importance of the source 2, situated in the south west of the source 1, seems to be lower.

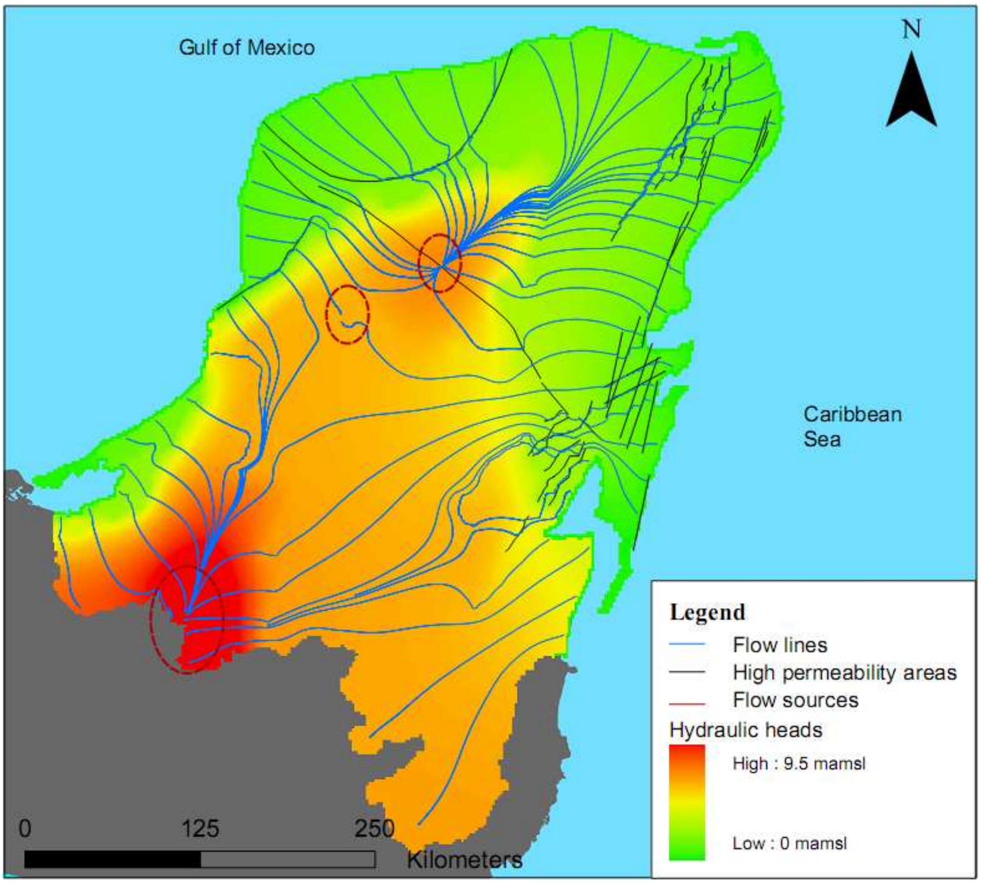

<u>Figure 40:</u> Flow pattern in the Yucatan Peninsula considering the Sierrita de Ticul as a Flow barrier

3.2. Flow pattern in the north of Quintana Roo

Figure 41 shows the flow pattern in the north-eastern part of the peninsula.

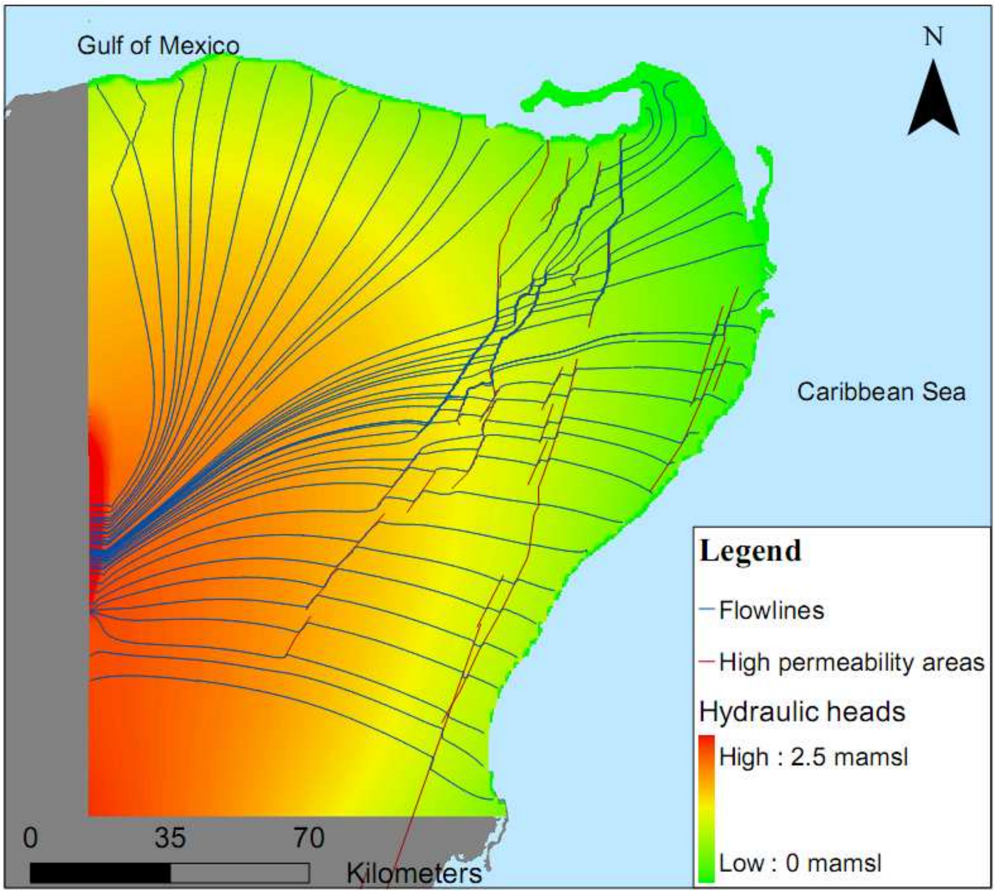

Figure 41: Flow pattern in the northern part of the peninsula

Figure 41 shows that the water is globally flowing from the western local hydraulic head maximum to the northern and eastern coasts.
The influence of the Holbox fracture is very important, but contrarily to some studies (Perry et al. 2002), except for the very southern part of the model area, there are no evidences of water flowing from the south to the north.
It is not surprising to see that the pumping wells do not have any influence on the general flow pattern as they do not have any influence on the hydraulic heads pattern.

4. Influence of the wells on the position of the saltwater/freshwater interface

When studying the influence of pumping wells in a coastal aquifer, it is important also to determine if the shape of the freshwater/saltwater interface is modified by the pumping of water. Bear et al. (1999), defined a relation between the pumping rate (Q) and the change in interface depth at the location of the well.

Figure 42 explains the different parameters of the problem.

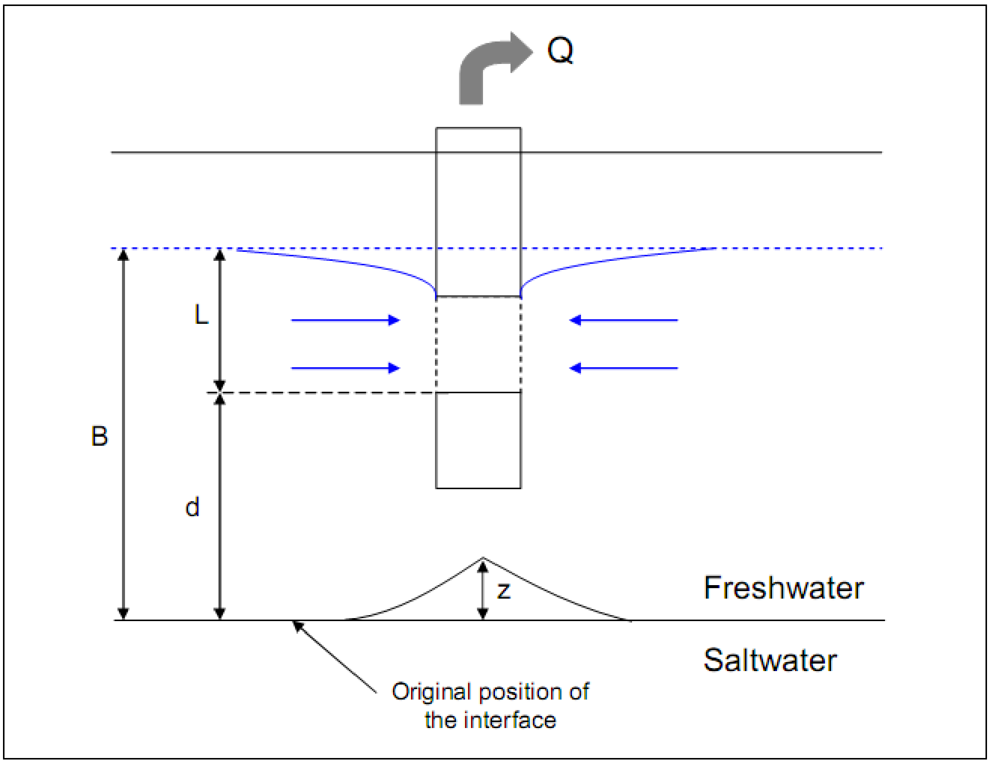

Figure 42: *Influence of the wells on the freshwater/saltwater interface*

Using the parameters defined in Figure 42, z is defined with the equation F.4.1.

$$z = \frac{Q \cdot \rho_w}{2\pi \cdot K \cdot d \cdot \Delta\rho}$$ **Equation F.4.1**

Where: *Q is the pumping rate ($L^3 \cdot T^{-1}$)*
K is the hydraulic conductivity ($L \cdot T^{-1}$)
d is the distance between the interface and the pumping depth (L)
$\Delta\rho$ is the difference of density between saltwater and freshwater($M \cdot L^3$)
ρ_w is the density of freshwater($M \cdot L^3$)

For a well not to be invaded by saltwater, z should be smaller than d and thus the maximum pumping rate (Q_{MAX}) can be calculated with the equation F.4.2 using the previous notations:

$$Q_{MAX} = 2\pi \cdot K \cdot d^2 \cdot \Delta\rho \qquad \textbf{Equation F.4.2}$$

Nevertheless in practice (for safety reasons), the value used for z_{max} is often equal to 0.3d (Bear et al., 1999). So Q_{MAX} in the rest of the calculations will be defined according to the equation F.4.3:

$$Q_{MAX} = 0.3 \cdot 2\pi \cdot K \cdot d^2 \cdot \Delta\rho \qquad \textbf{Equation F.4.3}$$

In the case of the wells supplying the water to Cancun, the depth of pumping (L) is not known. The depth to interface is in average B=36m in the pumping areas.
Figure 43 shows the value of z against the depth of pumping for the actual pumping rate (Q=13.38 L/s for a well) and in 4 different scenarios corresponding to pumping rates equal to 2.5, 5, 7.5 and 10 times the actual pumping rate.

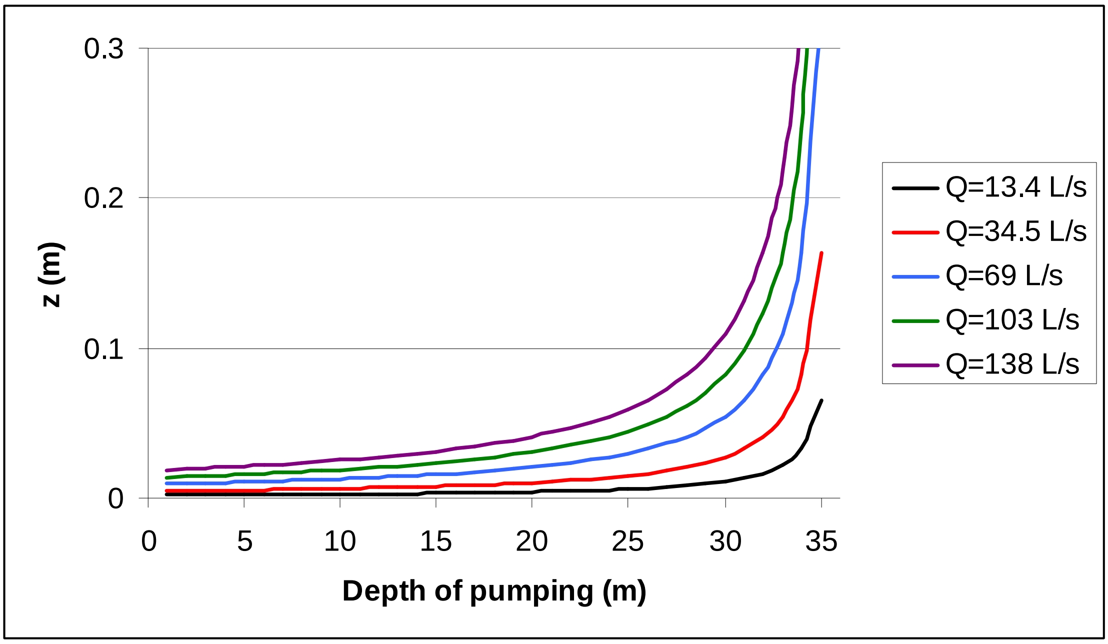

Figure 43: Acceptable pumping rates and pumping depth in order to avoid saltwater invasion in the well

It can be seen that the value of z is always less than 10 centimeters when the depth of pumping is below 30 meters. It means that the risk of contamination of extracted water by saltwater is very low. The situation of the pumping areas (not very close from the coast) and the current reasonable pumping rate prevent the wells from any risk of saltwater invasion.

5. Stochastic catchment study

5.1. *Implementation of the stochastic well catchment delineation*

5.1.1. *Determination of the set of inputs*

The stochastic well catchment study focused on the uncertainties of the four different hydraulic conductivities. These parameters have been defined during the calibration process and have high influence on the results. The samples have been generated using the procedure explained in chapter D.5.3 (page 48).

Figure 44 represents the set of values generated for a number of samples N=10000.

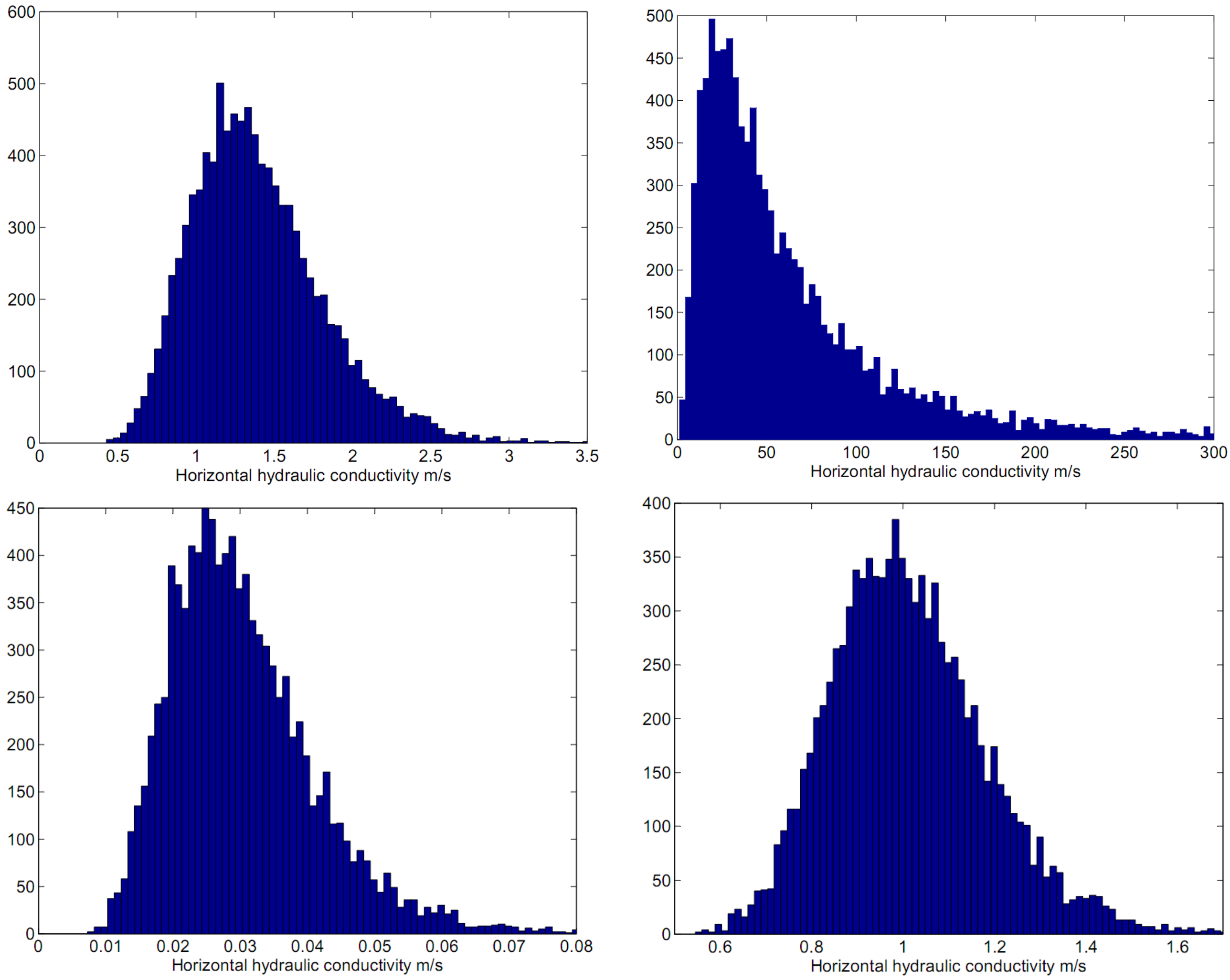

Figure 44: Probability distribution of the four parameters (P1, P2, P3, P4 from left to right and up to down)

5.1.2. Simulations

The models made in Modflow have been refined in 7 different layers as it is shown in Figure 45. Indeed Modpath do not take into consideration the vertical transport of particles when the model consists of one unconfined layer. The set of values generated with the Monte Carlo method is used to run N different simulations consecutively.
The values generated should be implemented in the input file of the flow simulation. The input file containing information on hydraulic conductivities is called “bcf.dat”. This file has to be rewrite for every simulation.
The programs Modflow and Modpath are then used consecutively and the output of modpath (pathline and endpoint files) is used to draw the well catchment.

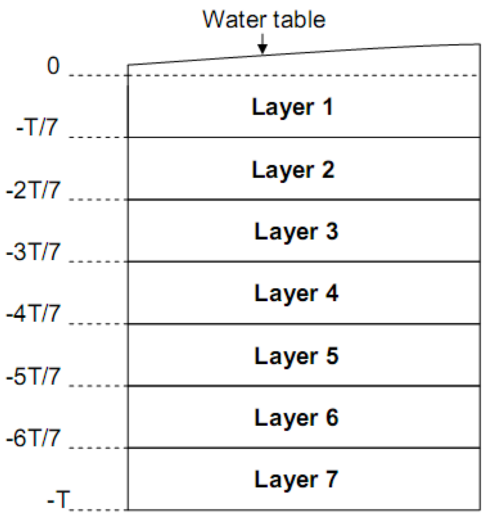

Figure 45: Discretization of the model in 7 layers. T represents the depth to saltwater/freshwater interface.

5.1.3. Results computation

A matrix representing the model grid is generated after each run. The values in the matrix represent cells of 500m × 500m. The value 1 is assigned to the cells which belong to the catchment and the value 0 is assigned to the other cells.
After the N runs, the N matrices that have been generated are summed and divided by the number of samples N. So the final matrix obtained represents the percentage of chances for a pixel to be part of the well catchment.

5.2. *Steady state well catchments*

Particles are assigned to the pumping areas and tracked backward. As the depth of pumping is not known, different situations have to be considered concerning the vertical location of the particles to be tracked. Three scenarios have been implemented assigning particles to different depths:

- Scenario 1 (T/14): particles are located at depth between -1.96m and -3.14m below mean sea level.
- Scenario 2 (3T/14): particles are located at depth between -5.88m and -9.42m below mean sea level.
- Scenario 3 (5T/14): particles are located at depth between -9.8m and -15.7m below mean sea level.

The number of simulations made to obtain the stochastic capture zones is N=100 in order to reduce the computational time. It has been seen that the steady state catchments do not change significantly when simulating for more than 100 runs.

It can be seen in Figure 46 that the wellhead catchment zones with particles assigned at depth equal to T/14 is rather stable. The changes in hydraulic conductivities do not lead to major changes in the shape of the delineated zone. This is probably due to the fact that the particles are not reaching any high permeability features (except in the very southern part of the capture zone).
On the contrary the shapes of the two other catchment areas are changing significantly in response to changes in hydraulic conductivities, especially du to the presence of high permeability areas.
The areas observed, in particular in the scenarios 2 and 3 are relatively large (corresponding for the 50 % probability to areas of respectively 680 km^2 and 820 km^2).

It has to be noted that the conduits have been mapped using SRTM data and previous studies, but their locations and descriptions are not precisely defined. Therefore it is not impossible to find in the reality conduits closer to the pumping areas than what we have modeled. In this case the scenario 1 would have given a less stable catchment zone.

The simple equivalent porous medium model, that we have chosen to represent the groundwater flow in the Yucatan aquifer, does not allow us to get realistic travel times because of the effective porosity evaluation. Therefore no time dependant protection zones have been delineated.

Stochastic well catchment zone with particles assigned at depth equal to T/14

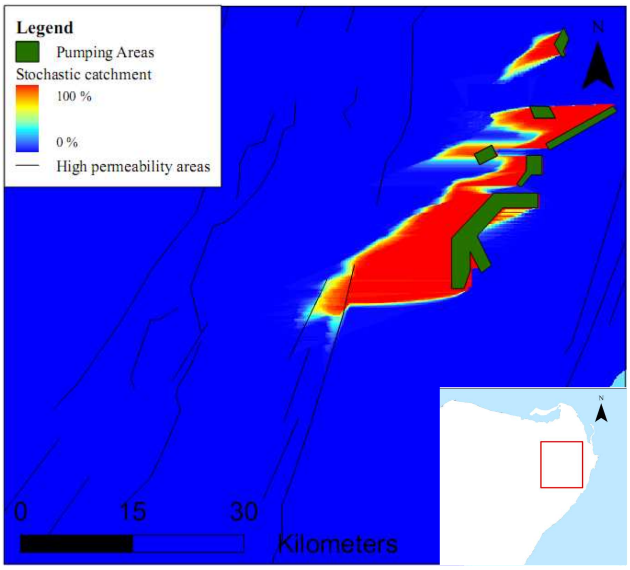

Stochastic well catchment zone with particles assigned at depth equal to 3T/14

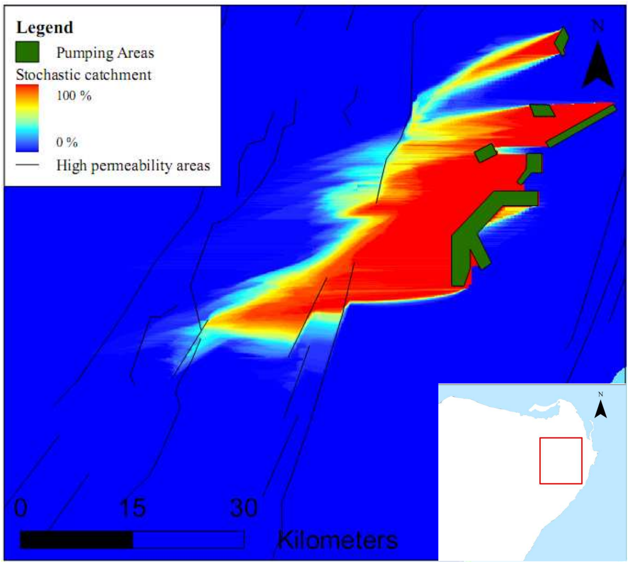

Stochastic well catchment zone with particles assigned at depth equal to 5T/14

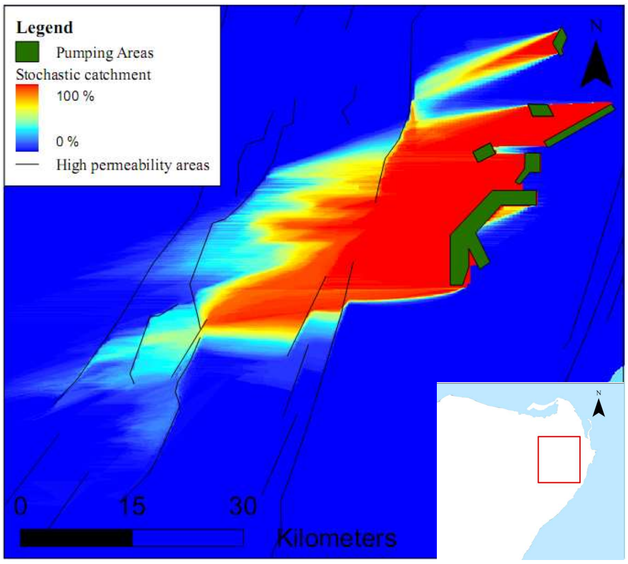

Figure 46: Steady state catchment for the 3 scenarios

G. DISCUSSIONS AND CONCLUSIONS

1. Discussion of the results

1.1.Groundwater flows at the scale of the Peninsula

In this study a hydrological model of the entire Yucatan peninsula has been made in order to investigate the flow pattern at this large scale. The flow simulations have brought to the light two main factors that highly influence the flow pattern.

On the one hand, high permeability areas, for which the calibration has assigned very high hydraulic conductivities (close to 50m/s), represent preferential flow paths. The shapes of the flow lines in their surroundings are also modified. This observation is especially true for the Sierrita de Ticul fault which seems to be the most important geological feature at the scale of the peninsula. This observation confirms the conclusions of Perry et al. (2002) who demonstrated that groundwater is flowing through this feature from the lake Chichancanab (located in the center of the Peninsula) to the western coast.

On the other hand, the important differencesin the hydraulic conductivities of the geological areas corresponding to the ages of Eocene and Paleocene (K=0.029m/s and K=1.00m/s respectively) are directly responsible for the presence of the three hydraulic head local maximums. (in fact the hydraulic head maximum situated in the north of the Sierrita de Ticul is not only due to this difference, but partly). This observation has to be taken carefully as the number of measurements available for the calibration of these two areas is low.

It is interesting to compare the two groundwater flow direction maps made for the Yucatan peninsula. Figure 47 has been obtained from the flow simulations made in this study and Figure 48 has been elaborated by local stakeholders, governmental organizations and non governmental organizations in a workshop organized by Amigos de Sian Ka´an in 2003.

First both maps show the presence of a groundwater flow divide in the south of the peninsula. Nevertheless in Figure 47, this divide is situated in the western part of the Peninsula (due to the presence of the Eocene geological formationin this zone). In Figure 48, it is located in the central part.

Secondly, some similarities concerning the flows in the area of the Sierrita de Ticul fault can be observed. In both cases there is a water divide located in the center of this fault; on the west side the water is flowing from east to west and, on the east side it is flowing from west to east. Nevertheless in the simulated map the direction of the flows in the north of the water divide is following the north to south axis. In Figure 48 the opposite situation is observed.

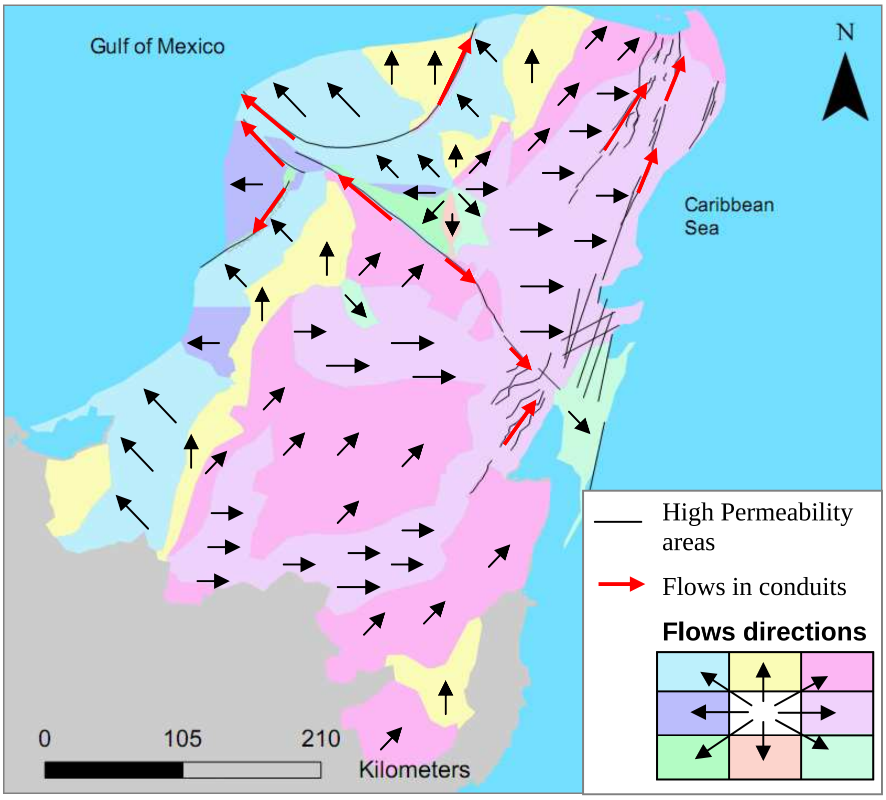

Figure 47: Simulated groundwater flow directions in the peninsula

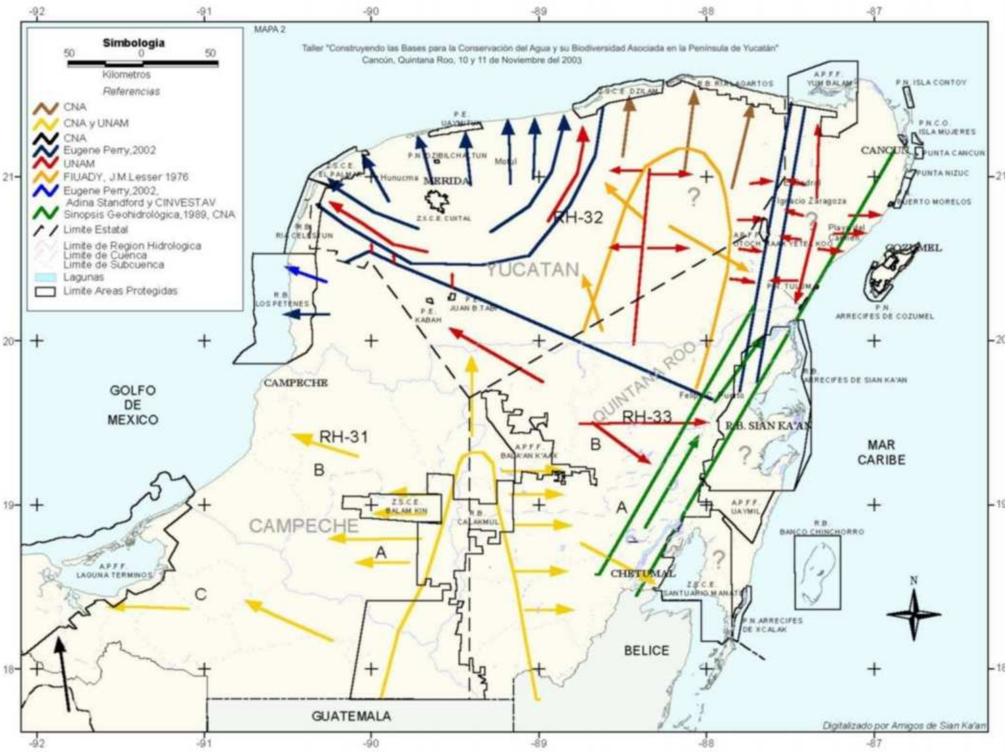

Figure 48: Flow pattern in the Peninsula elaborated in a workshop (ASK, 2003)

The comparison of the flow directions in the north-western part of the peninsula does not show significant differences. This may be due to the fact that the hydrological system in this area is relatively well known.

Finally concerning the zone of the Holbox fracture no evidence of north-south groundwater flows have been observed with the simulations made in this study. This contradicts the existence of a water flow divide in the center of the Holbox zone as it was stated in Figure 48.

1.2. *Groundwater flows in the north of Quintana Roo and influence of the pumping wells*

The hydrological model of the north-eastern part of the peninsula has shown that the water is globally flowing from south-west to north-east.

There are no flows from north to south except in the very southern part of the Holbox zone. This observation is of great importance considering that the Sian Ka´an Biosphere reserve is located in the south of this high permeability feature.

The simulations have also highlighted the importance of high permeability lineaments which represent preferential flow paths for the water flowing from south to north. This observation leads to important issues concerning the protection of the ecosystems situated in the north of the fracture zone (especially in the natural reserves of El Eden and Yum Balam).

The study seems to show that the actual characteristics of the pumping zones (locations and pumping rates) do not influence significantly the groundwater flow pattern of the north-eastern zone of the Peninsula. Additionally different scenarios have been simulated in order to see the impact of a potential increase of the volumes of water extracted and the flow lines appear to be significantly modified for pumping rates at least five times higher than the present ones.
Likewise it seems that the risk of contamination of drinking water by saltwater invasion into the wells is very small in the real situation.

Finally capture zones of the wells have been determined using a stochastic approach. This delineation has shown the impact of the pumping depth on the size of the capture zones. When the latter comprises high permeability features, their shapes become significantly more stretched (water flows along longer distances in the conduits than in the porous medium). As the standard deviation of the hydraulic conductivity in high permeability areas is high, the stability of these protection zones also depends on whether conduits features are situated in these areas or not.

2. Groundwater management possibilities with regards to the results

The two different hydrological models presented in this study, despite their uncertainties which will be further detailed, can support the elaboration of water management plans.

2.1. Groundwater management plans at the scale of the peninsula

The establishment of the map representing the groundwater flow patterns in the peninsula has confirmed that the high permeability features may lead to the existence of groundwater springs flowing through the entire peninsula. This demonstrates the necessity for the different states and municipalities to cooperate when designing groundwater management strategies.

The restriction on the volumes of water that can be extracted should be decided at the scale of the peninsula. The regions are interconnected and an excessive pumping in an up-gradient area leads to a significant decrease in the water volume for the down-gradient area (Younger, 2007).

The necessity of implementing management plans at the scale of the peninsula seems to be even more important to prevent groundwater pollution. Indeed the presence of flows in high permeability features leads to the possibility of contaminants spreading over large areas. In the case of pollutants released near underground conduits, the remediation is almost impossible considering the flow velocities.

A common strategy to protect heterogeneous aquifers from pollution is to established vulnerability maps (Polemio et al., 2009). This type of management plan has been defined and achieved in different countries and especially in Europe with the well known COST approach (COST, 2003). The basic principle of this method is to implement different levels of restrictions to the potential polluting activities according to the evaluation of the vulnerability of the location where they are located. In practice it means that polluting activities are highly restricted in the areas situated close to sinkholes or high permeability areas. The establishment of such maps for the Yucatan peninsula can be a useful tool to prevent pollution. It can be used to regulate existing activities in some sensitive locations but also to restrict the implementation of new potentially polluting activities in sensitive areas.

Finally the protection of the different natural reserves in the peninsula requires also a particular attention, especially concerning the coastal natural parks composed of large wetlands in direct interaction with groundwater. These protected reserves as well as the areas from where the groundwater comes should also be included in the groundwater management plans for the peninsula.

2.2. *Well field management plan in the north of Quintana Roo*

By looking at the results of the study, it seems that the volumes of water extracted today do not create significant drops in the water table elevations or changes in the shape of the freshwater/saltwater interface. Nevertheless it is important to regulate the extraction of water in order to avoid overexploitation of the aquifer in the coming years.

The diverse and important pollution threats present in the north-eastern part of the peninsula require the establishment of efficient water management plans in order to protect the wells supplying drinking water to Cancun.

Considering the high velocities of the groundwater in karstic aquifers, the entire steady state well capture zone should be protected. In practise this means that potentially polluting activities should be strictly restricted in these areas. Nevertheless as it has been seen in the study, these areas are large and situated close to Cancun. Therefore it is challenging to prohibit any threatening activity.
The previous chapter has described the method for establishing vulnerability maps for a karstic aquifer.

Taking into account the specificities of the aquifer, the following considerations might be included in the establishment of an efficient well field management plan:

- Regulation of the maximum groundwater volume extracted in order to ensure the sustainability of the aquifer.

- Establishment of a vulnerability map of the protection zones. Beforehand an extensive determination of the location of sinkholes and conduits should have been conducted. In the most sensitive locations a complete prohibition of polluting activities is required.

- Evaluation of the risk of pollution represented by the different types of activities in the capture zones. This classification should lead to the total prohibition of the most polluting activities (eg. landfills, industrial activities with discharge of liquid waste…) in the entire protection zone and a strong regulation concerning the other activities.

- Regular monitoring of water quality in wells as well as regular inspections at the locations of the different polluting activities classified before.

3. Conclusion

The hydrological model of the entire Yucatan penisula has allowed to characterize the hydraulic heads distribution and groundwater flow pattern in the region. The hydraulic conductivities in this numerical model have been calibrated in the different geological areas using water table elevation data. The limited fit between simulated and observed hydraulic heads has shown the difficulties of the implementation of a simple model for a large heterogeneous aquifer. Nevertheless several important outcomes have been found.

First the differences in the calibrated hydraulic conductivities of the geological areas are of great importance in the results. The three local hydraulic heads maximums originate partly or completely from this factor. However this result has to be taken carefully as the water table elevations used for the determination of hydraulic conductivities are mainly located in only one geological area.

The second observation that can be made based on the results of the large model is the influence of the high permeability features. The latter represent preferential flow paths inside which water flows along long distances. The direct consequence of this outcome is the need for implementing groundwater management plans at the scale of the peninsula. The different regions are interconnected and thus pollution can spread rapidly in large areas.

The equivalent porous medium model implemented for the north-eastern part of the peninsula has not been calibrated, but used the results found in the calibration of the large model. The regional groundwater flow system is believed to be highly influenced by the Holbox fracture zone. Water is flowing from south to north in its lineaments. No evidences of groundwater flow divide in the center of the high permeability zone have been found. Indeed it can be considered that no water originating from the north of Quintana Roo ends in the Sian Ka'an Biosphere. On the contrary the natural reserves situated near the north coastline (Yum Balam and El Eden reserve) receive high groundwater volumes coming from the entire north-eastern part of the peninsula.

The influence on the groundwater resources of the extraction wells located close to Cancun can not be considered as very important in the current situation. Scenarios performed using higher pumping rates have shown that the hydraulic heads distribution is modified significantly if water extraction exceeds 10,000 L/s in the pumping areas. The wells do also not have any major influence on the shape of the freshwater/saltwater interface.

Finally a stochastic delineation of the well protection zone has been made using Monte Carlo methods. The capture zone is large, but its size depends highly on the depth of pumping (which is not known). Different scenarios have been simulated for different pumping depths. The catchments obtained are stable as long as they do not comprise any high permeability features. Indeed the important standard deviation of the calibrated hydraulic conductivity in fractures leads to a lower stability of the capture zones when water is partly flowing in conduits. The protection of these areas require establishment of restrictive regulations for polluting activities. The use of vulnerability maps for the capture zone has been proposed as a basis for implementing efficient legislations.

4. Further work

The work presented here has led to the development of the first hydrological model of the entire peninsula and the first regional hydrological model of the north of Quintana Roo. The two models are representing first steps in the understanding of the groundwater flow pattern but further work (in terms of data acquisition and modeling improvements) is needed to confirm the results highlighted and to fill the gaps that have been seen.

The current data have not allowed to perform a proper calibration of the Yucatan Peninsula model. Water table elevations are especially needed in the central and southern part of the Peninsula where only 6 measurements are available. This will allow a better determination of the hydraulic conductivities and thus will narrow the location of the local hydraulic head maximums.
A better delineation of the different zones of hydraulic conductivities will also be an important step in the improvement process. Investigations on soil samples and additional geological studies have to be made.
The mapping of the high permeability features, based on remote sensing data so far, can be significantly improved by means of airborne electromagnetics (Supper et al., 2009). This is especially important for determining precise groundwater flow pattern at a regional scale. In particular, it will lead to a more detailed determination of the groundwater flow pattern in the Holbox zone and thus to a more clear delineation of Cancun's well head capture zone. Identification of water springs discharge locations and determination of their discharge flow rates can represent other information to correct the models.
Finally a characterization of the freshwater lens thickness is needed to evaluate the water resource magnitude. In the model the Ghyben Herzberg relation was used, nevertheless the validity of this formula has not been strongly assessed.

Modeling improvements can also be made. The seasonal variability has not been studied in these simulations. It is supposed to be important due to the high permeability of the aquifer. The impacts of extreme rain events like hurricanes can also be studied.
At a regional scale, the implementation of a dual flow model can lead to a beter modeling of the aquifer's heterogeneities.

References

AGUAKAN (2008), Electrical conductivity profiles measured in different monitoring wells of Aguakan. Data given personally by Ing. Rodriguez.

Alcocer J. and Escobar E. (1996), *Limnological regionalization of Mexico*. Lakes Reserv.Resources Management, 2, 55-69.

Allen R.G., Perreira L.S., Raes D., and Smith M. (1998), *Crop Evapotranspiration (guidelines for computing crop water requirements)*. FAO irrigation and drainage paper, 56.

Andreo, B., Goldscheider, N., Vadillo, I., Vias, J. M., Neukum, C., Sinreich, M., Jimenez, P., Brechenmacher, J., Carrasco, F., Hotzl, H., Perles, M. J., and Zwahlen, F. (2006), *Karst groundwater protection: First application of a Pan-European Approach to vulnerability, hazard and risk mapping in the Sierra de Libar (Southern Spain)* . Science of the Total Environment, 357, 54-73.

ASCE (American Society of Civil Engineers) (2000), *NAVSTAR global positioning system surveying*. ASCE Press.

ASK (2003), *Tratamiento de Aguas Residuales*. Report prepared by Amigos de Sian Ka'an A. C. Document from the cd-rom of the workshop: Construyendo las Bases Para la Conservación del Agua y su Biodiversidad Asociada en la Península de Yucatan". 10 y 11 de noviembre 2003, Cancún Quintana Roo, Organizado por Amigos de Sian Ka'an, The Nature Conservancy y la Comisión de Áreas Naturales rotegidas.

Aster R.C., Thurber C.H., and Borchers B. (2005), *Parameter estimation and inverse problems*. Published by Elsevier Inc.

Atkinson, T. C. (1977), *Diffuse Flow and Conduit Flow in Limestone Terrain in Mendip Hills, Somerset (Great-Britain)*. Journal of Hydrology, 35, 93-110.

Back W. and Hanshaw B.B. (1970), *Comparison of chemical hydrogeology of the carbonate Peninsulas of Florida and Yucatan*. Journal of Hydrology, 10, 330-368.

Bahremand, A. and De Smedt, F. (2008), *Distributed hydrological modeling and sensitivity analysis in Torysa watershed, Slovakia*. Water Resources Management, 22, 393-408.

Bear and Jacob (1965), *On the movement of water bodies injected into aquifers*. Journal of Hydrology, 3.

Bear J., Sorek S., and Ouazar D. (1999), *Seawater intrusion in coastal aquifers: concepts, methods, and practices*. Kluwer academic publishers.

Bear, J. and Bensabat, J. (1989), *Advective Fluxes in Multiphase Porous-Media Under Non-Isothermal Conditions*. Transport in Porous Media, 4, 423-448.

Beddows P.A. (2003), *Cave Hydrology of the Carribean Yucatan Coast*. Association for Mexican Cave studies - AMCS - Bulletin 11.Reformatted and slightly revised version of the M.Sc.thesis by the same author from McMaster University, Canada, 1999.Austin, Texas.2003.

Beddows P.A. (2004), *Groundwater hydrology of a Coastal Conduit Aquifer: Caribbean Coast of the Yucatan Peninsula, Mexico. Phd Thesis*. School of Geographical Sciences, University of Bristol.

Beddows P.A., Hendrickson M.R., Webster K.H., and Kras S.M. (2007), *Mapping flooded caves from above: surface karst inventory of the Yucatan Peninsula*. National Cave and karst Management Symposium, 193-197.

Bonacci, O., Ljubenkov, I., and Roje-Bonacci, T. (2006), *Karst flash floods: an example from the Dinaric karst (Croatia)*. Natural Hazards and Earth System Sciences, 6, 195-203.

Carlson, T. (2007), *An overview of the "triangle method" for estimating surface evapotranspiration and soil moisture from satellite imagery*. Sensors, 7, 1612-1629.

Cheng, J. M. and Chen, C. X. (2005), *An integrated linear/non-linear flow model for the conduit-fissure-pore media in the karst triple void aquifer system*. Environmental Geology, 47, 163-174.

CNA (Comisiòn Nacional del Agua, Servicio Meteorologico Nacional) (2008), Climate data. Data collected in the field by S. Lerrer.

Connors, M., Hildebrand, A. R., Pilkington, M., OrtizAleman, C., Chavez, R. E., UrrutiaFucugauchi, J., GranielCastro, E., CamaraZi, A., Vasquez, J., and Halpenny, J. F. (1996), *Yucatan karst features and the size of Chicxulub crater*. Geophysical Journal International, 127, F11-F14.

Cornaton, F. and Perrochet, P. (2002), *Analytical 1D dual-porosity equivalent solutions to 3D discrete single-continuum models. Application to karstic spring hydrograph modelling*. Journal of Hydrology, 262, 165-176.

COST (2003), *Vulnerability and risk mapping for the protection of carbonate (karst) aquifers*, European Commission,Directorate-General for Research, Report EUR 20912, Luxemburg.

Curtis, J. H., Brenner, M., Hodell, D. A., Balser, R. A., Islebe, G. A., and Hooghiemstra, H. (1998), *A multi-proxy study of Holocene environmental change in the Maya lowlands of Peten, Guatemala*. Journal of Paleolimnology, 19, 139-159.

Doehring, D. O. and Butler, J. H. (1974), *Hydrogeologic Constraints on Yucatans Development* . Science, 186, 591-595.

Doherty, J. (1994) *PEST Model-Independant parameter estimation, user manual*. Watermark numerical modelling.

Ebbing, J., Janle, P., Koulouris, J., and Milkereit, B. (2001), *3D gravity modelling of the Chicxulub impact structure*. Planetary and Space Science, 49, 599-609.

El Rabbany A. (2002), *Introduction to GPS: the Global Positioning System*. Artech house, inc.

FAO (Food and Agriculture Organization of the United Nations (1997), *Seawater intrusion in coastal aquifers, Guidelines for study, monitoring and control*. FAO 1997.

Farrell J. and Barth M. (1999), *The global positioning system and inertial navigation*. Mc Graw-hill companies.

Fetter C.W. (2001), *Applied Hydrogeology*. Pearson Education International, Prentice-Hall, Inc.Upper Saddle River, New Jersey 07458.

Fishman G.S. (1995), *Monte Carlo: concepts, algorithms, and applications*. Springer-Verlag New York Inc.

Fleury, P., Bakalowicz, M., and de Marsily, G. (2007), *Submarine springs and coastal karst aquifers: A review*. Journal of Hydrology, 339, 79-92.

Ford D.C. and Williams P.W. (2007), *Karst hydrogeology and geomorphology*. John Wiley & Sons.562pp.

Franssen, H. J. H., Stauffer, F., and Kinzelbach, W. (2004), *Joint estimation of transmissivities and recharges - application: stochastic characterization of well capture zones*. Journal of Hydrology, 294, 87-102.

Franzetti, S. and Guadagnini, A. (1996), *Probabilistic estimation of well catchments in heterogeneous aquifers*. Journal of Hydrology, 174, 149-171.

Fratini C. (2007), *Field surveys in the Yucatan Peninsula, Mexico-Special Course Report*. Institute for Environment and Resources, Technical University of Denmark.

Ginsberg M. and Palmer A. (2002), *Delineation of sourcewater protection areas in karst aquifers of the Ridge and Valley and Appalachian Plateaus Physiographic Provinces*. United Sates Environmental protection agency (EPA).

Gonzalez-Herrera, R., Pinto, I., and Gamboa-Vargas, J. (2002), *Groundwater-flow modeling in the Yucatan karstic aquifer, Mexico*. Hydrogeology Journal, 10, 539-552.

Gopi S. (2005), *Global Positioning System: Principles And Applications*. Tata Mc Graw-Hill.

Guha, H. (2008), *A stochastic modeling approach to address hydrogeologic uncertainties in modeling wellhead protection boundaries in karst aquifers*. Journal of the American Water Resources Association, 44, 654-662.

Guochang Xu (2003), *GPS: theory, algorithms, and applications*. Springer.

Haitjema H.M. (1995), *Analytic element modeling of groundwater flow*. Academic Press, INC.

Hansen N. (2008), *The CMA Evolution Strategy: A Tutorial*. Technical University of Berlin, accessed on URL: www.bionik.tu-berlin.de/user/niko/cmatutorial.pdf in september 2009.

Hargreaves, G. H. and Allen, R. G. (2003), *History and evaluation of Hargreaves evapotranspiration equation*. Journal of Irrigation and Drainage Engineering-Asce, 129, 53- 63.

Hatzopoulos J.N. (2008), *Topographic mapping: covering the wider field of geospatial information*. Universal publishers.Boca Raton, Florida.

Hill M.C. and Tiedeman C.R. (2007), *Effective groundwater model calibration: with analysis of data, Sensitivities, Predictions and Uncertainty*. John Wiley & Sons.

Holmbeck-Pelham, S. A., Rasmussen, T. C., and Fowler, L. A. (2000), *Regulation of injected ground water tracers*. Ground Water, 38, 541-549.

Hornberger G.M., Raffensperger J.P., Wiberg P.L., and Eshleman K.N. (1998), *Elements of physical hydrology*. Baltimore: Johns Hopkins University Press, 302p.

ILWIS (2007), ILWIS 3.3 Academic. International Institute for Geo-Information Science and Earth Observation (ITC). Unit Geo Software Development (GSD), Sector Remote Sensing & GIS (RSG). Software for Remote sensing and GIS.

INEGI (2005), Website of Instituto Nacional de Estadistica Geografia e Informatica (INEGI) displaying general data for the different states of Mexico. Accessed on URL: http://www.inegi.org.mx.

Ingebritsen S., Sanford W., and Neuzil C. (2006), *Groundwater in geologic processes - Second edition*. Cambridge 536p.

Kinsland, G. L., Hurtado, M., and Pope, K. O. (2000), *Detection of groundwater conduits in limestones with gravity surveys: Data from the area of the Chicxulub Impact Crater, Yucatan Peninsula, Mexico*. Geophysical Research Letters, 27, 1223-1226.

Kinzelbach, W., Marburger, M., and Chiang, W. H. (1992), *Determination of Groundwater Catchment Areas in 2 and 3 Spatial Dimensions*. Journal of Hydrology, 134, 221-246.

Kresic N. (2007), *Hydrogeology and groundwater modeling-second edition*. CRC Press, Taylor & Francis group.

Larocque, M., Banton, O., Ackerer, P., and Razack, M. (9-19-0099), *Determining karst transmissivities with inverse modeling and an equivalent porous media*. Ground Water, 37, 897-903.

Leibundgut C., Gunn J, and Dassargues A. (1998), *Karst hydrology*. IAHS Publication, 247.

Lerner, D. N. (1992), *Well Catchments and Time-Of-Travel Zones in Aquifers with Recharge*. Water Resources Research, 28, 2621-2628.

Lerrer S. and . (2008), *Estimation of actual evapotranspiration using remote sensing data for the Yucatan Peninsula, Mexico* . Institute of Environment & Resources, Technical University of Denmark.

Limpert, E., Stahel, W. A., and Abbt, M. (2001), *Log-normal distributions across the sciences: Keys and clues*. Bioscience, 51, 341-352.

Madsen K, Nielsen H.B., and Tingleff O. (2004), *Methods for non linear least squares problems*. Informatics and mathematical modelling, Technical university of Denmark.

Marin L.E. (1990), *Field investigations and numerical simulation of Ground-Water flow in the karstic aquifer of Northwestern Yucatan, Mexico, Phd Thesis*. Department of Geology, Northern Illinois University.

MATLAB (2008), Matlab v7.7 The language of technical computing. The mathworks inc.

McDonald M.G. and Harbaugh A.W. (1988), *A modular three-dimensional finite difference ground-water flow model*. US Geological survey (USGS).

Mcwhorter D.B. and Sunada D.K. (1977), *Ground-Water hydrology and hydraulics*. Water resources publications.

Mendez Ramos R. (1991), *Modelo de Comportamiento del Acuifero de la ciudad de Merida, Yucatan*. Comision Nacional del Agua, Gerencia Estatal Yucatan, Subgerencia de Administracion del Agua, Merida, Yucatan, Mexico.

Milanovic P.T. (2004), *Water Resources Engineering in Karst*. CRC Press.Boca Raton.

MODFLOW-96 US Geological survey (2000), Modflow 96 v3.3, Modular three-dimensional finite-difference ground-water flow model.

MODPATH, US Geological Survey (2000), Modpath v3.2, A particle-tracking postprocessor model for MODFLOW.

Moon (2009), Map of the Yucatan Peninsula. Accessed on URL: http://www.moon.com/maps?filter0=11413&apage=Y in September 2009.

Moore, C. and Doherty, J. (2006), *The cost of uniqueness in groundwater model calibration*. Advances in Water Resources, 29, 605-623.

Moore, Y. H., Stoessell, R. K., and Easley, D. H. (1992), *Fresh-Water Sea-Water Relationship Within A Groundwater-Flow System, Northeastern Coast of the Yucatan Peninsula*. Ground Water, 30, 343-350.

Morgan, J., Warner, M., Brittan, J., Buffler, R., Camargo, A., Christeson, G., Denton, P., Hildebrand, A., Hobbs, R., Macintyre, H., Mackenzie, G., Maguire, P., Marin, L., Nakamura, Y., Pilkington, M., Sharpton, V., Snyder, D., Suarez, G., and Trejo, A. (1997), *Size and morphology of the Chicxulub impact crater*. Nature, 390, 472- 476.

NASA (2008), Specification sheet for Modis. Accessed on URL: http://modis.gsfc.nasa.gov/about/specifications.php in September 2009.

Neal R.M. (1993), *Probabilistic Inference Using Markov Chain Monte Carlo Methods*. Technical Report CRG-TR-93-1, Department of computer science, University of Toronto.

Neuman B.R. and Rahbeck M.L. (2006), *Modeling Concepts for the Sustainable Management of the Sian Ka'an Biosphere Reserve, Quintana Roo, Mexico.* Institute of Environment & Resources, Technical University of Denmark..

Neuman B.R. (2007), *GPS for Groundwater Modeling-Special Course Report*. Institute for Mathematical Modeling , Technical University of Denmark..

Niell, A. E. (1996), *Global mapping functions for the atmosphere delay at radio wavelengths*. Journal of Geophysical Research-Solid Earth, 101, 3227-3246.

Oosterbaan R.J. and Nijland H.J. (1994), *Determination of the Saturated Hydraulic conductivity.* In: H.P. Ritzema (ed.) *Drainage Principles and Applications-chapter12*. ILRI Publication 16, International Institute for Land Reclamation and Improvement, Wageningen, The Netherlands, 435-476.

Parise M. and Gunn J. (2007), *Natural and anthropogenic hazards in karst areas: recognition, analysis and mitigation*. Geological Society, special publication 279.

Perry, E., Swift, J., Gamboa, J., Reeve, A., Sanborn, R., Marin, L., and Villasuso, M. (1989), *Geologic and Environmental Aspects of Surface Cementation, North Coast, Yucatan, Mexico*. Geology, 17, 818-821.

Perry, E., Velazquez-Oliman, G., and Marin, L. (2002), *The hydrogeochemistry of the karst aquifer system of the northern Yucatan Peninsula, Mexico*. International Geology Review, 44, 191-221.

Perry, E., Paytan, A., Pedersen, B., and Velazquez-Oliman, G. (2009), *Groundwater geochemistry of the Yucatan Peninsula, Mexico: Constraints on stratigraphy and hydrogeology*. Journal of Hydrology, 367, 27-40.

PEST Pest v4.1, Model independant Parameter estimaion. Watermark numerical computing.

Polemio, M., Casarano, D., and Limoni, P. P. (2009), *Karstic aquifer vulnerability assessment methods and results at a test site (Apulia, southern Italy)*. Natural Hazards and Earth System Sciences, 9, 1461-1470.

Pollock D.W. (1994), *User guide for Modpath/Modpath plot version 3*. US Geological Survey.

Pope, K. O., Ocampo, A. C., and Duller, C. E. (1993), *Surficial Geology of the Chicxulub Impact Crater, Yucatan, Mexico*. Earth Moon and Planets, 63, 93-104.

Pope, K. O., Ocampo, S. C., Kinsland, G. L., and Smith, R. (1996), *Surface expression of the Chicxulub crater*. Geology, 24, 527-530.

Reeve A. and Perry E.C. (1990), *Aspects and tidal analysis along the western north coast of the Yucatan Peninsula, Mexico.* WRA: International Symposium on Tropical Hydrogeology, 23-27 July 1990, San Juan, Puerto Rico.

Riva, M., Guadagnini, A., and Ballio, F. (1999), *Time-related capture zones for radial flow in two dimensional randomly heterogeneous media*. Stochastic Environmental Research and Risk Assessment, 13, 217-230.

Rosencrantz, E. (1990), *Structure and Tectonics of the Yucatan Basin, Caribbean Sea, As Determined from Seismic-Reflection Studies*. Tectonics, 9, 1037-1059.

Rzedowski J. (2006), *La vegetacion de Mexico*. Ediciòn digital, Comision Nacional para el conocimiento y Uso de la Biodiversidad, Mexico, 504pp.

Scanlon, B. R., Mace, R. E., Barrett, M. E., and Smith, B. (2003), *Can we simulate regional groundwater flow in a karst system using equivalent porous media models? Case study, Barton Springs Edwards aquifer, USA*. Journal of Hydrology, 276, 137-158.

Schmitter-Soto, J. J., Comin, F. A., Escobar-Briones, E., Herrera-Silveira, J., Alcocer, J., Suarez-Morales, E., Elias-Gutierrez, M., Diaz-Arce, V., Marin, L. E., and Steinich, B. (2002), *Hydrogeochemical and biological characteristics of cenotes in the Yucatan Peninsula (SE Mexico)*. Hydrobiologia, 467, 215-228.

Schmoll O., Howard G., Chilton J., and Chorus I. (2006), *Protecting groundwater for health: managing the quality of drinking-water Sources*. World Health organization, IWA publishing, London-Seattle.

Schönian F, Tagle R., Stöffler D., and Kenkmann T (2005), *Geology of Southern Quintana Roo (Mexico)and the Chicxulub Ejecta Blanket*. Abstract#2389, in: 36th Lunar and Planetary Science conference, March 2005, League city.Lunar and Planetary Institute, Houston,

SEDETUR (2009), Secretaria de Turismo del Estado de Quintana Roo, accessed on URL: http://www.caribemexicano.gob.mx/ in september 2009.

Segol, G. and Pinder, G. (1975), *Transient Simulation of Saltwater Intrusion in Southeastern Florida*. Transactions-American Geophysical Union, 56, 980-980.

SGM (2007), Carta geológica de México. Escala 1:2,000,000. 6a edición. Servicio Geológico Mexicano (SGM).

Smart P.L., Beddows P.A., Coke J., Doerr S., Smith S., and Whitaker F.F. (2006), *Cave development on the Caribbean coast of the Yucatan Peninsula, Quintana Roo,Mexico*. Geological Society of America.Special Paper., 404.

Soon, B. K. H., Scheding, S., Lee, H. K., Lee, H. K., and Durrant-Whyte, H. (2008), *An approach to aid INS using time-differenced GPS carrier phase (TDCP) measurements*. Gps Solutions, 12, 261-271.

Spitz K and Moreno J. (1996), *A practical guide to groundwater and solute transport modeling*. John Wiley & Sons.

Springer, A. E. and Bair, E. S. (1992), *Comparison of Methods Used to Delineate Capture Zones of Wells .2. Stratified-Drift Buried-Valley Aquifer*. Ground Water, 30, 908-917.

Stauffer, F., Guadagnini, A., Butler, A., Franssen, H. J. H., Van den Wiel, N., Bakr, M., Riva, M., and Guadagnini, L. (2005), *Delineation of source protection zones using statistical methods*. Water Resources Management, 19, 163-185.

Steinich, B. and Marin L.E. (1997), *Determination of Flow characteristics in the aquifer of the Northwestern Peninsula of Yucatan, Mexico*. Journal of Hydrology, 191, 315- 331.

Stewart B.A. and Howell T.A. (2003), *Encyclopedia of water science*. Marcel Dekker, Inc..

Supper R., Motschka K., Ahl A., Bauer-Gottwein P., Gondwe B., Merediz Alonso G., Römer A., Ottowitz D., and Kinzelbach, W. (2009), *Spatial mapping of submerged cave systems by means of airborne electromagnetics: an emerging technology to support protection of endangered karst aquifers*. Near Surface Geophysics, 7, 613-627.

Trimble® Navigation Limited, 1999-2007 Trimble® Data Transfer Software. Heidi Hofmann, Legal Department Trimble Navigation Limited, 935 Stewart Drive, Sunnyvale, CA 94085 Web site: http://www.trimble.com.

Tulaczyk S.M., Perry E.C., Duller C.E., and Villaluso M. (1993), *Influence of the Holbox fracture zone on the karst geomorphology and hydrogeology of northerm Quintana Roo, Yucatan Peninsula, Mexico*. Applied karst Geology, Beck (ed.), 181-188.

USGS (2004), Seamless Shuttle Radar Topography Mission (SRTM) "finished" 3 Arcsecond (~90meter). Online document. Accessed on URL: http://seamless.usgs.gov/website/seamless/products/srtm3arc.asp in February 2009.

Valero A., Schipper J., and Alnutt T. (2009), *Yucatan Dry forests*. Unreviewed document.Accessed on URL: http://www.worldwildlife.org/wildworld/profiles/terrestrial/nt/nt0235_full.html in September 2009.

Vassolo, S., Kinzelbach, W., and Schafer, W. (1998), *Determination of a well head protection zone by stochastic inverse modelling*. Journal of Hydrology, 206, 268-280.

Villaluso M.J. and Ramos R.M. (2000), *A conceptual model of the aquifer of the Yucatan peninsula.* Chapter 6 in: Lutz, W., Priesto, L., Sanderson, W. (Eds.) (2000), *Population, development and environment on the Yucatan Peninsula: From Ancient Maya to 2030.* International Institute for Applied Systems Analysis.Vienna.Austria.

Villaluso M.J. (2007), *Informe Final Estudio Geohidrologico Predio Excelence, Quintana Roo, México*.

White, W. B. (2002), *Karst hydrology: recent developments and open questions*. Engineering Geology, 65, 85-105.

Wolff, D. B., Marks, D. A., Amitai, E., Silberstein, D. S., Fisher, B. L., Tokay, A., Wang, J., and Pippitt, J. L. (2005), *Ground Validation for the Tropical Rainfall Measuring Mission (TRMM)*. Journal of Atmospheric and Oceanic Technology, 22, 365-380.

Worthington, S. R. H. (1993), *Fresh-Water Sea-Water Relationship Within A Groundwater-Flow System, Northeastern Coast of the Yucatan Peninsula - Discussion*. Ground Water, 31, 321-321 .

Yeh G. (2000), *Computational subsurface hydrology: reactions, transport, and fate*. Library of Congress Cataloging-in-Publication data by Kluwer academic publishers.

Younger (2007), *Groundwater in the environment: an introduction*. Blackwell Publishing Ltd..

Appendixes

Appendix 1: Illustration of the Holbox fracture zone 2
Appendix 2: Water table elevation measurements... 4
Appendix 3: Field measurement locations description 6
Appendix 4: Electrical conductivity profiles 12
Appendix 5: Matlab script for the stochastic catchment study 15

Appendix 1: Illustration of the Holbox fracture zone

This appendix displays pictures taken during the field trip and showing evidences of the presence of the elongated flat bottomed swales.

Wetland in an elongated swale (10 km in the east of San Angel)

Elongated swale with grass and short palms surrounded by forest (20 km in the east of San Angel)

Appendix 2: Water table elevation measurements

Number	Date	Location	GPS Coordinates N	E	Water level [m]	Elevation of cross at well (H) (=h-N) [mamsl]	final water table elevation [mamsl]
1	6-Apr-09	Leona Vicario	20°59'14.85" N	87°12'14.94" W	5.670	6.731	1.1
2	7-Apr-09	Cenote 7 bocas	20°52'35.51" N	87°02'37.56" W	4.410	5.395	1.0
3	8-Apr-09	Ranch de la dama y del caballero	21°05'05.09" N	87°05'24.70" W	8.100	9.179	1.1
4	8-Apr-09	Ranch la calandaria	21°09'50.88" N	87°05'22.33" W	7 .810	9.115	1.3
5	13-Apr-09	El Delirios	20°50'52.37" N	87°13'24.22" W	11.550	12.303	0.8
6	13-Apr-09	Agua Azul	20°51'26.67" N	87°19'33.43" W	4.740	5.767	1.0
7	14-Apr-09	La granja	20°48'00.58" N	87°19'45.96" W	8.870	9.905	1.0
8	14-Apr-09	Valladolid nueva	20°56'37.99" N	87°19'23.62" W	3.51 5	4.741	1.2
9	14-Apr-09	Victoria	20°47'27.40" N	87°16'46.44" W	9.590	10.579	1.0
10	15-Apr-09	Chulutan	20°34'03.12" N	87°57'45.56" W	20.530	22.434	1.9
11	15-Apr-09	Felipe Carillo	20°29'43.65" N	87°52'04.95" W	18.050	19.764	1.7
12	15-Apr-09	Xalau	20°40'25.35" N	88°00'24.04" W	20.530	22.845	2.3
13	16-Apr-09	Santa Rosa	20°29'35.07" N	88°05'43.81" W	22.080	23.891	1.8
14	16-Apr-09	Chamul	20°22'42.63" N	88°03'55.66" W	22.360	23.917	1.6
15	16-Apr-09	San Juan	20°25'01.14" N	87°43'32.55" W	6.800	8.224	1.4
16	16-Apr-09	Camp. Hidalgo	20°35'46.88" N	87°40'06.57" W	21.130	22.762	1.6
17	20-Apr-09	Ranch el viejo	21°14'43.51" N	86°53'03.95" W	8.240	9.067	0.8
18	21-Apr-09	Solferino	21°21'36.90" N	87°25'34.63" W	8.370	10.444	2.1
19	21-Apr-09	San Eusebio	21°23'58.37" N	87°20'14.93" W	8.770	10.136	1.4
20	22-Apr-09	San Angel	21°14'11.436" N	87°26'03.264" W	5.020	7.820	2.8
21	22-Apr-09	Rancho san Juan	21°12'57.312" N	87°20'33.54" W	6.930	8.344	1.4
22	23-Apr-09	El Tintal	20°53'41.24" N	87°27'51.91" W	6.020	7.368	1.3
23	23-Apr-09	Nuevo Xcan	20°52'12.13" N	87°36'03.47" W	19.970	21.753	1.8
24	23-Apr-09	Kantanulikin	21°01'45.91" N	87°29'49.57" W	6.420	8.301	1.9
25	23-Apr-09	Esperanza	20°58'20.74" N	87°23'42.05" W	12.580	13.699	1.1
26	25-Apr-09	Aguakan Pozo 1B	21°03'49.16" N	87°01'59.25" W	9.410	10.439	1.0

27	25-Apr-09	Aguakan Pozo 3B	21°03'32.88" N	87°01'37.17" W	8.870	9.899	1.0
28	25-Apr-09	Aguakan Pozo 12	21°00'34.19" N	87°03'13.21" W	8.600	9.648	1.0
29	25-Apr-09	Aguakan Pozo 23a	20°58'41.98" N	87°06'21.97" W	7.900	9.240	1.3
30	25-Apr-09	Aguakan Pozo 23b	20°58'42.23" N	87°06'21.51" W	8.050	9.112	1.1
31	25-Apr-09	Aguakan vallarta	20°51'44.24" N	87°02'28.74" W	4.890	5.954	1.1
32	26-Apr-09	Pabalan	20°44'13.41" N	87°49'44.45" W	19.260	21.149	1.9
33	26-Apr-09	Estrella	20°48'27.72" N	87°44'15.16" W	19.190	21.024	1.8
34	28-Apr-09	Cenote en el eden	21°10'59.58" N	87°09'38.76" W	3.990	5.119	1.1

Appendix 3: Field measurement locations description

In this appendix are presented pictures of the wells that have been measured during the field trip. Unfortunately some wells have not been photographed. The number of the measurement referred to those displayed in the table in Appendix 2. Most of the wells measured are old dug wells and a cross has been drawn on their casings in order to identify the exact point from where the water level has been measured.

Measurement 1: Leona Vicario, old dug well situated in the center of the village 	Measurement 2: Cenote 7 bocas, cenote situated 4km in the north of Central Vallarta (the red arrow indicates the location from where the measurement was taken. 

Measurement 3: Ranch de la dama y del caballero, pipe well used for irrigation of the ranch, the water level has been measured at the top of the pipe.	Measurement 4: Ranch de la calandaria, old dug well situated at the entrance of the ranch.
Measurement 5: El Delirios, dug well situated in the center of the village 	Measurement 6: Agua azul, cenote situated in the center of the village. The red arrow indicates the location of the water level measurement. 
Measurement 7: La granja, Dug well in the village	Measurement 8: Valladolid nueva, Dug well in the village
Measurement 9: Victoria, Dug well in the center of the village 	Measurement 10 Chulutan, well in situated in the main place in the village 

Measurement 11: Felipe Carillo, dug well with underground cenote in the center of the village 	Measurement 12 Xalau, dug well in the center of the village
Measurement 13: Santa rosa, dug well in the center of the village 	Measurement 14: Chamul, dug well in the center of the village 

Measurement 15: San Juan, well situated in the center of the village 	Measurement 16: Camp. Hidalgo, well in the village, on the place
Measurement 17: Ranch el viejo, well situated in a ranch 2km in the east of the village el Viejo. In the ranch, horses are raised for races.	Measurement 18: Solferino,
Measurement 19: San Eusebio, well situated in the center of the village 	Measurement 20 San Angel

<table>
<tr>
<td><u>Measurement 21:</u> Rancho San Juan, private well situated in the ranch
</td>
<td><u>Measurement 22</u> El tintal, private well situated in the house of a flower raiser.</td>
</tr>
<tr>
<td><u>Measurement 23:</u> Nuevo Xcan</td>
<td><u>Measurement 24:</u> Kantunilkin, well situated along the road, few km in the south of Kantunilkin
</td>
</tr>
</table>

Measurement 25: Esperanza, well situated in the village	Measurement 26-31: Aguakan wells (pozo3B, 12, 23a, 23b, and central Vallarta), The measurements were made in the monitoring wells of Aguakan. All the water levels were taken from the top of the red box (all monitoring wells look the same). 
Measurement 32: Pabalan, well situated in the center	Measurement 33: Estrella, well situated in the center
Measurement 34: Cenote El Eden, cenote situated in the reserve el eden	

Appendix 4: Electrical conductivity profiles

The different profiles have been measured by Aguakan and collected during the field trip. These 5 profiles have been taken close to a location where the water table elevation has been measured. The table below presents the characteristics of these profiles. The latter are also displayed in this appendix.

Characteristics of the Electrical conductivity profiles

Date of the measurement	Location	Latitude	Longitude	Depth to saline water (relative to ground surface)	Topographical height	Depth to saline water (relative to mean Sea level)	Water table elevations
				[m]	[m]	[m]	[mamsl]
30-Mar-07	Cenote 7 bocas	20° 52' 33.6" N	87° 02' 38.4" W	- 30.4	5.395	- 25.005	0.985
4-May-08	Leona Vicario	20º 59’ 05.7” N	87º 12’ 39.2” W	- 43.5	6.7311	- 36.769	1.06
4-Apr-08	Pozo 12	21º 00’ 34.0” N	87º 03’ 13.1” W	- 39	9.648	- 29.353	1.048
4-Apr-08	Pozo 23a	20º 58’ 42.0” N	87º 06’ 21.9” W	- 33.5	9.240	- 24.260	1.062
4-Apr-08	Pozo 23b	20º 58’ 43.0” N	87º 06’ 21.0” W	- 35	9.112	- 25.888	1.062

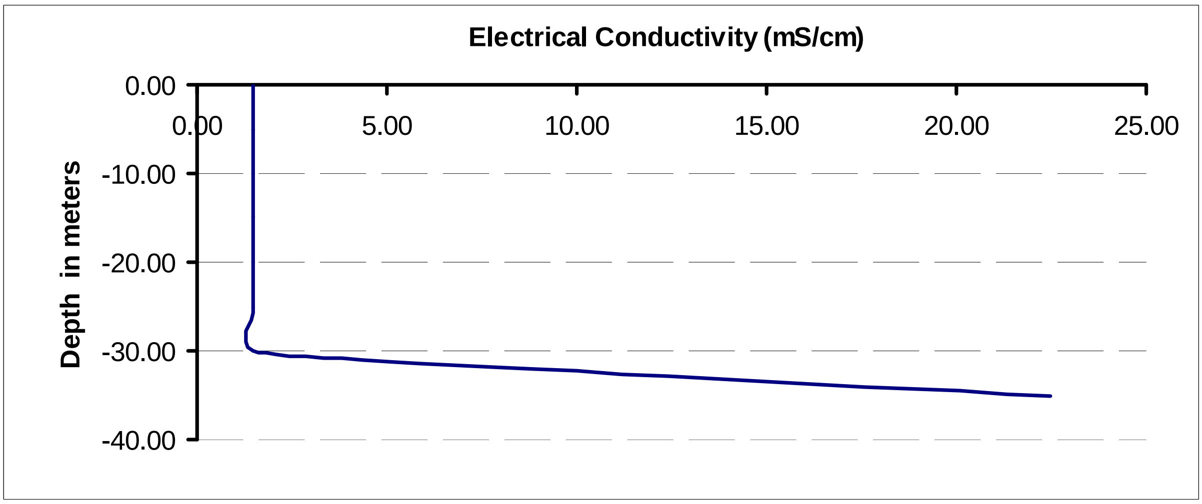

Electrical conductivity profile measured in Cenote 7 bocas.

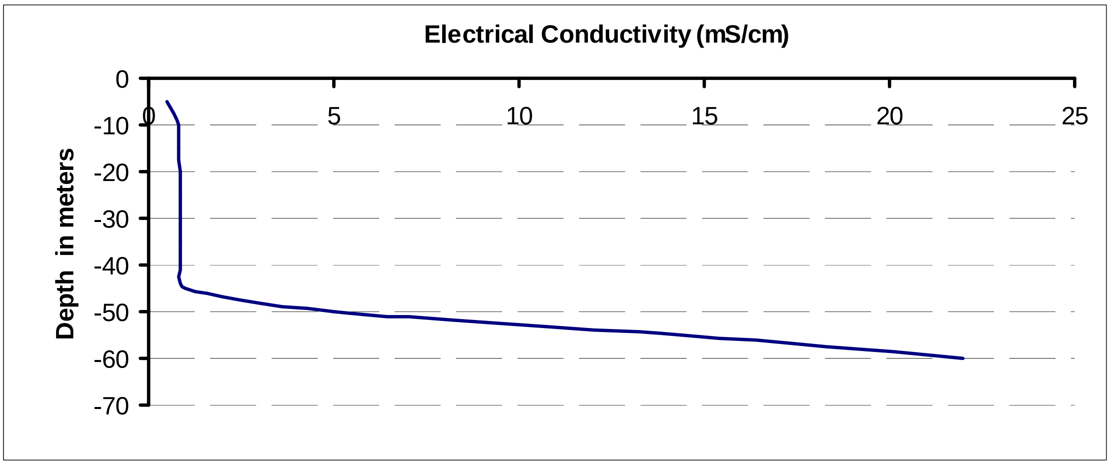

Electrical conductivity profile measured in Leona Vicario.

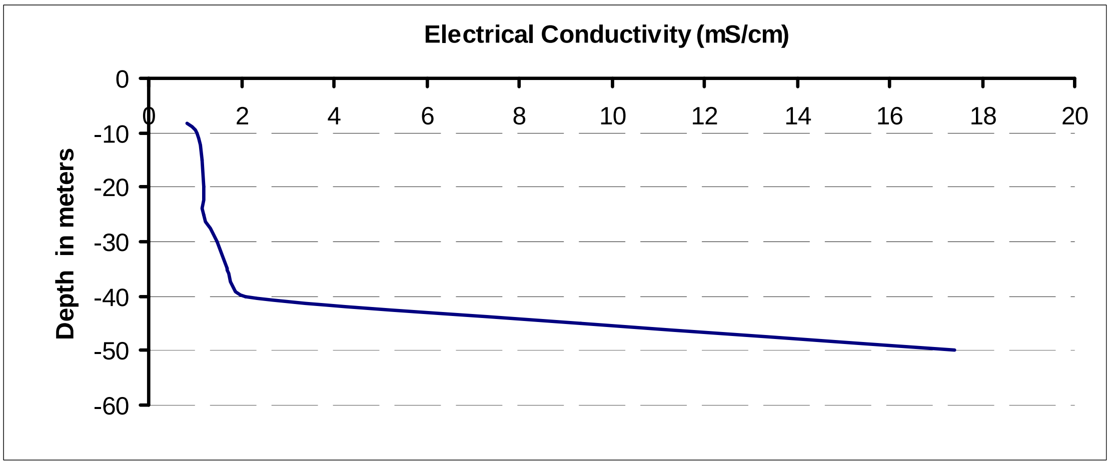

Electrical conductivity profile measured in Pozo 12.

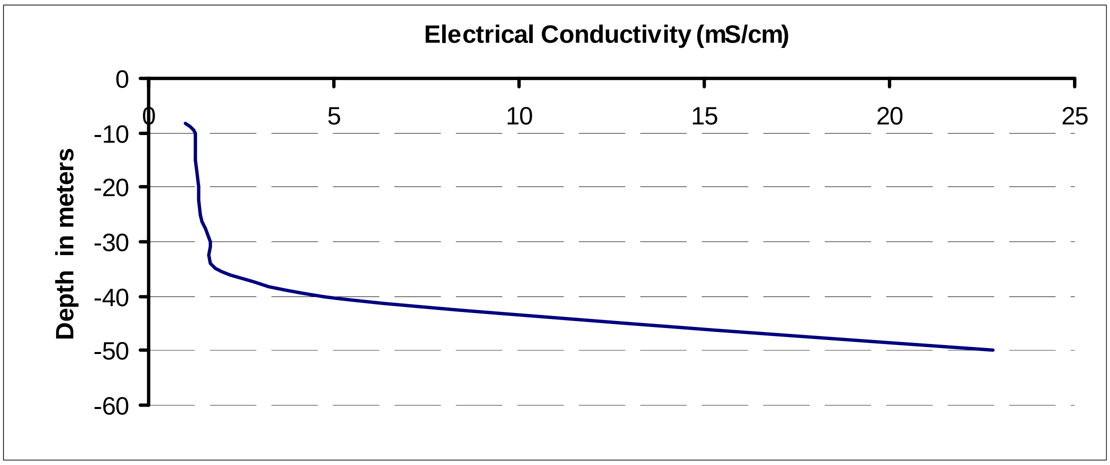

Electrical conductivity profile measured in Pozo 23a

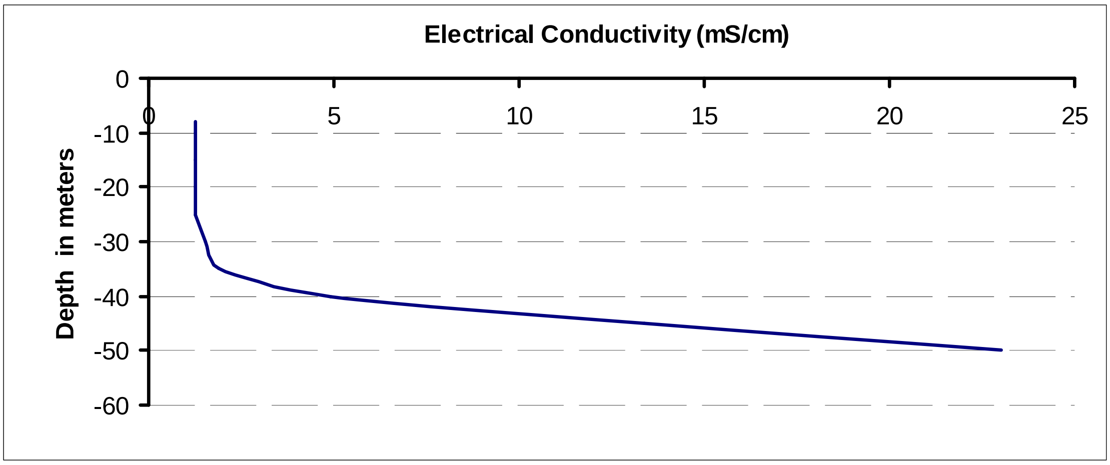

Electrical conductivity profile measured in Pozo 23b

Appendix 5: Matlab script for the stochastic catchment study

The script corresponding to the Monte Carlo study can basically be separated in 3 parts: the generation of the set of inputs, the simulations and the computation of the results.

```
%%%%%%%%%%%%%%%%%%%%%%%%%%Generation of the inputs%%%%%%%%%%%%%%%%%%%%%%

%input 95% confidence intervals (lower and upper value)
loga=log10(0.723512)
logb=log10(2.47893)
logc=log10(7.38327)
logd=log10(295.791)
loge=log10(1.385831E-02)
logf=log10(5.951406E-02)
logg=log10(0.704857)
logh=log10(1.40988)

%input number of samples
nsamples=10000

%input calibrated hydraulic conductivities
mu_matrix1=log10(1.33923)
mu_matrix2=log10(46.7323)
mu_matrix3=log10(2.871871E-02)
mu_matrix4=log10(0.996878)

%input covariance matrix
covB=[ 1.8614E-02  -5.4786E-02   3.8073E-03  -3.9287E-03; -5.4786E-02
0.1672      -1.1907E-02   9.7423E-03;  3.8073E-03  -1.1907E-02
2.6068E-02  -1.0210E-02; -3.9287E-03   9.7423E-03  -1.0210E-02
5.8992E-03 ]

%calculation of standard deviations
stdev_matrix1=(logb-loga)/(2*1.95996);
stdev_matrix2=(logd-logc)/(2*1.95996);
stdev_matrix3=(logf-loge)/(2*1.95996);
stdev_matrix4=(logh-logg)/(2*1.95996);

%Metropolis Hastings algorithm

start=[mu_matrix1 mu_matrix2 mu_matrix3 mu_matrix4];
MU= [mu_matrix1 mu_matrix2 mu_matrix3 mu_matrix4];
SIGMA=covB;
delta=[(stdev_matrix1/2) ; (stdev_matrix2/2); (stdev_matrix3/2) ;
(stdev_matrix4/2)];
R = chol(SIGMA);

pdf = @(x) mvnpdf(x, MU, SIGMA);

proppdf = @(x,y) 1*gt(gt(unifpdf(y(1,1)-x(1,1),-delta(1,1),
delta(1,1)),0) + gt(unifpdf(y(1,2)-x(1,2),-delta(2,1), delta(2,1)),0) +
```

```
gt(unifpdf(y(1,3)-x(1,3),-delta(3,1), delta(3,1)),0) +
gt(unifpdf(y(1,4)-x(1,4),-delta(4,1), delta(4,1)),0),1);

proprnd = @(x) repmat(MU,1,1) + randn(1,4)*R;

x=mhsample(start,nsamples,'pdf',pdf, 'proppdf',
proppdf,'proprnd',proprnd);

%convertion to real K-values
Kmatrix1=10.^(x(:,1));
Kmatrix2=10.^(x(:,2));
Kmatrix3=10.^(x(:,3));
Kmatrix4=10.^(x(:,4));

%save the results just to have a copy of the vectors generated
save( 'Kmatrix1.mat', 'Kmatrix1')
save( 'Kmatrix2.mat', 'Kmatrix2')
save( 'Kmatrix3.mat', 'Kmatrix3')
save( 'Kmatrix4.mat', 'Kmatrix4')


%%%%%%%%%%%%%%%%%%%%%%%%%%%%%%%%%Simulations%%%%%%%%%%%%%%%%%%%%%%%%%%%%%%%%%
for i=1:nsamples
    i

    cd 'C:\Documents and Settings\s070729\Desktop\New'

%bcf_firstpart.dat is a text file containing the 45 first lines of the
bcf.dat file. These lines are not changing between samples

    copyfile('bcf_firstpart.dat', 'bcf.dat')

%bcf2.dat is a file containing the matrix of hydraulic conductivities
(with, instead of the normal conductivity values, the values 11, 22, 33,
44 corresponding respectively to the 4 different conductivities) and the
matrix describing the bottom of layer.

    A1=dlmread('bcf2.dat','',[45 0 7244 19]);
    A2=dlmread('bcf2.dat','',[7246 0 14445 19]);

    B1=A1.';
    B2=A2.';

  %Writing of the new values in the bcf.dat file

    fid=fopen('bcf.dat','a');

    B1(B1==11111)=Kmatrix1(i,1);
    B1(B1==22222)=Kmatrix2(i,1);
    B1(B1==33333)=Kmatrix3(i,1);
    B1(B1==44444)=Kmatrix4(i,1);
```

```
    %calculation of vertical leakance
    B3=-((0.1*B1)./B2);

    %calculation of transmissivity
    B4=-B1.*B2;

    % Layer 1
        %write horyzontal hydraulic conductivity for layer 1


fprintf(fid,'%14.5f%14.5f%14.5f%14.5f%14.5f%14.5f%14.5f%14.5f%14.5f%14.5
f%14.5f%14.5f%14.5f%14.5f%14.5f%14.5f%14.5f%14.5f%14.5f%14.5f\r\n',B1);

        %write header botom layer 1
        %write matrix botom layer 1

        fprintf(fid,'        11          1(20G14.0)                   -1
Elevation of the bottom of the layer : 1\r\n');

fprintf(fid,'%14.5f%14.5f%14.5f%14.5f%14.5f%14.5f%14.5f%14.5f%14.5f%14.5
f%14.5f%14.5f%14.5f%14.5f%14.5f%14.5f%14.5f%14.5f%14.5f%14.5f\r\n',B2);


        %write header vertical leakance layer 1
        %write matrix vertical leakance layer 1

        fprintf(fid,'        11          1(20G14.0)                   -1
10. DATA Vcont: Calculated Vertical Leakance of layer 1\r\n');

fprintf(fid,'%14.5f%14.5f%14.5f%14.5f%14.5f%14.5f%14.5f%14.5f%14.5f%14.5
f%14.5f%14.5f%14.5f%14.5f%14.5f%14.5f%14.5f%14.5f%14.5f%14.5f\r\n',B3);

    % Layer 2
        %write header transmissivity layer 2
        %write matrix transmissitivity layer 2

        fprintf(fid,'        11          1(20G14.0)                   -1
7. DATA Tran(): Transmissivity = Hydr. Conductivity * thickness of layer
2\r\n');

fprintf(fid,'%14.5f%14.5f%14.5f%14.5f%14.5f%14.5f%14.5f%14.5f%14.5f%14.5
f%14.5f%14.5f%14.5f%14.5f%14.5f%14.5f%14.5f%14.5f%14.5f%14.5f\r\n',B4);

        %write header vertical leakance layer 2
        %write matrix vertical leakance layer 2

        fprintf(fid,'        11          1(20G14.0)                   -1
10. DATA Vcont: Calculated Vertical Leakance of layer 2\r\n');

fprintf(fid,'%14.5f%14.5f%14.5f%14.5f%14.5f%14.5f%14.5f%14.5f%14.5f%14.5
f%14.5f%14.5f%14.5f%14.5f%14.5f%14.5f%14.5f%14.5f%14.5f%14.5f\r\n',B3);
% Layer 3
        %write header transmissivity layer 3
```

```
        %write matrix transmissivity layer 3

        fprintf(fid,'        11         1(20G14.0)                   -1
7. DATA Tran(): Transmissivity = Hydr. Conductivity * thickness of layer
3\r\n');

fprintf(fid,'%14.5f%14.5f%14.5f%14.5f%14.5f%14.5f%14.5f%14.5f%14.5f%14.5
f%14.5f%14.5f%14.5f%14.5f%14.5f%14.5f%14.5f%14.5f%14.5f%14.5f\r\n',B4);

        %write header vertical leakance layer 3
        %write matrix vertical leakance layer 3

        fprintf(fid,'        11         1(20G14.0)                   -1
10. DATA Vcont: Calculated Vertical Leakance of layer 3\r\n');

fprintf(fid,'%14.5f%14.5f%14.5f%14.5f%14.5f%14.5f%14.5f%14.5f%14.5f%14.5
f%14.5f%14.5f%14.5f%14.5f%14.5f%14.5f%14.5f%14.5f%14.5f%14.5f\r\n',B3);

    % Layer 4
        %write header transmissivity layer 4
        %write matrix transmissivity layer 4

        fprintf(fid,'        11         1(20G14.0)                   -1
7. DATA Tran(): Transmissivity = Hydr. Conductivity * thickness of layer
4\r\n');

fprintf(fid,'%14.5f%14.5f%14.5f%14.5f%14.5f%14.5f%14.5f%14.5f%14.5f%14.5
f%14.5f%14.5f%14.5f%14.5f%14.5f%14.5f%14.5f%14.5f%14.5f%14.5f\r\n',B4);

        %write header vertical leakance layer 4
        %write matrix vertical leakance layer 4

        fprintf(fid,'        11         1(20G14.0)                   -1
10. DATA Vcont: Calculated Vertical Leakance of layer 4\r\n');

fprintf(fid,'%14.5f%14.5f%14.5f%14.5f%14.5f%14.5f%14.5f%14.5f%14.5f%14.5
f%14.5f%14.5f%14.5f%14.5f%14.5f%14.5f%14.5f%14.5f%14.5f%14.5f\r\n',B3);

    % Layer 5
        %write header transmissivity layer 5
        %write matrix transmissivity layer 5

        fprintf(fid,'        11         1(20G14.0)                   -1
7. DATA Tran(): Transmissivity = Hydr. Conductivity * thickness of layer
5\r\n');

fprintf(fid,'%14.5f%14.5f%14.5f%14.5f%14.5f%14.5f%14.5f%14.5f%14.5f%14.5
f%14.5f%14.5f%14.5f%14.5f%14.5f%14.5f%14.5f%14.5f%14.5f%14.5f\r\n',B4);

        %write header vertical leakance layer 5
        %write matrix vertical leakance layer 5
```

```
        fprintf(fid,'        11          1(20G14.0)                   -1
10. DATA Vcont: Calculated Vertical Leakance of layer 5\r\n');

fprintf(fid,'%14.5f%14.5f%14.5f%14.5f%14.5f%14.5f%14.5f%14.5f%14.5f%14.5
f%14.5f%14.5f%14.5f%14.5f%14.5f%14.5f%14.5f%14.5f%14.5f%14.5f\r\n',B3);

   % Layer 6
        %write header transmissivity layer 6
        %write matrix transmissitivity layer 6

        fprintf(fid,'        11          1(20G14.0)                   -1
7. DATA Tran(): Transmissivity = Hydr. Conductivity * thickness of layer
6\r\n');

fprintf(fid,'%14.5f%14.5f%14.5f%14.5f%14.5f%14.5f%14.5f%14.5f%14.5f%14.5
f%14.5f%14.5f%14.5f%14.5f%14.5f%14.5f%14.5f%14.5f%14.5f%14.5f\r\n',B4);

        %write header vertical leakance layer 6
        %write matrix vertical leakance layer 6

        fprintf(fid,'        11          1(20G14.0)                   -1
10. DATA Vcont: Calculated Vertical Leakance of layer 6\r\n');

fprintf(fid,'%14.5f%14.5f%14.5f%14.5f%14.5f%14.5f%14.5f%14.5f%14.5f%14.5
f%14.5f%14.5f%14.5f%14.5f%14.5f%14.5f%14.5f%14.5f%14.5f%14.5f\r\n',B3);

fprintf(fid,'        11          1(20G14.0)                   -1  7. DATA
Tran(): Transmissivity = Hydr. Conductivity * thickness of layer
7\r\n');

fprintf(fid,'%14.5f%14.5f%14.5f%14.5f%14.5f%14.5f%14.5f%14.5f%14.5f%14.5
f%14.5f%14.5f%14.5f%14.5f%14.5f%14.5f%14.5f%14.5f%14.5f%14.5f\r\n',B4);

    fclose(fid)



    %run Modflow with the batch file

        !test.bat


    %copy output files from Modflow in the Modpath folder and run the
particle tracking

    cd C:\Progra~1\USGS\mpath3.2\bin

   copyfile('C:\Documents and Settings\s070729\Desktop\New\heads.dat',
'C:\Program Files\USGS\mpath3.2\bin')
   copyfile('C:\Documents and Settings\s070729\Desktop\New\ddown.dat',
'C:\Program Files\USGS\mpath3.2\bin')
   copyfile('C:\Documents and Settings\s070729\Desktop\New\budget.dat',
'C:\Program Files\USGS\mpath3.2\bin')
```

```
   copyfile('C:\Documents and Settings\s070729\Desktop\New\output.dat',
'C:\Program Files\USGS\mpath3.2\bin')

!mpathstartpath.bat


%%%%%%%%%%%%%%%%%%%%%%%%Results computation%%%%%%%%%%%%%%%%%%%%%%%%%%%

%read the pathline file

l=size(dlmread('pathline','',1,0),1);
A=dlmread('pathline','',[1 6 l 7]);


% write a matrix containing with 1 assigned to every cells where a
particle passes through


C=zeros(360,400);

for j=1:l
    j

    C(A(j,1),A(j,2))=1;

end

mask=C;

%concatenate data

    if i==1
        finmask=mask;
    else
        finmask=cat(3,finmask,mask);
        finmask=sum(finmask,3);
    end
```

```
%for every 10 outputs, generate a separate file of the stacked results,
so that the development in catchment can be evaluated. The files are
written as ASCII file readable directly with ArcGIS.

   cd C:\s070729\results

    if eq(mod(i,10),0)
       endnum=i;
       startnum=i-9;

 name3=strcat('finmask_',num2str(startnum),'_',num2str(endnum),'.asc');
       mask2=((100*finmask)/i);
       save('mask2','mask2','-ASCII');

     F=dlmread('mask2');
     fid=fopen('mask2','wt');
     fprintf(fid,'ncols          1800\r\n');
     fprintf(fid,'nrows          2000\r\n');
     fprintf(fid,'xllcorner      350000\r\n');
     fprintf(fid,'yllcorner      2200000\r\n');
     fprintf(fid,'cellsize       100\r\n');
     fprintf(fid,'NODATA_value   0\r\n');
     fprintf(fid,' %u',F);
     fclose(fid)
     copyfile('mask2',name3);


    end


end
```